2012

Allosteric Mechanisms in Recombinant Human Hexokinase Type I

Lu Shen
Iowa State University

Allosteric mechanisms in recombinant human hexokinase type I

by

Lu Shen

A dissertation submitted to the graduate faculty

In partial fulfillment of the requirements for the degree of

DOCTOR OF PHILOSOPHY

Major: Biochemistry

Program of Study Committee:

Richard B. Honzatko, Major Professor

Scott W. Nelson

Mark S. Hargrove

Michael Shorgen-Knaak

Mei Hong

Iowa State University

Ames, Iowa

2012

Table of Contents

Abbreviations

HKI: hexokinase I

Glc-6-P: glucose 6-phosphate

Glc: glucose

P_i: phosphate

1,5-anhydroGlc-6-P: 1,5-anhydroglucitol 6-phosphate

2-deoxy Glc-6-P: 2-deoxy glucose-6-phosphate

Man-6-P: mannose 6-phosphate

Glc-1,6-P_2: glucose 1,6-bisphosphate

TNP-ADP: 2'-(or-3')-O-(2,4,6-trinitrophenyl)-adenosine 5'-diphosphate

To indicate amino acids in protein sequences or names of the mutant enzymes, one letter or three letters abbreviation was used.

Abstract

Hexokinase I (HKI) is the pacemaker of glycolysis in brain and red bold cells, being subject to potent feedback inhibition by its product glucose 6-phosphate (Glc-6-P) and the relief of that inhibition by inorganic phosphate (P_i) and glucose (Glc). Presented here is a comprehensive model of inhibition and relief of inhibition for recombinant human HKI derived from crystal structures, molecular dynamics simulations, kinetics and directed mutations. Ligand interactions at each half of HKI are comparable in crystal structures, but in simulations, 2-deoxyglucose 6-phosphate (2-deoxyGlc-6-P) and mannose 6-phosphate (Man-6-P) lose hydrogen bonds at the C-terminal half, consistent with early stages of ligand dissociation. 1,5-Anhydroglucose 6-phosphate (1,5-anhydroGlc-6-P), adopts an alternative binding mode, and stabilizes a slightly open C-terminal half. The kinetics of D413N and/or D861N enzymes (D413 and D861 interact with the 1-OH group of Glc-6-P) are consistent only with synergistic binding of two molecules of 1,5-anhydro-Glc-6-P to sites with unequal constants of dissociation. The crystal structure and simulation of HKI with glucose 1,6-bisphosphate (Glc-1,6-P_2) implicate Lys418 (N-terminal half) and Lys866 (C-terminal half) in stabilizing inhibited conformations of HKI, a finding support by directed mutations. P_i displaces 1,5-anhydroglucitol 6-phosphate from the N-terminal half, but not from the C-terminal half. Glucose (Glc) up to concentration of 1 mM interacts synergistically with 1,5-anhydroGlc-6-P, but at higher concentrations becomes an antagonist of inhibition. A site-affinity model quantitatively accounts for these observed phenomena in wild-type and mutant forms of HKI. For wild-type HKI, inhibitor binds to sites of unequal affinity, coupled by negative coorperativity, with the site of highest affinity at the N-terminal half. Pi-displaces inhibitor from the N-terminal half, but does not prevent inhibition at the C-terminal half. Potent inhibition requires two molecules of bound glucose to HKI, and the binding of Glc to the active site seems primarily responsible for creating a state of HKI susceptible to potent inhibition. The mapping of mutations that affect allosteric mechanism in HKI clearly define the N-terminal inhibitor pocket and the flexible subdomain as key components of allostery in HKI.

Chapter I. General Introducation & Literature Review

Hexokinase (ATP: D-hexose 6-phosphotransferase, EC2.7.1.1) catalyzes the initial and crucial step of glycolysis, the phosphorylation of 6-hydroxyl group of glucose (Glc) using $[ATP\text{-}Mg]^{2-}$ as the phosphoryl donor[1-3].

$$\text{Glucose} + [ATP{\bullet}Mg]^{2-} \longrightarrow \text{Glc-6-P}^{2-} + [ADP{\bullet}Mg]^{1-} + H^{+}$$

The focus of work here is human hexokinase Type I (HKI), and as the name implies, HKI can phosphorylate several six-carbon sugars (mannose, 2-deoxy glucose, and 2,5-anhydro-glucitol, for example); however, only Glc binds to HKI with high affinity. As early as 1954, Crane demonstrated the importance of the 2-hydroxyl group in the binding of 6-phosphorylated hexoses to an inhibitory site of HKI, whereas the 2-hydroxyl group was not important for substrate binding[4]. Only the 4-hydroxyl group is important for both hexose and hexose-6-phosphate binding[4]. Later studies showed that a doubly charged anionic group at the 6-position is necessary for effective inhibition[4-6]. A 5-thio group increases the binding affinities, both for the hexose and hexose-6-phosphate[6]. ATP is the best substrate for HKI (highest k_{cat}, lowest K_m). The K_m values for other triphosphate nucleosides, such as ITP, GTP, CTP and UTP do not differ significantly from that of ATP, while the k_{cat} values are significantly lower[7].

Evolution of Hexokinase Family

Four isozymes of hexokinase have been identified in mammalian tissues[8](Table I). The type I, II and III hexokinase isozymes, all with molecular weights of approximately 100 kDa, share 70% sequence identity[9]. N- and C- halves of isozymes I–III show extensive internal sequence similarity (~50% sequence identity) and structure similarity[9]. Hexokinase Type IV, commonly named glucokinase, is similar to yeast hexokinase isoforms A and B, having a molecular weight of 50 kDa, and exhibiting significant sequence similarity to both halves of isozymes I–III[9]. Presumably, all members in the hexokinase family derived from a common ancestor, a 30 kDa glucomannokinase-like enzyme which utilized poly(P) as substrate in primordial age before the appearance of ATP (Figure 1)[10]. One branch of the evolutionary

pathway led to poly(P)/ATP utilizing hexokinase, whereas the other led to a 50 kDa ATP-specific hexokinase such as yeast hexokinase and hexokinase IV[10]. Whether the 50 kDa ATP-specific hexokinase, however, evolved independently from the 30 kDa glucomannokinase-like enzyme or from the poly(P)/ATP utilizing hexokinase is unclear. During evolution, the ATP-specific hexokinase acquired a new property of regulation, feedback inhibition by product, just like the isoforms in starfish and other marine organisms[9-10]. The 100 kDa hexokinase architecture appeared then through gene duplication and fusion[11-14]. The N-domain lost catalytic properties in becoming mammalian hexokinase types I and III[10]. The 100 kDa Glc-6-P insensitive hexokinase might have evolved directly from the 50 kDa Glc-6-P insensitive enzyme, or from the 50/100 kDa Glc-6-P sensitive enzyme, thereafter losing product inhibition. Some researchers suggest that the gene duplication and fusion occurred prior to the diversification of the hexokinase family, and that glucokinase evolved from the 100 kDa isozyme by losing its N-terminal regulatory domain[15].

General Kinetics Properties of Mammalian Hexokinases

Besides sequence and structural similarities, isozymes I-III also share several properties, such as K_m for glucose is in the sub-millimolar range and product inhibition is at physiologically relevant concentrations (micromolar level)[9]; however, they differ significantly in catalytic and regulatory properties. Both halves of hexokinase II possess catalytic activity[16], whereas the N-halves of hexokinase I and III are devoid of activity[9, 17-18]. Given the fact that both hexokinase I and II have special binding sites for Glc, Glc-6-P, P_i and ATP in both N- and C-domains, it is believed that during evolution, the N-terminal domain of hexokinase I lost its activity and evolved into a regulatory domain[9]. Inorganic phosphate (P_i) potently inhibits hexokinase II and III, and at high concentrations (millimolar) is an inhibitor of hexokinase I. At relatively low concentrations (100 μM), however, P_i antagonizes the inhibition of hexokinase I by Glc-6-P[9]. Among all four isozymes, only Hexokinase III is substrate-inhibited by glucose at physiologically relevant concentrations (1 mM)[19-20]. In contrast, the K_m for glucose is 100 times higher for glucokinase than the other mammalian hexokinase

isozymes. Glucokinase exhibits no substrate inhibition and is insensitive to physiologically relevant levels of Glc-6-P[9].

Tissue Distribution of Mammalian Hexokinases

Given the different kinetics properties associated with each isozyme, it's reasonable to expect the expression of different isozymes in different tissues. Hexokinase I, as a "housekeeping enzyme", is found in all mammalian tissues and is highly or even exclusively expressed in brain and red blood cells[1-3]. Hexokinase II is mainly expressed in insulin-sensitive tissues such as skeletal muscle and adipose tissue[19]. Hexokinase III is expressed in very low levels, and is associated with the cell nucleus[19]. Hexokinase IV is mainly present in liver, but also found in neuoroendocrine cells[19].

Both Hexokinase I and II are overexpressed in many cancer cells[21-22]. The overexpression leads to protection against apoptotic cell death[21-22]. Other studies show that mitochondrial hexokinase I and II binding increases with insulin treatment and ischemia in an isoform-specific way in heart[23]. HKI gene promoter mutation in humans causes hexokinase I deficiency and chronic hemolysis[24]. All these make hexokinase a good therapeutic target for a number of diseases.

Physiological functions of hexokinase type I

Hexokinase I is highly expressed in brain and red blood cells[1-3]. In brain, hexokinase I exists predominantly as mitochondrial bound form[9]. The bound enzyme preferentially uses ATP generated by oxidative phosphorylation, putatively allowing efficient cycling of adenine nucleotide to and from the inner matrix of the mitochondrion[9]. The first 15 residues of hexokinase I (HKI) are predicted to form a hydrophobic helix and are necessary and sufficient for targeting HKI to the mitochondrial outer membrane[25-27].

When bound to mitochondrial outer membrane, HKI is likely to interact with the cytosollic face of the voltage dependent anion channel (VDAC), while the other end of VDAC interacts directly with the adenylate nucleotide translocator (ANT) of mitochondrial

inner membrane. In turn, ANT interacts with cyclophilin D (Cph.D) inside the mitochondrial matrix[26]. The HKI-VDAC-ANT-Cph.D complex is the mitochondrial permeability transition pore, which opens putatively during cell apoptosis and necrosis. Recent studies show that glucose phosphorylation and mitochondrial binding are required for the anti-apoptotic effect of hexokinase I and II[28].

HKI may form a tetramer when bound to mitochondria[26, 29]. Binding of human HKI to rat liver mitochondria is cooperative with a Hill coefficient of 3.1-3.3[30-32], but earlier investigations from at least three different groups provide no evidence for cooperativity in the binding of HKI to mitochondria[29, 33-34]. Glc-6-P can release ~60% HKI from mitochondria[33]. The presence of Mg^{2+} or P_i antagonizes Glc-6-P induced release effect[9]. The mechanism of Glc-6-P release of hexokinase I may be due to a conformational change induced by Glc-6-P binding to the N-terminal domain[9, 34]. The nucleoside triphosphates, ATP, CTP, GTP, UTP and ITP, are also capable of releasing 90% of the enzyme from the membrane[33]. The release mechanism due to nucleotides is probably distinct from that of Glc-6-P [33].

In solution at physiological concentrations (1-10 μg/ml), HKI functions as a monomer, but dimerizes as protein concentration increases (>1 mg/ml)[9]. Small angle scattering experiments show that HKI exists exclusively as monomer up to a concentration of 3.6 mg/ml when P_i present, though the enzyme dimerizes as protein concentration increases[35]. Unlike P_i, Glc-6-P helps HKI dimerize with 80% dimer at 0.9 mg/ml as shown in the small angle scattering experiment[35].

X-ray Crystallography Structure of HKI

The structure of recombinant HKI (Figure 2) has been solved by X-ray crystallography[32,35-40]; however, compared to the functional monomeric enzyme in solution, HKI exists as a dimer in the crystal, with Glc·Glc-6-P or Glc·Pi binding in both N- and C-half[36-37]. Subunits in the HKI dimer align head-to-tail with twofold rotational symmetry. The N-terminal domain of one monomer interacts with the C-terminal domain of another monomer[32, 36-39]. Triple-mutant HKI (E280A/R283A/G284Y) eliminates subunit interactions of the crystalline

dimer, exhibits wild-type functional properties, and crystallizes as a monomer[40]. The structure of the monomeric HKI adopts a rod-like conformation, similar to subunits in the dimer[35, 40]. Furthermore, small angle x-ray scattering indicates HKI retains the conformation observed in crystallographic structures in solution in the presence and absence of ligands (Glc-6-P, glucose, P_i, and ADP) [35].

The monomer of hexokinase I is composed of two structurally similar halves (N-terminal and C-terminal) separated by a transition helix[35-41]. Each half is composed of large domain (residues 13-74, 210-447 in N-terminal half and residues 466-522, 658-895 in C-terminal half) and the small domain (residues 75-209, 448-465 in N-terminal half and residues 523-657, 896-913 in C-terminal half)[40]. The relative position of the two domains in C-terminal half of HKI define two conformational states, open and closed states, differing by a 17° rotation of the small domain relative to the large domain[40]. In the Glc-6-P·Glc structure, both N-terminal and C-terminal halves are in the closed state, whereas in the P_i·Glc structure, the N-terminal half is closed and the C-terminal half is open[36-37]. HKI structures are consistent with that N-terminal half possessing a “tighter” conformation with respect to C-terminal half, and C-terminal half unfolding before the N-terminal half[41-42].

Although the N-terminal half of hexokinase I is catalytically inactive, it does contain a binding pocket for glucose and Glc-6-P which is nearly identical to that of C-terminal half[37]. The crystal structures reveal a high affinity binding site for P_i at the N-terminal half, overlapping the binding site of the 6-phosphoryl group of Glc-6-P[36-37]. The conformation of the N-terminal of hexokinase I in its P_i and Glc-6-P complexes differs slightly: the conformation of loop 445-450 is different and the N-terminal half pivots at the N-terminal end of the transition helix. The monomeric triple mutant HKI structure with ligands ADP·P_i·Glc reveals two ADP binding sites, one at the distant end of N-terminal half and one at the active site[40]. Although the phosphoryl groups of the ADP molecule at the C-terminal half do not bind as would be predicted for a productive substrate complex, the structures reveals the adenine ring binding pocket and conformational changes in the active site thought to be necessary for catalysis. The major difference between this structure and the previous structures is that the residue T784 is in an “up” position, providing space for the base of the adenine nucleotide.

The extremely limited interaction demonstrated in the structures between the two halves of the enzyme, as well as between two monomers, makes it very hard to imagine and understand how the N-terminal half delivers regulatory information to its catalytic C-terminal half (Figure 3).

Glc-6-P Inhibition Mechanism Puzzle of HKI

Crystal structures reveal two binding sites for Glc-6-P at high concentration in the presence of 1 mM glucose, whereas binding studies in solution indicate that only one molecule of Glc-6-P binds to HKI with high affinity in the presence or absence of glucose[34, 43-45]. High affinity binding is thought to be responsible for potent Glc-6-P inhibition, but the kinetics mechanism of HKI inhibition is nonlinear competitive with ATP consistent with a second, weaker binding site for inhibitor[46]. Investigators have differed as to the site of high affinity binding (N-terminal half or C-terminal half) since the 1970s. Based on kinetics, Fromm suggested that Glc-6-P inhibits the enzyme by binding to the C-terminal half, the 6-phosphoryl group competing with the γ-phosphate of ATP[44, 47]. Wilson assigned Glc-6-P inhibition to a site at the N-terminal half, on the basis of Glc-6-P protection against proteolysis[17, 41]. Both models have extensive supporting evidence[9, 17, 41, 44, 47]. The Fromm and Wilson models agree however that P_i antagonizes Glc-6-P inhibition by binding to a high-affinity site at the N-terminal half[9, 36]. P_i competes with Glc-6-P for the same phosphoryl binding site in the Wilson model, whereas P_i competes via an allosteric mechanism with Glc-6-P bound at the C-terminal half in the Fromm model.

Results from numerous investigations from laboratories of Fromm and Wilson clearly indicate that each model individually cannot account for all observed phenomena. When HKI is cleaved proteolytically into two halves, the C-terminal half (mini-HKI) is active and inhibited potently by Glc-6-P without P_i-relief of inhibition[48]. On the other hand, the N-terminal half binds Glc-6-P tightly[17,49]. Moreover, mutational studies have shown that Glc-6-P is capable of inhibiting HKI when binding to either of the two binding sites on the enzyme[46, 50]. Only mutations at both Glc-6-P binding sites eliminate the inhibition[50]. Mutant forms of HKI exhibit reduced P_i-relief of Glc-6-P inhibition, which is inconsistent

with the P_i and Glc-6-P competing for the same phosphoryl binding site (Wilson model)[46]. The existence of a single high-affinity site for Glc-6-P in HKI can be reconciled with high affinity sites in each of the C- and N-terminal halves by a mechanism of anticooperativity in Glc-6-P binding[50] or by a conformational change in the N-terminal or C-terminal half when they become separated.

The effect of Glc in the binding of Glc-6-P, while not entirely unrecognized, may be under-appreciated. The binding of Glc-6-P or Pi to HKI is synergistic with Glc[17]. Nonetheless, Glc-6-P still binds with high affinity in the absence of Glc[44], and Wilson has assigned this Glc-independent binding site to N-terminal half[49]. Synergistic interactions between the Glc and Glc-6-P are also observed with miniHKI but not the N-terminal half[17]. The observation of synergism between P_i and Glc in HKI is puzzling given the absence of synergism between Glc and Glc-6-P in the separate N-terminal half.

Table I. Mammalian Hexokinase Isozymes

Isozyme	M.W. (KDa)	Glc-6-P Inhibition	P_i-relief	Tissue Distribution	Mitochondrial Binding
I	100	+	+	brain, red blood cells	+
II	100	+	–	skeletal muscle, adipose tissue	+
III	100	+	–	cell nucleus	–
IV	50	–	–	liver, pancreas neuroendocrine cells	–

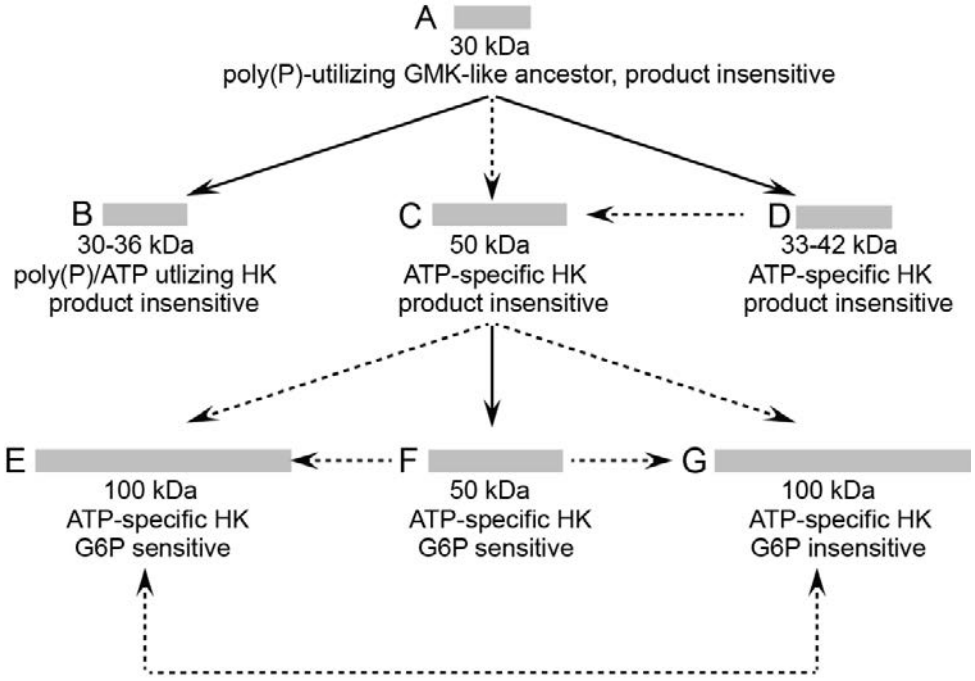

Figure 1. Putative ancestor and evolutionary process of hexokinase family[9-10]. 100 kDa HK formed through gene duplication. Consensus evolutionary transitions are shown by solid arrows, whereas possible transitions are indicated by dotted arrows. A: Putative ancestor of the HK family. B: HK from $Gram^+$ bacteria, crenarchaeota. C: HK from yeast. D: HK from $Gram^-$ bacteria, cyanobacteria and amitochondriate protists. E: HK from mammalian HKI-III .F: HK from starfish and other marine organisms and *S. mansoni*. G: HK from tapeworm *Hymenolepsis diminuta* and lamprey (90 kDa). HK: hexokinase.

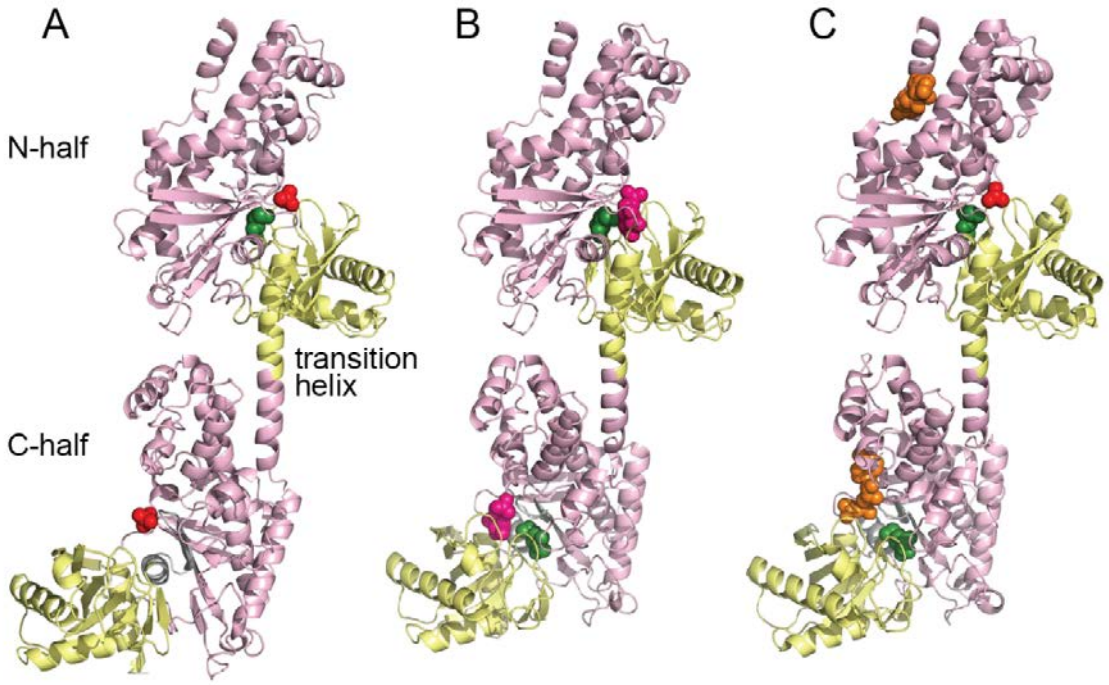

Figure 2. Crystal structures of HKI. A, HKI with Pi·Glc bound (PDB:1HKC); B, HKI with Glc-6-P·Glc bound (PDB:1HKB); C, monomeric triple mutant of HKI with ADP·Pi·Glc bound (PDB:1DGK). The N-half and C-half is connected via a transition helix. Only the C-half of Pi·Glc bound structure is in open conformation, all others are in closed conformation. Color key: large domain, violet; small domain, yellow; P_i, red; Glc, green; Glc-6-P, pink; ADP, brown. (The illustration was generated with PyMOL).

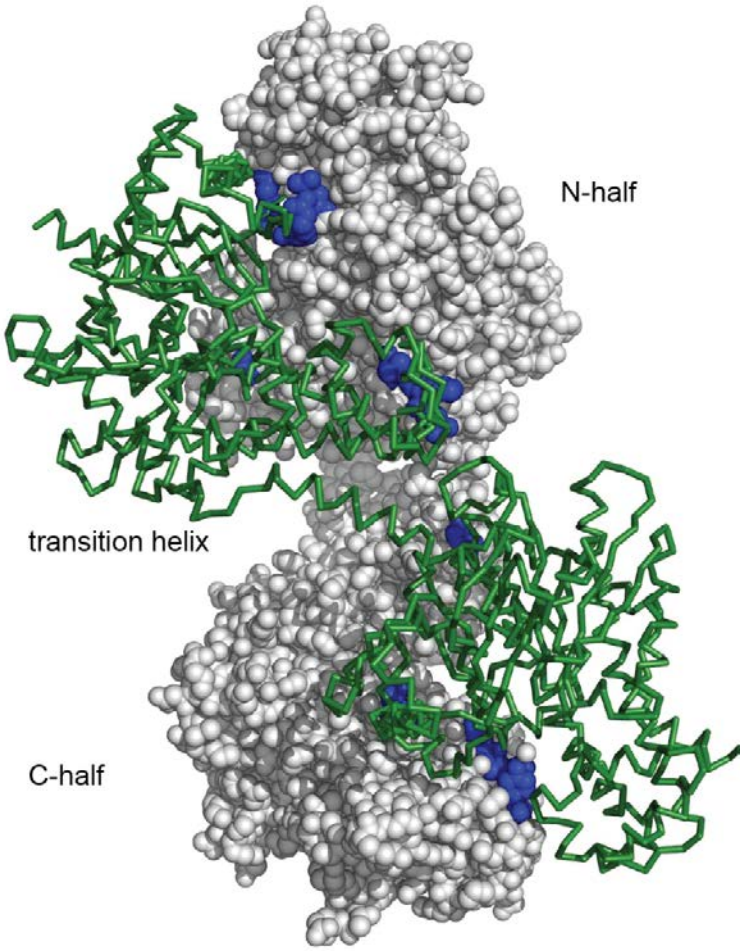

Figure.3. Dimer crystal structures of HKI (PDB:1HKB). Residues in contact between subunits are in blue. (The illustration was generated with PyMOL).

Thesis Organization

This thesis contains 6 chapters.

Chapter I is the general introduction and literature review about hexokinase I.

Chapter II is the study of a series of crystalline complexes and molecular dynamics simulations of recombinant human wild-type HKI and D413N with different phosphoryl ligands: Glc-6-P, 1,5-anhydro-Glc-6-P, 2-deoxy-Glc-6-P and Man-6-P. Studies here reveals an alternative binding mode for 1,5-anhydro-Glc-6-P. A positive binding synergism also appears for the mutant D413N and/or D861N.

Chapter III is the study of crystalline complex and molecular dynamics simulations of D413N HKI with glc-1,6-P_2. The new structure reveals two important residues K418 and K866 that are crucial for high affinity binding of 1,5-anhydro-Glc-6-P. A model of phosphate relief requires the present of EPI complex is derived and fitted.

Chapter IV demonstrates the dual mechanism of Glc on Glc-6-P inhibition for recombinant human HKI. At low glucose concentration, the binding of Glc-6-P is synergistic with Glc. However at high concentrations, glucose is acting as an antagonist to 1,5-anhydro-Glc-6-P.

Chapter V is the study of allosteric inhibition of Glc-6-P for HKI. The following residues which are not directly interact with Glc-6-P are found to be important for the allosteric inhibition : Gly448, Ser449, Ile781, Thr784, Leu795, Leu797 and L867. Results are consistent with a proposed mechanism in which the ligation of the N-terminal half by Glc-6-P induces a rotation of the N-terminal half that alters nonbonded contacts with and within the flexible subdomain of the C-terminal half. Conformational changes in the flexible subdomain, which involve the re-organization of hydrophobic residues within the core of that domain, stabilize an open binding pocket for ATP.

Chapter VI presents general conclusions about the above studies.

References

1. Gonzalez, C., Ureta, T., Sánchez, R., and Niemeyer, H. (1964) Multiple molecular forms of ATP: hexose 6-phosphotransferase from rat liver. *Biochem. Biophys. Res. Commun.* **16**, 347-352
2. Grossbard, L., and Schimke, R.T. (1966) Multiple hexokinases of rat tissues. Purification and comparison of soluble forms. *J. Biol. Chem*. **241**, 3546-3560
3. Katzen, H.M. (1967) The multiple forms of mammalian hexokinase and their significance to the action of insulin. *Adv. Enzyme Regul*. **5**, 335-356
4. Crane, R.K., and Sols, A. (1954) The non-competitive inhibition of brain hexokinase by glucose-6-phosphate and related compounds. *J. Biol. Chem*. **210**, 597-606
5. Magnani, M., Stocchi, V., Serafini, G., and Chiarantini, L. (1988) The interaction of phosphorylated sugars with human hexokinase I. *Biochim. Biophys. Acta*. **954**, 336-342
6. Wilson, J.E., and Chung, V. (1989) Rat brain hexokinase: further studies on the specificity of the hexose and hexose 6-phosphate binding sites. *Arch. Biochem. Biophys*. **269**, 517-525
7. Liu, X.F. (2000) Human hexokinase: multiple mechanisms of Glc-6-P inhibition. Ph.D. thesis, Iowa State University
8. Katzen, H.M., and Schimke, R.T. (1965) Multiple forms of hexokinase in the rat: tissue distribution, age dependency, and properties. *Proc. Natl. Acad. Sci. U.S.A.* **54**, 1218-1225
9. Wilson, J.E. (1995) Hexokinase. *Rev. Physiol. Biochem. Pharmacol*. **126**, 65-198
10. Kawai, S., Mukai, T., Mori, S., Mikami, B., and Murata, K. (2005) Hypothesis: structures, evolution, and ancestor of glucose kinases in the hexokinase family. *J. Biosci. Bioeng*. **99**, 320-330
11. Easterby, J.S, and O'Brien, M.J. (1973) Purification and properties of pig-heart hexokinase. *Eur. J. Biochem*. **38**, 201-211
12. Holroyde, M.J., and Trayer, I.P. (1976) Purification and properties of skeletal muscle hexokinase. *FEBS Lett*. **62**, 215-219
13. Ureta, T. (1982) The comparative isozymology of vertebrate hexokinases. *Comp. Biochem. Physiol*. **71B**, 549-555
14. Manning, T.A., and Wilson, J.E. (1984) Inhibition of brain hexokinase by a multisubstrate analog results from binding to a discrete regulatory site. *Biochem. Biophys. Res. Commun.* **118**, 90-96
15. Irwin, D.M., and Tan, H. (2008) Molecular evolution of the vertebrate hexokinase gene family: Identification of a conserved fifth vertebrate hexokinase gene. *Comp. Biochem. Physiol. Part D Genomics Proteomics.* **3**, 96-107

16. Tsai, H.J. and Wilson, J.E. (1996) Functional organization of mammalian hexokinases: both N- and C-terminal halves of the rat type II isozyme possess catalytic sites. *Arch. Biochem. Biophys.* **329**, 17-23

17. White, T.K., and Wilson, J.E. (1989) Isolation and characterization of the discrete N- and C-terminal halves of rat brain hexokinase: retention of full catalytic activity in the isolated C-terminal half. *Arch. Biochem. Biophys*. **274**, 375-393

18. Arora, K.K., Filburn, C.R., and Pedersen, P.L. (1993) Structure/function relationships in hexokinase. Site-directed mutational analyses and characterization of overexpressed fragments implicate different functions for the N- and C-terminal halves of the enzyme. *J. Biol. Chem*. **266**, 5359-5362

19. Wilson, J.E. (2003) Isozymes of mammalian hexokinase: structure, subcellular localization and metabolic function. *J. Exp. Biol.* **206**, 2049-2057

20. Palma, F., Agostini, D., Polidori, E., and Stocchi, V. (2002) The overexpressed hexahistidine-tagged human hexokinasetype III is inhibited by D-glucose. *Prep. Biochem. Biotechnol.* **32**, 393-403

21. Pedersen, P.L., Mathupala, S., Rempel, A., Geschwind, J.F., and Ko, Y.H. (2002) Mitochondrial bound type II hexokinase: a key player in the growth and survival of many cancers and an ideal prospect for therapeutic intervention. *Biochim. Biophys. Acta*. **1555**, 14-20

22. Bryson, J.M., Coy, P.E., Gottlob, K., Hay, N., and Robey, R.B. (2002) Increased hexokinase activity, of either ectopic or endogenous origin, protects renal epithelial cells against acute oxidant-induced cell death. *J. Biol. Chem.* **277**, 11392-11400

23. Southworth, R., Davey, K.A., Warley, A., and Garlick, P.B. (2007) A reevaluation of the roles of hexokinase I and II in the heart. *Am. J. Physiol. Heart Circ. Physiol*. **292**, H378-386

24. de Vooght, K.M., van Solinge, W.W., van Wesel, A.C., Kersting, S., and van Wijk, R. (2009) First mutation in the red blood cell-specific promoter of hexokinase combined with a novel missense mutation causes hexokinase deficiency and mild chronic hemolysis. *Haematologica*. **94**, 1203-1210

25. Xie, G.C., and Wilson, J.E. (1988) Rat brain hexokinase: the hydrophobic N-terminus of the mitochondrially bound enzyme is inserted in the lipid bilayer. *Arch. Biochem. Biophys*. **267**, 803-810

26. Beutner, G., Rück, A., Riede, B., and Brdiczka, D. (1998) Complexes between porin, hexokinase, mitochondrial creatine kinase and adenylate translocator display properties of the permeability transition pore. Implication for regulation of permeability transition by the kinases. *Biochim. Biophys. Acta*. **1368**, 7-18

27. Gelb, B.D, Adams, V, Jones, S.N, Griffin, L.D, MacGregor, G.R, and McCabe, E.R. (1992) Targeting of hexokinase 1 to liver and hepatoma mitochondria. *Proc. Natl. Acad. Sci. U.S.A.* **89**, 202-206

28. Sun, L., Shukair, S., Naik, T.J., Moazed, F., and Ardehali, H. (2008) Glucose phosphorylation and mitochondrial binding are required for the protective effects of hexokinases I and II. *Mol. Cell Biol*. **28**, 1007-1017

29. Xie, G., and Wilson, J.E. (1990) Tetrameric structure of mitochondrially bound rat brain hexokinase: a crosslinking study. *Arch. Biochem. Biophys*. **276**, 285-293

30. Wicker, U., Bücheler, K., Gellerich, F.N., Wagner, M., Kapischke, M., and Brdiczka, D. (1993) Effect of macromolecules on the structure of the mitochondrial inter-membrane space and the regulation of hexokinase. *Biochim. Biophys. Acta*. **1142**, 228-239

31. Aflalo, C., and Azoulay, H. (1998) Binding of rat brain hexokinase to recombinant yeast mitochondria: effect of environmental factors and the source of porin. *J. Bioenerg. Biomembr*. **30**, 245-255

32. Rosano, C., Sabini, E., Rizzi, M., Deriu, D., Murshudov, G., Bianchi, M., Serafini, G., Magnani, M., and Bolognesi, M. (1999) Binding of non-catalytic ATP to human hexokinase I highlights the structural components for enzyme-membrane association control. *Structure*. **7**, 1427-1437

33. Rose, I.A., and Warms, J.V. (1967) Mitochondrial hexokinase. Release, rebinding, and location. *J. Biol. Chem*. **242**, 1635-1645

34. Skaff, D.A., Kim, C.S., Tsai, H.J., Honzatko, R.B., and Fromm, H.J. (2005) Glucose 6-phosphate release of wild-type and mutant human brain hexokinases from mitochondria. *J. Biol. Chem*. **280**, 38403-38409

35. Aleshin, A.E., Malfois, M., Liu, X., Kim, C.S., Fromm, H.J., Honzatko, R.B., Koch, M.H., and Svergun, D.I. (1999) Nonaggregating mutant of recombinant human hexokinase I exhibits wild-type kinetics and rod-like conformations in solution. *Biochemistry*. **38**, 8359-8366

36. Aleshin, A.E., Zeng, C., Bartunik, H.D., Fromm, H.J., and Honzatko, R.B. (1998) Regulation of Hexokinase I: Crystal Structure of Recombinant Human Brain Hexokinase Complexed with Glucose and Phosphate. *J. Mol. Biol*. **282**, 345-357

37. Aleshin, A.E., Zeng, C., Bourenkov, G.P., Bartunik, H.D., Fromm, H.J., and Honzatko, R.B. (1998) The mechanism of regulation of hexokinase: new insights from the crystal structure of recombinant human brain hexokinase complexed with glucose and glucose-6-phosphate. *Structure.* **6**, 39-50

38. Mulichak, A.M., Wilson, J.E., Padmanabhan, K., and Garavito, R.M. (1998) The structure of mammalian hexokinase-1. *Nat. Struct. Biol*. **5**, 555-560

39. Aleshin, A.E., Fromm, H.J., and Honzatko, R.B. (1998) Multiple crystal forms of hexokinase I: new insights regarding conformational dynamics, subunit interactions, and membrane association. *FEBS Lett*. **434**, 42-46

40. Aleshin, A.E., Kirby, C., Liu, X., Bourenkov, G.P., Bartunik H.D., Fromm, H.J., and Honzatko, R.B. (2000) Crystal structures of mutant monomeric hexokinase I reveal multiple ADP binding sites and conformational changes relevant to allosteric regulation. *J. Mol. Biol*. **296**, 1001-1015

41. Smith, A.D., and Wilson, J.E. (1991) Effect of ligand binding on the tryptic digestion pattern of rat brain hexokinase: relationship of ligand-induced conformational changes to catalytic and regulatory functions. *Arch. Biochem. Biophys*. **291**, 59-68

42. White, T.K., Kim, J.Y., and Wilson, J.E. (1990) Differential scanning calorimetric study of rat brain hexokinase: domain structure and stability. *Arch. Biochem. Biophys*. **276**, 510-517

43. Ellison, W.R., Lueck, J.D., and Fromm, H.J. (1974) Studies on the kinetics and mechanism of orthophosphate activation of bovine brain hexokinase. *Biochem. Biophys. Res. Commun*. **57**, 1214-1220

44. Ellison, W.R., Lueck, J.D., and Fromm, H.J. (1975) Studies on the mechanism of orthophosphate regulation of bovine brain hexokinase. *J. Biol. Chem*. **250**, 1864-1871

45. Chou, A.C., and Wilson, J.E. (1974) Rat brain hexokinase: glucose and glucose-6-phosphate binding sites and C-terminal amino acid of the purified enzyme. *Arch. Biochem. Biophys.* **165**, 628-633

46. Fang, T.Y., Alechina, O., Aleshin, A.E., Fromm, H.J., and Honzatko, R.B. (1998) Identification of a Phosphate Regulatory Site and a Low Affinity Binding Site for Glucose 6-Phosphate in the N-terminal Half of Human Brain Hexokinase. *J. Biol. Chem*. **273**, 19548-19553

47. Purich, D.L., and Fromm, H.J. (1971) The kinetics and regulation of rat brain hexokinase. *J. Biol. Chem*. **246**, 3456-3463

48. Zeng, C., and Fromm, H.J. (1995) Active site residues of human brain hexokinase as studied by site-specific mutagenesis. *J. Biol. Chem*. **270**, 10509-10513

49. White, T.K., and Wilson, J.E. (1987) Rat brain hexokinase: location of the allosteric regulatory site in a structural domain at the N-terminus of the enzyme. *Arch. Biochem. Biophys*. **259**, 402-411

50. Liu, X., Kim, C.S., Kurbanov, F.T., Honzatko, R.B., and Fromm, H.J. (1999) Dual Mechanisms for Glucose 6-Phosphate Inhibition of Human Brain Hexokinase. *J. Biol. Chem.* **274**, 31155-31159

Chapter II. Inhibitor Sites of Unequal Affinity Linked by Binding Synergism in Mutant Forms of Recombinant Human Hexokinase Type-I

A paper to be submitted to the Journal of Biological Chemistry

Lu Shen, Yang Gao and Richard B. Honzatko

Department of Biochemistry, Biophysics and Molecular Biology,

Iowa State University, Ames IA 50011

Abstract

Hexokinase I (HKI) is the pacemaker of glycolysis in the red bold cell, being subject to potent feedback inhibition by its product glucose 6-phosphate (Glc-6-P) and the relief of that inhibition by inorganic phosphate (P_i). Mechanisms of inhibition and relief have been subjects of controversy, as no model adequately accounts for all observations. Presented here are crystalline complexes and molecular dynamics simulations of recombinant human HKI with Glc-6-P, 1,5-anhydro-D-glucitol 6-phosphate (1,5-anhydroGlc-6-P), 2-deoxy-β-D-glucose 6-phosphate (2-deoxyGlc-6-P) and β-D-mannose 6-phosphate (Man-6-P). Ligand interactions at each half of HKI are comparable in crystal structures, but in simulations, 2-deoxyGlc-6-P and Man-6-P lose hydrogen bonds at the C-terminal half, consistent with early stages of ligand dissociation, and 1,5-anhydroGlc-6-P, relative to Glc-6-P, stabilizes slightly open conformations of N- and C-terminal halves. The kinetics of D413N and/or D861N enzymes (D413 and D861 interact with 1-OH groups of Glc-6-P) are consistent only with synergistic binding of two molecules of 1,5-anhydroGlc-6-P to sites with unequal constants of dissociation. A dynamics simulation of the D413N HKI demonstrates global conformational change that affects Glc-6-P recognition at N- and C-terminal halves. Studies here clarify the mechanism of action of 1,5-anhydroGlc-6-P, but also indicate a differential response of HKI to Glc-6-P and 1,5-anhydroGlc-6-P.

Introduction

Hexokinase (ATP: D-hexose 6-phosphotransferase, EC2.7.1.1) catalyzes the initial step of glycolysis, the phosphorylation of 6-hydroxyl group of glucose (Glc) using $[ATP\text{-}Mg]^{2-}$ as the phosphoryl donor[1-3]. Four isozymes of hexokinase have been identified in mammalian tissues[4]. Type I, II and III hexokinase isozymes have molecular weights of 100 KDa, and share 70% sequence identity[5]. N- and C-terminal halves of isozymes I–III have ~50% sequence identity[5], putatively a result of the duplication and fusion of a gene of a primordial hexokinase[6-9]. Hexokinase IV (glucokinase) and yeast hexokinase isoforms A and B have molecular weights of 50 KDa, and exhibit significant sequence similarity to both halves of isozymes I–III[5].

Despite sequence and structural similarities, isozymes I-III differ significantly in functional properties. Both halves of hexokinase II possess catalytic activity[10], whereas the N-terminal halves of hexokinase I and III are inactive[5, 11-12]. The reaction product glucose 6-phosphate (Glc-6-P) potently inhibits isozymes I-III (but not isoform IV) at physiological concentrations[5]. Inorganic phosphate (P_i) is a weak inhibitor of hexokinase II and III[5]; however, P_i antagonizes the inhibition of hexokinase I by 1,5-anhydroglucitol 6-phosphate (1,5-anhydroGlc-6-P, an analog of Glc-6-P used in kinetics) at low (micromolar) concentrations, whereas, at millimolar concentrations it inhibits catalysis competitively with ATP[5].

In crystal structures, Glc-6-P binds to both halves of HKI[13-15]. Proteolytic cleavage of HKI produces an active C-terminal half (mini-HKI) that is inhibited potently by 1,5-anhydroGlc-6-P with no P_i-relief[12, 16]. The N-terminal half of HKI is inactive, but it still binds Glc-6-P tightly[11-12]. Mutational studies have shown that 1,5-anhydroGlc-6-P inhibits HKI potently at either of two binding sites[17-18]. Only mutations at both Glc-6-P binding sites eliminate 1,5-anhydroGlc-6-P inhibition[18]. Data from equilibrium binding and kinetics experiments, however, indicate only one molecule of Glc-6-P binds to HKI with high-affinity, suggesting the dominance of one inhibitory mechanism or the possibility of negative cooperativity in Glc-6-P binding[18-22]. Crystal structures and experiments in directed mutations, kinetics and equilibrium binding have not identified the site of high

binding affinity for Glc-6-P.

As early as 1954, Crane and Sols recognized the significance of the 2-hydroxyl group in the binding of 6-phosphorylated hexoses to an inhibitory site of HKI. Millimolar levels of 2-deoxyGlc-6-P and Man-6-P are ineffective in inhibiting HKI activity[23]. Magnani *et al.* reported that the K_Is for 2-deoxyGlc-6-P and Man-6-P are at least 20-fold higher than that of Glc-6-P[24]. In crystal structures, the 2-OH group of Glc-6-P hydrogen bonds with Ser449/897 and Asp84/532 (N-half/C-half) and the 1-OH group with Asp413/861[13]. Yet 1,5-anhydroGlc-6-P has potent inhibition without a 1-OH group and 2-deoxyGlc-6-P is without potent inhibition. The accepted conclusion from these observations: the 1-OH group is unimportant, but the 2-OH group is critical to inhibition.

Structures of crystalline complexes of HKI with Glc-6-P, 1,5-anhydroGlc-6-P, 2-deoxyGlc-6-P, and Man-6-P reported here indicate all phosphoryl ligands bind with lower thermal parameters to the C-terminal half relative to the N-terminal half. Molecular dynamics simulations indicate stable binding of phosphoryl ligands to the N-terminal half (consistent with interactions observed in crystal structures); however, 1,5-anhydroGlc-6-P, 2-deoxy-Glc-6-P, and Man-6-P exhibit binding modes to the C-terminal half which are not consistent with crystal structures. In fact, a significant binding mode for 1,5-anhydroGlc-6-P appears in a slightly open C-terminal half (a conformation not observed in crystal structures) in which its 2-OH group interacts with Asp861 (residue that interacts with the 1-OH of Glc-6-P in crystal structures). Mutations of Asp861 and/or Asp413 result in stoichiometric dissociation constants that require binding synergism between two molecules of 1,5-anhydroGlc-6-P. The behavior of the mutant forms of HKI examined here cannot be reconciled with a model that couples two sites of nearly equal, high-binding affinity by a mechanism of negative cooperativity[18], but instead support the synergistic binding of two molecules of 1,5-anhydroGlc-6-P to sites of unequal affinity. In such a model, the binding of P_i to the high-affinity site would elevate the dissociation constant of the low-affinity site, and hence eliminate inhibition.

Materials and methods

Materials— A full-length cDNA of human hexokinase I, cloned into vector pET-11a was available from previous studies[16, 25-26]. Oligonucleotides came from IDT-DNA. DNA sequencing was done by the Iowa State University DNA Sequncing and Synthesis Facility. *Escherichia coli* strain DH5a and BL21 were from Invitrogen. DNaseI, phenylmethanesulfonyl fluoride (PMSF), leupeptin, bovine serum albumin (BSA), ATP, NADP, ampicillin, glucose 6-phosphate, mannose 6-phosphate and 2-deoxy-D-glucose 6-phosphate were from Sigma. 1,5-Anhydro-D-sorbitol was from Toronto Research Chemicals. Isopropyl-β-D-thiogalactopyranoside (IPTG) was from Bio-World. DEAE sepharose CL-6B and CHT ceramic hydroxyapatite (HA) Type II were from Bio-Rad. DEAE-5PW HPLC media was from Tosohaas. Glusoe-6-phosphate dehydrogenase (G6PDH) was from Roche. 2'-(or-3')-*O*-(2,4,6-Trinitrophenyl)-adenosine 5'-diphosphate (TNP-ADP) was from Invitrogen.

Construction, Expression and Purification of Wild-type and Mutant Hexokinase I— The oligonucleotide primers for directed mutations are as follows: 5’-CG-GTT-GGT-GTC-AAC-GGA-TCT-CTT-TAC-AAG-ACG-3’ for D413N and 5’-CT-GTG-GGA-GTG-AAC-GGG-ACA-CTC-TAC-AAG-C-3’ for D861N, where the altered codon is underlined.

A 200 ml culture of the transformed *Escherichia coli* BL21 was grown overnight at 37 ºC in LB medium (33mg/L ampicillin) and then 1.5% cell were transferred to 9.6L LB medium (33mg/L ampicillin). The culture was grown at 300 rpm and 37 ºC to A_{600}=1.0. The temperature then was reduced to 16 ºC, isopropyl-β-D-thiogalactopyranoside (IPTG) was added to a final concentration of 0.5 mM and the culture was grown at 200 rpm for 20-22 hr. at 16 ºC. The cells were re-suspended in 25 mM KP_i (pH 7.5), 5 mM glucose, 3 mM $MgCl_2$, 1 mM dithiothreitol (DTT), 1 mM phenylmethanesulfonyl fluoride (PMSF), 50 μg/ml DNaseI and 5 μg/ml leupeptin. The cells were broken by sonication and then centrifuged (33,000*x*g, 1 hr.). The supernatant fluid was adjusted to pH 7.5 and loaded onto a DEAE-anion exchange column, using 25 mM KP_i, 5 mM glucose, 1 mM dithiothreitol DTT (pH 7.5), with a gradient of 0–400 mM NaCl. The fractions containing HKI activity were pooled,

concentrated and dialyzed against 50 mM KP_i (pH 7.0), 5 mM glucose, 1 mM dithiothreitol (DTT) and loaded onto a ceramics hydroxyapatite column with a gradient of 0.05–1 M KP_i (pH 7.0). HKI was collected and dialyzed against 25 mM KP_i, 5 mM glucose, 1 mM dithiothreitol (DTT) (pH 7.5), and further purified by DEAE-5PW HPLC chromatography with a gradient of 0–500 mM NaCl. The pure protein was identified by sodium dodecylsulfate polyacrylamide gel electrophoresis (SDS-PAGE)[27]. Protein concentration was determined by the method of Bradford with BSA as a standard[28].

TNP-ADP Binding and Displacement— Wild-type HKI was prepared in a buffer of 50 mM Tris (pH 7.5) and 1mM Glc. In all experiment involving TNP-ADP binding and displacement, the enzyme concentration is 2 μM. In binding experiments, TNP-ADP concentrations range from 0–10 μM, whereas in displacement experiments, the TNP-ADP concentration is 3.66 μM. Fluorescence measurements were made at room temperature using a 1-cm^2 quartz cuvette on a SLM Amico 8000 fluorometer with entrance/exit slits of 4 mm. The excitation wavelength is 409 nm and emission scans are from 530 to 560 nm. Fluorescence intensity (average of three scans for each datum) was integrated over 530–560 nm using 30 increments and an accumulation time of 1 sec per increment. Fluorescence data were analyzed by the method described by Faller[29-30] with modifications as provided in the next paragraph.

The observed fluorescence from a mixture of TNP-ADP and HKI comes from free TNP-ADP, TNP-ADP bound to HKI and HKI itself:

$$F_{obs} = F_{free} + F_{bound} + F_{protein}$$

$$F_{free} = a + b[L] - c[L]^2$$

$$F_{bound} = Gb([L_0] - [L])$$

$$F_{obs} = a + b[L] - c[L]^2 + Gm([L_0] - [L]) + S \qquad \text{Eqn.1}$$

$F_{protein}$ is an adjustable parameter (S) that accounts for background fluorescence due to the protein sample. As HKI has no native fluorophore sensitive to an excitation wavelength of 409 nm the parameter S should be a small value and nearly constant over the experiment presented here. $[L_o]$ and $[L]$ represent the total and free TNP-ADP concentrations,

respectively. G is a fluorescence enhancement factor of the bound fluorescent ligand relative to the free state. Parameters *a*, *b* and *c* are determined by fitting fluorescence versus $[L]$ in the absence of protein, the data for which comes from the addition of TNP-ADP to buffer. The same buffer is used for the binding and displacement experiments.

A single binding-site model adequately accounts for the F_{obs} of the bound state as well as the displacement of TNP-ADP by phosphoryl ligand Glc-6-P, or 2-deoxyGlc-6-P or Man-6-P:

$$P + L = PL \quad , \qquad K_L = \frac{[P][L]}{[PL]}$$

$$P + A = PA \quad , \qquad K_A = \frac{[P][A]}{[PA]}$$

$$[L_o] = [L] + [PL];\ [A_o] = [A] + [PA];\ [P_o] = [P] + [PL] + [PA];$$

$[A_o]$ and $[A]$ are total and free phosphoryl ligand concentrations, respectively; $[P_o]$ and $[P]$ are total and free protein concentrations, respectively. K_L and K_A are constants for the dissociation of TNP-ADP and phosphoryl ligand from protein, respectively. The equilibrium and mass conservation relationships for $[L_o]$ (total fluorophore concentration), $[A_o]$ (total concentration of displacing ligand) and $[P_o]$ (total concentration of protein) lead to a third-order equation in the concentration of free protein [P]. Substitution of the equilibrium relationships into mass conservation relationships for protein leads to a third-order equation in the concentration of free protein [P]. For circumstances here, $K_A >>$ [P], allowing an approximation that reduces the third-order equation to one of second order:

$$\left(1 + \frac{[A_0]}{K_A}\right)[P]^2 + \left(\frac{K_A - [P_0] + [A_0]K_L}{K_L + [L_0]}\right)[P]^2 - P_0 K_L = 0$$

The physical root of this quadratic relationship is the concentration of free protein, and determines the concentration of free fluorophore $[L]=[L_o]K_L/(K_L+[P])$ at a given total concentration of fluorophore, $[L_o]$. GraFit software optimizes the fit of the observed fluorescence to the right-hand side of Eqn. 1 at fixed $[P_o]$ and varying $[L_o]$ and $[A_o]$ by adjusting parameters K_A, K_L, G and $F_{protein}$[31].

Hexokinase Kinetics— Hexokinase activity was determined by the glucose-6-phosphate

dehydrogenase (G6PDH, E.C.1.1.1.49) coupled spectrometric assay[26]. Commercial G6PDH, as precipitate from ammonium sulfate, was dialyzed against 80 mM Tris (pH 8.0) extensively to remove sulfate, which at millimolar concentrations causes relief of 1,5-anhydroGlc-6-P inhibition in the manner of P_i. 1,5-AnhydroGlc-6-P, which is not a substrate for G6PDH, is a surrogate for Glc-6-P in inhibition kinetics of HKI. The dicyclohexylamine salt of 1,5-anhydroGlc-6-P was prepared as described by Ferrari and Crane[32] and its concentration determined by the method of Drueckes *et al.*[33]. The concentration of hexokinase in kinetics assays was 1.2–2.0 μg/ml and the assay volume was 1 ml. The assay buffer was 80 mM Tris (pH 8.0), 0.4 mM NADP, 3 mM $MgCl_2$ and 2 mM Glc.

Crystal Preparation— All the crystals were grown by the hanging drop method. Wild-type or mutant forms of HKI stored in 25 mM KP_i (pH 7.5), 1 mM glucose, 1mM dithiothreitol (DTT) was concentrated to 20–30 mg/ml in 50-kDa cut-off centrifugational filtration tube, then subject to 12–15 cycles of wash at 4 ºC with 2–3 volumes of a ligand buffer. The ligand buffers are 40 mM 1,5-anhydroGlc-6-P, 40 mM 2-deoxyGlc-6-P, 40 mM Man-6-P or 20 mM Glc-6-P, all pH 7.5 with 1 mM Glc. 3 μl of the resulting solutions, containing 15–20 mg/ml protein and in the ligand buffer, was combined with an equal volume of precipitant solution containing 4.5-6.5% (w/v) polyethylene glycol 4000 or polyethylene glycol 8000, 0.1 M sodium acetate and 0.1 M sodium citrate, pH 6.0. The drops equilibrated against 0.5 ml of the precipitant solution. Prismatic needles of length 0.5–0.8 mm and width 0.2–0.3 mm grew in two to three weeks at 4 ºC. Crystals were transferred sequentially to a solution containing 1:1 ratio of the corresponding precipitant solution and 20% glycerol, and then to 1:1 ratio of the corresponding precipitant solution and 40% glycerol before flash freezing in liquid nitrogen.

X-ray Diffraction Data— X-ray diffraction data for Glc-6-P, 2-deoxyGlc-6-P and Man-6-P were collected at ALS beamline 4.2.2. Diffraction data were processed with d*trek[34]. X-ray diffraction data for 1,5-anhydroGlc-6-P and D413N/Glc-6-P were collected at APS SBC-sec19. Diffraction data were processed with HKL-3000[35].

Structure Determination, Model Building and Refinement— All crystals has unit cell parameters isomorphous to those of the $P2_1$ crystal form published previously[13-15, 36]. In these crystal forms, HKI is a homodimer consistent with the results of ultracentrifugation studies[37], which reports the dimer prevails at concentrations of protein above 1 mg/ml in the presence of saturating concentrations of Glc and Glc-6-P. Crystal structures were solved by molecular replacement using the HKI•Glc-6-P•Glc complex (PDB entry 1HKB)[13], less ligands and water molecules. The program AMoRe or Molrep from CCP4 suite was used in calculation of rotation and translation functions, based on data to 3 Å resolution[38-39]. The program RefMac from CCP4 suite was used to refine the structures[40]. Further refinement employed CNS with hydrogen bond restraints[41]. Manual adjustments in the conformation of specific residues employed the program XTALVIEW[42].

Molecular Dynamics Simulations— NAMD package with the CHARMM 27 force field was used for molecular dynamics simulations on hexokinase I[43-44]. The initial coordinates came from chain A of each of the crystalline complexes. TIP3P water molecules were added into a rectangular water box surrounding the single molecule of HKI with a buffering distance of 15 Å[45]. To balance the net charge of system, sodium and chloride ions were added. Periodic boundary conditions were applied and the Particle mesh Ewald algorithm was used for the calculation of long-range electrostatic interactions[46]. Non-bonded *Van der Waals* interactions were applied with a cutoff of 12 Å. The integration time step was 2.0 fs. All models were energy-minimized for 100 ps and gradually heated to 300 K to relax unfavorable contacts (if any), followed by another 100 ps simulation to equilibrate the system. Finally, simulations of 10 ns were carried out at constant pressure and temperature (1.01325 bar and 300 K).

Principal Component Analysis (PCA)— Principal component analysis was applied to extract functionally important motions from simulations. Rigid-body translations and rotations of the tetramer were removed before PCA by aligning trajectory structures onto the starting structure. Principle components were calculated by decomposing the covariance matrix *C* which was calculated from the molecular dynamics trajectory as:

$$C_{ij} = \left\langle \left(r_i - \left\langle r_i \right\rangle\right) \bullet \left(r_j - \left\langle r_j \right\rangle\right) \right\rangle,$$

where $i,j = 1,...3N$, N is the total number of C_α atoms in the structure, r is the Cartesian coordinates of i^{th} C_α atom, and the angle brackets denote an average over the entire trajectory. The Carma package was used in PCA analysis and VMD was used to visualize the principal motions[47,48].

Results

TNP-ADP binding and displacement experiment— Two assays have been used in studies of kinetics of HKI. One couples Glc-6-P formation through G6PDH to the formation of NADPH and the other couples ADP formation through pyruvate kinase (E.C.2.7.1.40) and lactate dehydrogenase (E.C.1.1.1.28)[26, 49]. The latter assay, because of the accumulation of Glc-6-P, would provide nonlinear progress curves, complicating the determination of initial velocities. The assay which couples to Glc-6-P formation, however, limits the choice of inhibitors to 1,5-anhydroGlc-6-P; as 2-deoxyGlc-6-P and Man-6-P, are substrates of G6PDH, albeit poor ones. Here we measure binding affinities of phosphoryl ligands through the displacement of TNP-ADP for HKI. TNP-ADP is a linear competitive inhibitor with respect to [ATP-Mg]$^{2-}$[30]. TNP-ADP binds with high-affinity to the single site at the C-terminal half of hexokinase I, and the binding of TNP-ADP and ATP are mutually exclusive[30]. The K_L and G for TNP-ADP are 0.47 ± 0.04 μM and 5.51 ± 0.06, respectively (Figure 2). Glc-6-P displaces TNP-ADP from wild-type HKI with a K_A of 0.51 ± 0.02 μM, whereas K_A values for 2-deoxyGlc-6-P and Man-6-P are at least 100 fold higher (Figure 2). All the fluorescence enhancement parameters (G) are similar. Results here are consistent with those of Crane and Sols[23] and Magnani *et al.*[24], indicating weak inhibition of HKI due to 2-deoxy-Glc-6-P and Man-6-P.

Kinetics of wild-type, D413N, D861N and D413/861N hexokinases— Asp413 and Asp861 hydrogen bond with the 1-OH group of Glc-6-P at the N- and C-terminal halves, respectively. Mutations here were not expected to have a substantial effect on the inhibition of HKI by 1,5-anhydroGlc-6-P, as this molecule lacks the 1-OH group. The biggest effect is the 90% reduction in k_{cat} due to the mutation of Asp861 to asparagines (Table I). Conceivably Asp861 could play a role in the localization of Mg^{2+} in the active site for catalysis. Of more

relevance to the study here, however, are effects on nonlinear competitive inhibition by 1,5-anhydroGlc-6-P with respect to $[ATP\text{-}Mg]^{2-}$. The dissociation constant for the first inhibitor molecule from hexokinase K_I increases slightly, whereas the dissociation constant for the second inhibitor molecule K_{II} decreases (Table I). P_i-relief of 1,5-anhydroGlc-6-P appears comparable for mutant and wild-type enzymes.

Crystalline complexes of wild-type or D413N HKI with different phosphoryl ligands— For the most part, structures of wild-type HKI co-crystallized with Glc (1 mM) and Glc-6-P, 1,5-anhydroGlc-6-P, 2-deoxyGlc-P or Man-6-P are isomorphous and are of comparable resolution, the exception being the complex of 1,5-anhydroGlc-6-P, which is of lower resolution and higher average thermal parameter (Table II). The same crystal forms grew from buffers that contained only the 6-phosphoryl ligand (data not shown), but retained Glc and are in all respects identical to the structures reported in Table II. HKI in crystallization experiments came from a storage buffer of 25 mM KP_i (pH 7.5) and 1 mM Glc. Evidently, multiple exchanges of HKI with buffers that contained 6-phosphoryl ligands without glucose failed to remove enzyme-bound glucose, as has been reported by other investigators[51].

Crystalline complexes of Table II are isomorphous to Glc/Glc-6-P complex previously reported[13]. Superimpositions of a single chains from each structure give root-mean-square deviations of less than 0.5 Å. Each asymmetric unit contains a homodimer with observable electron density for residues 16–914. The polypeptide chain crosses three times between large and small domains; residues 16–74 and 210–447 belong to the large domain and residues 75–209 and 448–466 to the small domain of the N-terminal half and residues 467–522 and 658–895 belong to the large domain and residues 523–657 and 896–914 to the small domain of C-terminal half. The two halves of each subunit contain molecules of Glc and 6-phosphoryl ligand bound to a crevice between large and small domains. A common trend for all structures is a higher B-parameter for ligands bound to the N-terminal half relative to the C-terminal half. The systematic difference in B-parameter is consistent with the appearance of systematically weaker electron density at the N- relative to the C-terminal half.

Difference density maps generated from Fourier coefficients $(F_{obs} - F_{calc})e^{i\alpha_{calc}}$

indicate the presence of both α- and β-anomers of Glc (Figure 3). If refinement employs the β-anomer or α-anomer of Glc, positive difference density appears at the α-anomer or β-anomer position of the 1-OH group, respectively. The 1-OH group of β-D-Glc forms hydrogen bonds with Glu294 (N-terminal half) or Glu742 (C-terminal half) and the 1-OH group of α-D-Glc forms hydrogen bonds with Thr234 (N-terminal half) or Ser682 (C-terminal half). Indeed, both anomers are substrates for HKI with comparable values for K_m and V_{max}[5].

Difference electron difference density for the anomer alternative to the one used in refinement for Glc indicates the crystallographic data can distinguish 1,5-anhydroGlc-6-P, 2-deoxyGlc-6-P and Man-6-P from Glc-6-P (Figure 4). Refinement was repeated with Glc-6-P in place of the actual ligand used in co-crystallization experiments. In each instance negative and/or positive difference density appeared at the expected locations, indicating the that the electron density at binding sites for the 1,5-anhydroGlc-6-P, 2-deoxyGlc-6-P and Man-6-P was not due to Glc-6-P (as could happen if a small impurity of Glc-6-P were present in any of the samples).

Differences in hydrogen bonding interactions between 6-phsophoryl ligands and the N-and C-terminal halves of HKI (Table III) are localized to the altered functional group of the ligand. The absence of the 1-OH group in 1,5-anhydroGlc-6-P eliminates hydrogen bonds with Asp413 (N-terminal half) and Asp861 (C-terminal half) without noticeable effects on hydrogen bonds between protein and ligand involving the other hydroxyl groups or the 6-phosphoryl group. The absent 2-OH group in complexes 2-deoxyGlc-6-P eliminates hydrogen bonds with Asp84 and Ser447 (N-terminal half) and Asp532 and Ser897 (C-terminal half). The re-positioning of the 2-OH group in the Man-6-P complex eliminates hydrogen bonds with Asp84 (N-terminal half) and Asp532 (C-terminal half) without the loss of hydrogen bonds to Ser447 (N-terminal half) and Ser897 (C-terminal half). In all ligated states, the subunits of HKI remain the same in crystal structures, giving no clear indication of the relative importance of hydroxyl groups in the inhibition of HKI.

MD Simulations of Wild-type and D413N HKI— All simulations presented here begin with the equilibration of a crystallographic structure of a ligated complex of HKI.

Root-mean-square deviations (RMSD) of 6-phosphoryl ligands at the C-terminal half are higher than those at the N-terminal half (Figure 5), and for simulations of 1,5-anhydroGlc-6-P, 2-deoxyGlc-6-P and Man-6-P, the differences are substantial. Difference in RMSD values are due primarily to a transition of the C-terminal half to a more open conformation relative to that present in crystal structures; however, for the Glc-6-P simulation, the N-terminal half moves toward a more closed conformation relative to that observed in crystal structures.

Simulations of HKI with Glc-6-P reveal similar interactions at the N- and C-terminal halves except for the 6-phosphoryl group (Tables IV&V). Thr536 forms hydrogen bonds with the 6-phosphoryl group of Glc-6-P in the crystal structure, but hydrogen bonds exist in only 4% of the frames over the simulation. In contrast, hydrogen bonds between Ser88 and the 6-phosphoryl group of Glc-6-P are present at levels of 100%. The simulation implies a less important role for the 6-phosphoryl group in Glc-6-P binding to the C- relative to the N-terminal half, whereas crystallographic results indicate no discernible difference (Table III). Interestingly, the C-terminal half in its open conformation binds phosphate through hydrogen bonds involving Thr680[50], a residue that in simulations plays a significant role in the binding of the 6-phosphoryl group of Glc-6-P.

1,5-Anhydro-Glc-6-P has two binding modes to the C-terminal half in simulations (Figures 6&7). Initially, 1,5-anhydroGlc-6-P binds like Glc-6-P save for one distinction: its 6-phosphoryl group forms hydrogen bonds with Thr536 (Table IV, Figure 7). At approximately the mid-point of the simulation the C-terminal half undergoes a transition, whereupon the 2-OH group of 1,5-anhydroGlc-6-P forms a hydrogen bond with Asp861 (a residue that interacts with the 1-OH group of Glc-6-P), while retaining hydrogen bonds with Thr536. Principal component analysis (Figure 6) reveals two clusters of conformations for the C-terminal half in the 1,5-anhydroGlc-6-P simulation, each differing from that of the C-terminal half in the Glc-6-P simulation. The two clusters in the 1,5-anhydroGlc-6-P simulation correlate with the two binding modes of the ligand. The alternative (non-Glc-6-P) binding mode appears in a C-terminal half with a more open conformation relative to the conformation of C-terminal half in the Glc-6-P simulation (Figure 7). In contrast, principal component analysis reveals single clusters for the N-terminal half ligated

by Glc-6-P or 1,5-anhydroGlc-6-P (Figure 6). Although the two ligands have comparable sets of hydrogen bonds (Table IV), the N-terminal half with 1,5-anhydroGlc-6-P is more open than that of the N-terminal half with Glc-6-P (Figure 8).

The effect of Glc-6-P on the N-terminal half (stabilization of a more closed conformation relative to the N-terminal half ligated with 1,5-anhydroGlc-6-P) is not observed in the simulation of D413N HKI ligated with Glc-6-P (Figure 8). The conformation of the N-terminal half of D413N HKI ligated by Glc-6-P is similar to that of wild-type N-terminal half ligated by 1,5-anhydroGlc-6-P. The D413N mutation could well have a global influence on the conformation of HKI (Figure 9). Small movements in the N-terminal half due to mutation cause big changes in the relative position of the N- and C-terminal halves. Most significantly, the 6-phosphoryl group of Glc-6-P at the C-terminal half establishes a full set of hydrogen bonds with Thr536 which are absent in the simulation of Glc-6-P with the wild-type enzyme (Table IV). The mutation D413N seemingly weakens Glc-6-P interactions at the N-terminal half, but strengthen interactions at the C-terminal half.

Man-6-P and 2-deoxyGlc-6-P appear as though each is dissociating from the C-terminal half as simulations progress (Figure 10). Initially, hydrogen bonds are present between the 6-phosphoryl group of each ligand and Thr536, but in simulations such interactions terminate due to the relative movement of small and large domains of the C-terminal half and the movement of the loop 533–588 (Figure 10). In addition, the interactions of the 1-OH group of 2-deoxyGlc-6-P with Asp861 end abruptly (Figure 10). The stable hydrogen bond involving the 2-OH group of Man-6-P with Asp861 is not unlike that of the 2-OH group of 1,5-anhydroGlc-6-P, the primary difference being the loss of hydrogen bonds between the 6-phosphoryl group of Man-6-P and Thr536 not observed in the case of 1,5-anhydroGlc-6-P.

The movements also result in the broken interactions between 3-OH group of Man-6-P and 2-deoxyGlc-6-P with Asp532 (Figure 10). In addition, the interactions between 2-OH group of Man-6-P and Asp532 disappear (Figure 10). Conceivably longer simulations might lead to further loss of ligand-protein hydrogen bonds at the C-terminal half. Man-6-P and 2-deoxyGlc-6-P retain stable interactions at the N-terminal half throughout

simulations (Tables IV, V & VI), with interactions dominated by 6-phosphoryl groups.

Discussion

Systematic differences in the thermal parameters and levels of electron density in the N- and C-terminal halves could be an artifact of packing contacts in the crystal. Simulations which do little more than relax the subunit in the absence of inter-subunit contacts, lead to a more open C-terminal half in general, and in the specific case of Glc-6-P ligation, a more closed N-terminal half than in crystal structures. The mildly acidic conditions of crystallization (pH 6.0) may also contribute to differences in crystal structures and simulations. At pH 6, phosphoryl ligands are predominantly monoanions, whereas at pH 7.5 (simulations) and pH 8.0 (conditions of assay) dianionic forms of phosphoryl ligands dominate. The N-terminal half binds P_i (as a dianion) with high affinity relative to the C-terminal half[50], and hence the level of protonation of the phosphoryl moiety may be critical to a high affinity interaction of the 6-phosphoryl group at the N-terminal half. Indeed, simulations clearly show favored binding of the 6-phosphoryl group of Glc-6-P to the N- relative to the C-terminal half (Table IV). Protonation of the 6-phosphoryl group then may disproportionately weaken the binding of Glc-6-P to the N-terminal half relative to the C-terminal half, contributing to effects observed in crystal structures.

Principal component analysis of simulations of wild-type HKI and D413N HKI reveal effects on Glc-6-P interactions distal and proximal to the site of mutation. For instance, simulations of D413N HKI with bound Glc-6-P exhibit enhanced interactions at the C-terminal half along with weakened interactions at the N-terminal half (Figures 8&9). Moreover, values of stoichiometric dissociation constants K_I and K_{II} require interactions between inhibitor binding sites at the N- and C-terminal halves for D413N, D861N and D413/861N forms of HKI (Table I). The requirement of interacting sites becomes clear when the stoichiometric model is recast as a site affinity model (Scheme I), recognizing four equilibriums and their constants of dissociation.

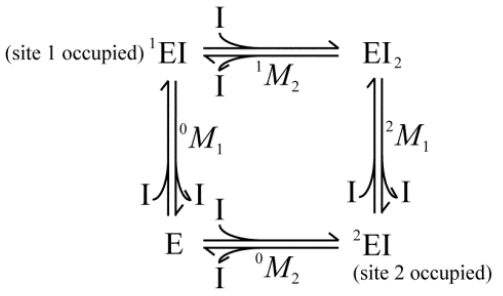

$$^0M_1 = \frac{[E][I]}{[^1EI]} \qquad ^0M_2 = \frac{[E][I]}{[^2EI]} \qquad ^2M_1 = \frac{[^2EI][I]}{[EI_2]} \qquad ^1M_2 = \frac{[^1EI][I]}{[EI_2]}$$

Site Affinity Model

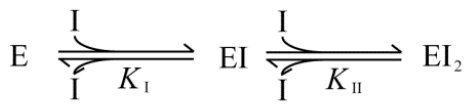

$$K_I = \frac{[E][I]}{[EI]} \qquad K_{II} = \frac{[EI][I]}{[EI_2]}$$

Stoichiometric Model

Scheme I

The known values of K_I and K_{II} do not uniquely determine values for site affinity constants; however, the definition of a site interaction parameter α allows a systematic exploration of allowable values for site dissociation constants given experimentally determined values of K_I and K_{II}. The relationships of Scheme I permit the determination of site affinity constants for an arbitrary value of α by way of Eqn. 2:

$$^0M_1 = \left. \alpha K_{II} - \sqrt{\alpha^2 K_{II}^2 - 4\alpha K_I K_{II}} \right/ 2$$

$$^0M_2 = \alpha K_{II} - {}^0M_1 \quad \text{and}$$

$$^2M_1 = {}^0M_1/\alpha$$

$$^1M_2 = {}^0M_2/\alpha \qquad \text{Eqn. 2}$$

Values of α greater (less) than unity represent positive (negative) cooperativity, whereas a value of unity represents independent binding sites. Values of K_I and K_{II} for the wild-type enzyme lead to physically acceptable site-dissociation constants for $0.35<\alpha<\infty$. At $\alpha = 0.35$,

the site dissociation constants are nearly equal and of low value (high affinity), and become progressively different as α increases (Table VII). The allowed range for D413N, D861N and D413/861N is $1.55<\alpha<\infty$. Site-dissociation constants must differ and ligand binding must be synergistic ($\alpha>1$) in order to reproduce observed values of K_I and K_{II}. In this model (synergistic binding to sites of unequal affinity), P_i-relief of 1,5-anhydroGlc-6-P occurs if P_i binds to the high-affinity site, which through the loss of synergism, causes the dissociation constant for the low affinity site to rise. Although The mutant enzymes here require synergistic binding of 1,5-anhydroGlc-6-P, the wild-type enzyme, on the basis of K_I and K_{II} values, is consistent with any model (antagonistic, independent, or synergistic inhibitory sites). The observation of a single high-affinity binding site for Glc-6-P[18-22] for wild-type HKI, however, is consistent only with a value of α less than unity.

The foregoing analysis does not fix the site of high-affinity interaction (N- or C-terminal half) for 1,5-anhydroGlc-6-P, and indeed the site of tight binding may change with mutation. Nonetheless results here favor tight-binding for 1,5-anhydroGlc-6-P at the N-terminal half. This assignment stems from the low root-mean-square-deviation (RMSD) for inhibitors bound to the N- relative to the C-terminal half (Figure 5), better recognition of the phosphoryl moiety at the N- relative to the C-terminal half as measured by hydrogen bonding persistence (Tables IV, V&VI), and the unimodal binding of 6-phosphoryl molecules at the N-terminal half (Figure 6). The C-terminal half in comparison has high root-mean-square-deviations for ligands (Figure 5), bimodal interactions involving 1,5-anhydroGlc-6-P (Figure 6), and a tendency to transition from a closed to partially open conformation (Figure 7). Binding synergism could arise from the tight-binding of a molecule of 1,5-anhydroGlc-6-P to the N-terminal half, forcing a partial opening of the C-terminal half, which in turn allows a second molecule of 1,5-anhydroGlc-6-P to bind in its alternative mode.

The mechanism of nonlinear competitive inhibition with respect to ATP exhibited by 1,5-anhydroGlc-6-P may also be a consequence of its alternative binding mode. Glc-6-P is a linear competitive inhibitor and has not exhibited an alternative binding mode, although in longer simulations alternative interactions could arise. Moreover, 1,5-anhydroGlc-6-P may not bind as tightly to the N-terminal half as Glc-6-P (Figure 8). Simulations of D413N HKI

with Glc-6-P and wild-type HKI with 1,5-anhydroGlc-6-P have similar effects on the conformation of the N-terminal half. The effects of mutation presumably weaken recognition of the 1-OH group of Glc-6-P, and cause K_I to increase and K_{II} to decrease. Arguably the proper recognition of the 1-OH group (as would be the case for wild-type HKI and Glc-6-P) should cause K_I to decrease and K_{II} to increase. Although the effects of Glc-6-P are not easily assayable by kinetics, the K_d for Glc-6-P in equilibrium dialysis experiments is less than 1 μM[21, 52] and in fluorescence titrations is 0.5 μM (Figure 2). Both values are significantly less than 20 μM (K_I of 1,5-anhydroGlc-6-P).

Simulations here also address potent inhibition of mini-HKI by 1,5-anhydroGlc-6-P and the effects due to mutations. The 6-phosphoryl group of 1,5-anhydroGlc-6-P in each of its modes of interaction with the C-terminal half of HKI binds Thr536. Regardless of binding mode, the mutation T536A will have an impact on 1,5-anhydroGlc-6-P inhibition. The mutation D861A also eliminates inhibition by 1,5-anhydroGlc-6-P[18], suggesting the possible significance of the alternative binding mode of 1,5-anhydroGlc-6-P in mini-HKI.

Finally, we come to the 2-OH group of Glc-6-P and its importance to inhibition proposed by Crane and Sols[23]. Fluorescence titrations suggest 100-fold weaker binding of the 2-OH variants relative to Glc-6-P (Figure 2). TNP-ADP is a competitive inhibitor with respect to $[ATP\text{-}Mg]^{2-}$, so loss of fluorescence arises from the displacement of TNP-ADP from the C-terminal half of HKI by the binding of ligands. The absence of the 2-OH group or the change in chirality of carbon-2 has a significant effect on ligand interactions at the C-terminal half in simulations. In contrast, interactions of 2-deoxy-Glc-6-P and Man-6-P at the N-terminal half appear similar to those of Glc-6-P. One possibility then has 2-deoxy-Glc-6-P and Man-6-P binding to the N-terminal half with relatively high affinity, but with no influence on the C-terminal half due to the absence of interactions involving the 2-position of the ligand. Inhibition would come about by weak interactions of 2-deoxy-Glc-6-P and Man-6-P with the C-terminal half. Alternatively, one could have weak association with the N-terminal half due to the absent or repositioned 2-OH group, but retain allosteric inhibition triggered by interactions of the 1-OH group.

Allosteric inhibition putatively stems from the nonbonded contacts between the loop

244–253 of the N-terminal half and the flexible subdomain of the C-terminal half[53] and in simulations an isosteric mutation (D413N) causes significant change to contacts between N-and C-terminal halves (Figure 9) that influence interactions of Thr536 at the active site. Moreover, ATP recognition by the C-terminal half of HKI correlates with the position and hydrogen bonding of Thr784 of the flexible subdomain[53], and even in a crystalline ATP complex of glucokinase[54], the corresponding threonine adopts the same ATP-favored conformation as observed in HKI.

The mechanism of allosteric regulation of HKI by Glc-6-P and P_i has been obscured by packing interactions in crystals, differences in pH, assumptions of localized effects due to mutations, and the use of metabolite analogs that may not elicit a response comparable to the physiological effector. Dynamics simulations offer a potential bridge from crystal structures, biased by packing interactions, to conformational states in solution that ultimately become the basis for a comprehensive of allostery in HKI.

Table I. Kinetics parameters for wild-type and mutant forms of HKI.[#]

HKI	k_{cat}	K_m^{Glc}	K_m^{ATP}	K_I	K_{II}	P_i-relief
	S^{-1}	μM	mM	μM	μM	%
Wild-type	92 ± 1	45 ± 3	1.03 ± 0.02	20 ± 3	240 ± 50	85
D413N	82 ± 1	57 ± 2	0.98 ±0.06	23 ± 4	80 ± 20	80
D861N	9.4 ± 0.1	37 ± 1	2.02 ± 0.09	30 ± 4	80 ± 20	86
D413N/D861N	10.0 ± 0.1	32 ± 2	1.59 ± 0.06	35 ± 5	110 ± 40	78

[#]Assays were in 80 mM Tris, pH 8.0, 1 mM DTT, 0.4 mM NADP, 3 mM $MgCl_2$ along with varying amounts of $[ATP\text{-}Mg]^{2-}$, Glc, P_i and/or 1,5-anhydroGlc-6-P. In the determination of K_m^{Glc}, the concentration of Glc varied from 1/ 6 K_m^{Glc} to 10 K_m^{Glc} and that of $[ATP\text{-}Mg]^{2-}$ was fixed at 9 mM. In the determination of K_m^{ATP}, the concentration of $[ATP\text{-}Mg]^{2-}$ varied from 1/6 K_m^{ATP} to 6 K_m^{ATP} and that of Glc was fixed at 2 mM. In the determination of K_I and K_{II}, the concentration of $[ATP\text{-}Mg]^{2-}$ varied from 1/2 K_m^{ATP} to 4 K_m^{ATP}, that of 1,5-anhydroGlc-6-P from 20 to 100 μM and that of Glc was fixed at 2 mM. Values for K_I and K_{II} for 1,5-anhydroGlc-6-P were obtained by fitting data to a model of nonlinear competitive inhibition, the equation for which is as follows:

$$V = {V_{max}} \Big/ \left[1 + (K_m^{ATP}) \times {1}/{S} + \left({K_m^{ATP}}/{K_I}\right) \times {I}/{S} + \left({K_m^{ATP}}/{K_I \times K_{II}}\right) \times {I^2}/{S}\right]$$

where S and I are concentrations of $[ATP\text{-}Mg]^{2-}$ and 1,5-anhydroGlc-6-P, respectively. P_i-relief of inhibition is defined as $100 \times (A\text{-}B)/A$, where A is the slope from plots of reciprocal relative velocity versus 1,5-anhydroGlc-6-P concentration in the absence of P_i, and B is the slope from plot of reciprocal relative velocity versus inhibitor concentration in the presence of 6 mM P_i. Relative velocity is the ratio of velocity at a specific concentration of inhibitor to the velocity in the absence of inhibitor. The $[ATP\text{-}Mg]^{2-}$ concentration is fixed at K_m^{ATP}.

Table II. Statistics for data collection and refinement of wild-type and mutant forms of HKI

Protein	Wild-type	D413N	Wild-type	Wild-type	Wild-type
Ligand [a]	Glc-6-P	Glc-6-P	1,5-anhydroGlc-6-P	2-deoxyGlc-6-P	Man-6-P
Space group	P2(1)	P2(1)	P2(1)	P2(1)	P2(1)
Unit cell parameters					
a (Å)	82.63	82.607	82.723	82.983	82.424
b (Å)	121.53	121.140	121.211	122.092	123.090
c (Å)	119.83	119.888	120.790	120.346	121.640
α (°)	90	90	90	90	90
β (°)	92.82	92.69	93.12	92.975	93.272
γ (°)	90	90	90	90	90
Resolution limits (Å)	37.90-2.65	44.15-2.48	46.24-3.00	35.36-2.65	45.78-2.70
No. of reflections	245322	3458364	665422	266419	237474
No. of unique reflections	68327	83067	56036	69139	64558
% Completeness (overall)	99.22	98.47	82.72	98.92	99.78
% Completeness (last shell)	98.99	84.92	22.74	98.32	99.85
R_{sym} [a]	0.061	0.070	0.112	0.086	0.071
R-factor[b]	0.2421	0.2391	0.2310	0.2397	0.2442
R_{free} [c]	0.2565	0.2527	0.2537	0.2578	0.2544
No. of atoms in refinement	14481	14394	14396	14508	14496
No. of water molecules	273	186	194	304	288
Mean B parameters (Å^2)					
Main chain	55	61	78	55	55
Side chain	57	63	79	57	56
Glucose, N-half	45	52	81	45	45
Glucose, C-half	35	40	55	34	37
Sugar-phosphate, N-half	51	78	80	51	63
Sugar-phosphate, C-half	35	42	62	34	37
Root mean square deviations					
Bond lengths (Å)	0.004	0.004	0.013	0.006	0.005
Bond angles (°)	0.907	0.889	1.014	0.865	0.887

[a] $R_{sys} = \Sigma_j \Sigma_i |I_{ij} - \langle I_j \rangle| / \Sigma_i \Sigma_j I_{ij}$, where *i* runs over multiple observations of the same intensity and *j* runs over crystallographically unique intensities.

[b] *R*-factor = $\Sigma \| F_{obs} - F_{calc} \| / \Sigma |F_{obs}|$, $F_{obs} > 0$.

[c] R_{free}- is based upon 10% of the data randomly culled and not used in the refinement.

Table III. Donor-acceptor distances between ligand and protein from crystal structures.

(Distances less than 3.2 Å for residues from the N- and C-terminal halves are listed for chains A and B.)

		Glc-6-P				D413N/Glc-6-P				1,5-anhydroGlc-6-P				2-deoxyGlc-6-P				Man-6-P			
Atom	Residue	NA	NB	CA	CB	NA	NB	CA	CB	NA	NB	CA	CB	NA	NB	CA	CB	NA	NB	CA	CB
	D/N413/861[#]: OD1	2.9	3.1			3.5	3.2							3.1	3.1						
O1	D/N413/861[#]: O/ND2	2.7	2.5	2.6	3.1	2.5	3.0	2.5	3.3					2.8	2.6	2.7	3.2	2.7	2.9	2.7	3.3
	D84/532:OD2	2.5	2.9	2.8	2.8	2.5	2.8	2.8	2.7	2.4	3.3	2.8	2.5								
	R91/539:NH1					2.7	4.9														
O2	D/N413/861:O/ND2																	2.5	2.9	2.9	3.0
	S449/897:N	3.7	3.1	2.9	2.8	3.3	3.2	2.8	3.0			2.8	2.8					3.6	2.9	3.1	3.0
	S449/897:OG			3.2	3.6							3.6	3.2					2.8	3.4	4.4	3.1
	D84/532:OD1	2.5	2.8	2.7	2.9	3.2	3.0	2.8	3.0	3.1	3.0	2.8	2.9	3.4	3.1	2.8	3.0	3.0	3.4	2.8	3.0
	D84/532:OD2	2.7	3.3			2.7	3.2			2.8	3.7			2.4	3.4			2.4	2.9		
O3	S449/897:OG	2.9	2.7	2.5	2.7	2.8	2.8	2.5	2.8	3.6	2.8	3.0	2.5	2.9	3.0	2.6	2.5	3.2	2.8	3.9	2.7
O4	D209/657:OD2	2.8	2.7	2.9	2.6	2.7	2.7	2.9	2.5	3.0	2.5	3.3	2.6	2.8	2.8	3.0	2.6	3.1	2.6	3.0	2.6
	S88/T536:N	3.1	3.6			3.1	3.6			3.2	3.2			3.0	3.0			2.7	3.8		
	S88/T536:OG																	3.2	4.0		
	T232/680:N	3.1	2.9	2.8	2.9	3.4	2.8	2.9	2.9			3.1	3.2	3.2	2.8	2.9	3.0	3.6	2.7	2.8	2.9
O1P	T232/680:OG	2.5	2.5	2.7	2.8	2.6	2.6	2.7	2.9	2.8	3.0	3.0	3.3	2.6	2.6	2.7	2.8	2.7	2.6	2.7	2.7
	S88/T536:OG	2.7	4.2			3.2	3.5			2.7	4.4			2.9	4.2			3.2	3.8		
	T232/680:N	3.3	3.2			3.1	3.8			2.9	3.0	3.0	3.4	3.2	3.4			2.7	3.9		
	S415/T863:N	2.8	2.9	2.9	2.9	2.8	3.1	2.8	2.8	3.2	3.2	3.1	2.8	3.0	2.8	2.9	2.9	3.0	2.9	2.9	2.9
O2P	S415/T863:OG	2.6	2.7	2.6	2.5	3.2	2.5	2.8	2.5	2.9	3.0	2.9	2.7	2.7	2.6	2.6	2.6	3.6	3.1	2.5	2.5
	S88/T536:N	2.8	2.9	2.9	2.9	3.3	2.7	2.8	3.0	3.0	3.0	3.1	3.4	2.9	2.9	2.8	2.8	3.6	2.8	2.9	3.0
O3P	S88/T536:OG	2.5	2.5	2.7	2.7	2.5	2.6	2.9	2.8	2.4	2.9	2.5	2.8	2.5	2.6	2.7	2.8	2.5	2.8	2.8	2.9

[#]D or N 413 from N-terminal half and D861 from C-terminal half.

Table III. Donor-acceptor distances between ligand and protein from crystal structures.

Table IV. Fractional ratio for phosphoryl ligands of all MD simulation structures

(distance ≤ 3.2Å between phosphoryl ligand and corresponding residues)

Atom	Residue	Glc-6-P		D413N/ Glc-6-P		1,5-anhydro Glc-6-P		2-deoxy Glc-6-P		Man-6-P	
		N	C	N	C	N	C	N	C	N	C
O1	D/N413/861:OD1	0.62	0.90	0.09	0.91	---	---	0.74	0.31	0.81	0.52
	D/N413/861:O/ND2	0.52	0.69	0.68	0.62	---	---	0.57	0.17	0.29	0.47
	K418/866:NZ	0.47	0.14	0.03	0.61	---	---	0.09	0.02	0.11	0.04
O2	D84/532:OD1	0.22	0.91	0.41	0.12	0.13	0.24	---	---	---	---
	D84/532:OD2	0.79	0.87	0.73	0.86	0.90	0.12	---	---	---	---
	R91/539:NH1	0.04	---	0.02	0.07	0.33	---	---	---	---	---
	R91/539:NH2	0.08	0.06	---	---	0.43	0.09	---	---	---	---
	T213/661:OG1	---	---	---	---	---	---	---	---	---	0.28
	D/N413/861:OD1	---	---	---	---	0.04	---	---	---	0.52	0.35
	D/N413/861:O/ND2	---	---	---	---	---	0.73	---	---	0.15	0.40
	S449/897:N	0.45	0.15	0.26	0.56	0.13	0.13	---	---	0.23	---
	S449/897:OG	0.01	---	0.01	0.03	0.26	0.22	---	---	0.76	0.17
O3	D84/532:OD1	0.85	0.98	0.81	0.81	0.85	0.72	0.52	0.14	0.72	0.11
	D84/532:OD2	0.70	---	0.64	0.33	0.69	0.10	0.39	---	0.84	---
	D209/657:OD2	---	---	---	0.05	0.01	---	0.21	0.67	---	0.76
	S449/897:OG	0.90	0.96	0.86	0.98	0.49	0.79	0.26	0.33	0.65	0.17
O4	G87/535:N	---	0.54	---	0.06	0.07	0.11	---	0.05	---	0.18
	D209/657:OD2	1.00	1.00	1.00	0.99	0.92	0.40	1.00	0.99	1.00	0.95
	Glc:O6	---	---	---	---	---	---	0.07	0.30	---	0.03
O1P	S88/T536:N	0.48	---	0.08	0.07	0.07	0.02	0.53	0.02	0.12	---
	S88/T536:OG(1)	0.45	---	0.20	---	0.32	---	0.57	---	---	---
	T232/680:N	0.25	0.42	0.46	0.98	0.30	0.98	0.51	1.00	0.87	0.68
	T232/680:OG1	0.25	0.43	0.44	1.00	0.30	0.97	0.53	1.00	0.98	0.98
	S415/T863:N	0.20	---	0.48	---	0.46	----	---	---	---	---
	S415/T863:OG(1)	0.30	---	0.58	---	0.66	---	0.02	---	---	---
O2P	S88/T536:N	0.33	---	0.56	---	0.57	---	0.10	---	---	---
	S88/T536:OG(1)	0.46	---	0.70	---	0.53	---	0.24	---	0.02	---
	T232/680:N	0.45	0.54	0.00	0.05	0.04	0.03	0.46	---	0.27	0.42
	T232/680:OG1	0.47	0.57	0.00	---	0.14	0.02	0.47	---	0.04	0.15
	S415/T863:N	0.19	0.39	0.37	0.86	0.25	0.64	0.42	0.73	0.75	0.46
	S415/T863:OG(1)	0.25	0.43	0.43	1.00	0.31	1.00	0.53	1.00	1.00	1.00
O3P	S88/T536:N	0.27	0.04	0.42	0.99	0.33	0.44	0.47	0.39	0.99	0.04
	S88/T536:OG(1)	0.27	0.04	0.29	1.00	0.28	0.45	0.35	0.45	1.00	0.03
	T232/680:N	0.27	0.05	0.56	---	0.62	---	0.01	---	---	---
	T232/680:OG1	0.29	---	0.57	---	0.65	0.02	---	---	---	0.03
	S415/T863:N	0.38	0.50	0.00	---	0.03	---	0.37	---	---	---
	S415/T863:OG(1)	0.48	0.57	0.00	---	0.06	---	0.47	---	---	---

--: value less than 0.01 or not exist.

Table V. Fraction of frames from molecular dynamics simulations with hydrogen bonds between protein residues and the 6-phosphoryl groups of ligands[$].

Residue	Glc-6-P		D413N/ Glc-6-P		1,5-anhydro Glc-6-P		2-deoxy Glc-6-P		Man-6-P	
	N	C	N	C	N	C	N	C	N	C
S88/T536:N[$]	0.99	0.04	0.98	0.99	0.93	0.99	0.88	0.44	0.97	0.39
S88/T536:OG(1)[$]	0.92	0.04	0.96	1.00	0.58	0.90	0.91	0.44	0.91	0.45
S88/T536[#]	1.00	0.04	1.00	1.00	0.96	1.00	0.98	0.45	1.00	0.47
T232/680:N[$]	0.96	0.97	0.99	0.98	0.97	0.69	0.95	0.98	0.97	1.00
T232/680:OG1[$]	1.00	1.00	1.00	1.00	1.00	1.00	1.00	0.98	1.00	1.00
T232/680[#]	1.00	1.00	1.00	1.00	1.00	1.00	1.00	1.00	1.00	1.00
S415/T863:N[$]	0.76	0.89	0.85	0.86	0.24	0.50	0.74	0.64	0.78	0.73
S415/T863:OG(1)[$]	1.00	1.00	1.00	1.00	1.00	0.64	1.00	1.00	1.00	1.00
S415/T863[#]	1.00	1.00	1.00	1.00	1.00	0.64	1.00	1.00	1.00	1.00

[$]A pair of polar atoms define a hydrogen bond if the corresponding donor-acceptor distance is less than or equal to 3.2 Å.

[#]Represents the fraction of frames with hydrogen bonds between any polar atom of the indicated protein residue and any atom of the 6-phosphoryl group.

Table VI. Fraction of frames from molecular dynamics simulations with hydrogen bonds between oxygen atoms of the 6-phosphoryl group and any polar atom from the protein[$].

6-P_i	Glc-6-P		D413N/ Glc-6-P		1,5-anhydro Glc-6-P		2-deoxy Glc-6-P		Man-6-P	
	N	C	N	C	N	C	N	C	N	C
O1P	0.99	0.44	1.00	1.00	0.88	0.83	1.00	0.99	0.98	1.00
O2P	0.99	1.00	1.00	1.00	0.98	0.97	0.98	1.00	1.00	1.00
O3P	1.00	0.61	0.99	1.00	0.81	0.92	0.98	0.47	0.97	0.48

[$]A pair of polar atoms define a hydrogen bond if the corresponding donor-acceptor distance is less than or equal to 3.2 Å.

Table VII. Values (μM) for site dissociation constants $^0M_1$ and $^0M_2$ of Scheme I for selected values of α for wild-type and mutant forms of HKI.

α	$^0M_1/^0M_2$			
	wt-HKI	D413N	D861N	D413/861N
0.35	33/51	--[a]	--[a]	--[a]
1.0	22/220	--[a]	--[a]	--[a]
1.5	21/340	31/89	--[a]	50/120
2.0	21/460	28/130	42/120	44/180

[a]No physical solution.

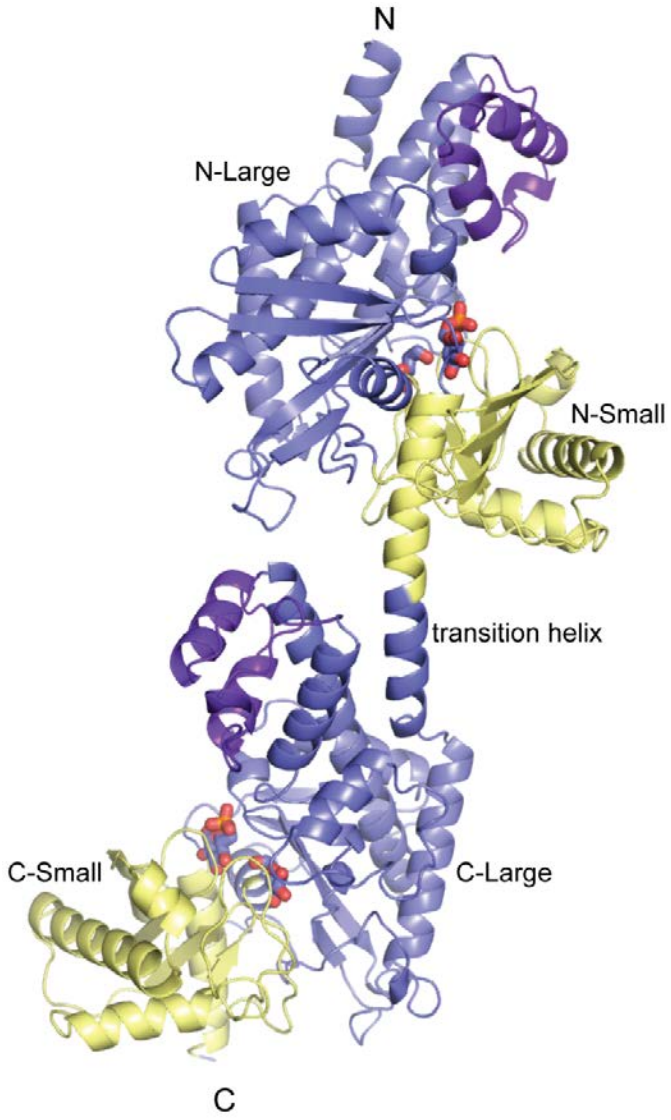

Figure 1. Overview of the wild-type HKI•Glc-6-P•Glc complex. Large domains are blue and small domains yellow. The flexible subdomain (residues 766–812) and corresponding residues of the N-terminal half (residues 318–364) are purple. Ligands Glc-6-P and Glc are sticks. The illustration was generated with PyMOL.

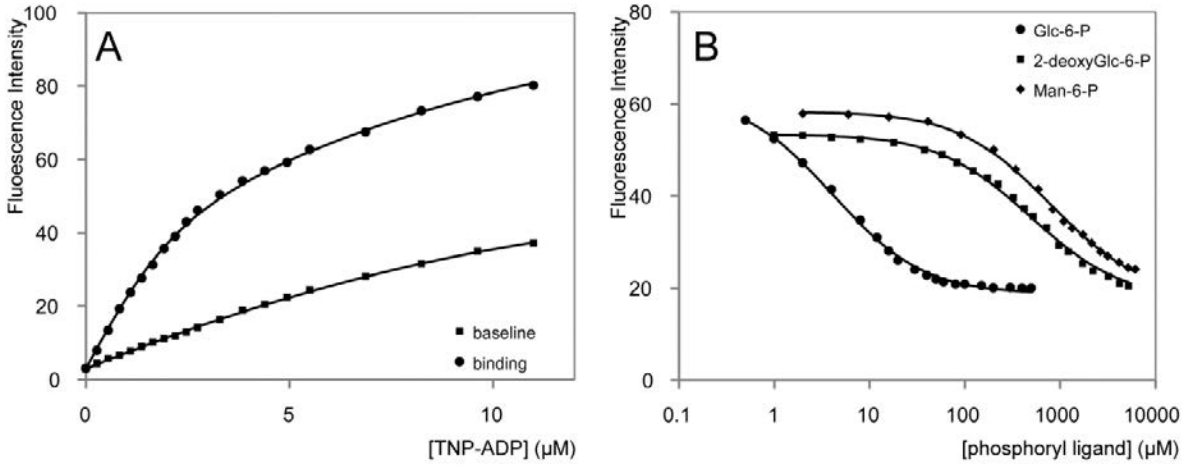

Baseline	*a*	*b*	*c*
	2.9 ± 0.1	4.51 ± 0.05	0.125 ± 0.003
Binding	K_L	*G*	*S*
	0.47 ± 0.04	5.51 ± 0.06	0

Displacement	K_A	*G*	*S*
Glc-6-P	0.51 ± 0.02	6.75 ± 0.06	1.0 ± 0.2
2-deoxyGlc-6-P	60 ± 2	5.69 ± 0.03	0
Man-6-P	97 ± 4	6.28 ± 0.06	0.6 ± 0.4

Figure 2. TNP-ADP binding and displacement curves for wild-type hexokinase I. A, Titration of 2 μM wild-type hexokinase I (binding curve) or buffer only (baseline) with TNP-ADP. B, Displacement of TNP-ADP from wild-type hexokinase I with different ligands. The fitted parameters are shown below.

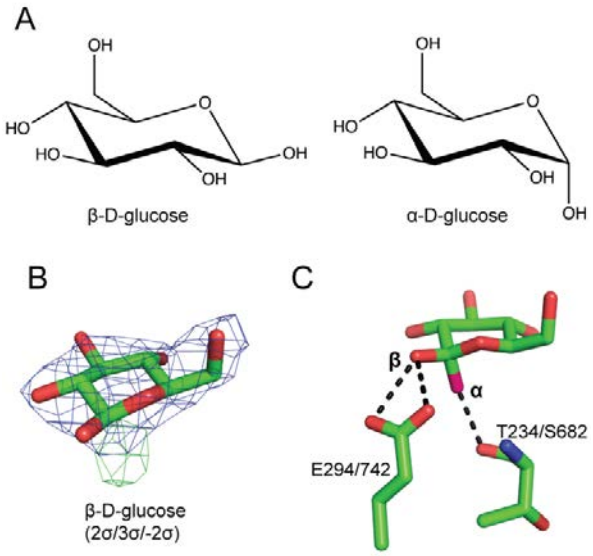

Figure 3. Electron density for glucose in structures of HKI. A, β-D-glucose and α-D-glucose. B, Electron density (2Fo-Fc) for β-D-glucose, contoured at 2σ (blue) in combination with Fo-Fc positive electron density (green) contoured at 3σ. (Fo-Fc negative electron density is not observed at levels above 2σ). C, Hydrogen bonds between the 1-hydroxyl group of β- and α-D-glucose and protein. Illustration generated with Chemdraw (*panel A*) and PyMOL (*panels B* and *C*).

.

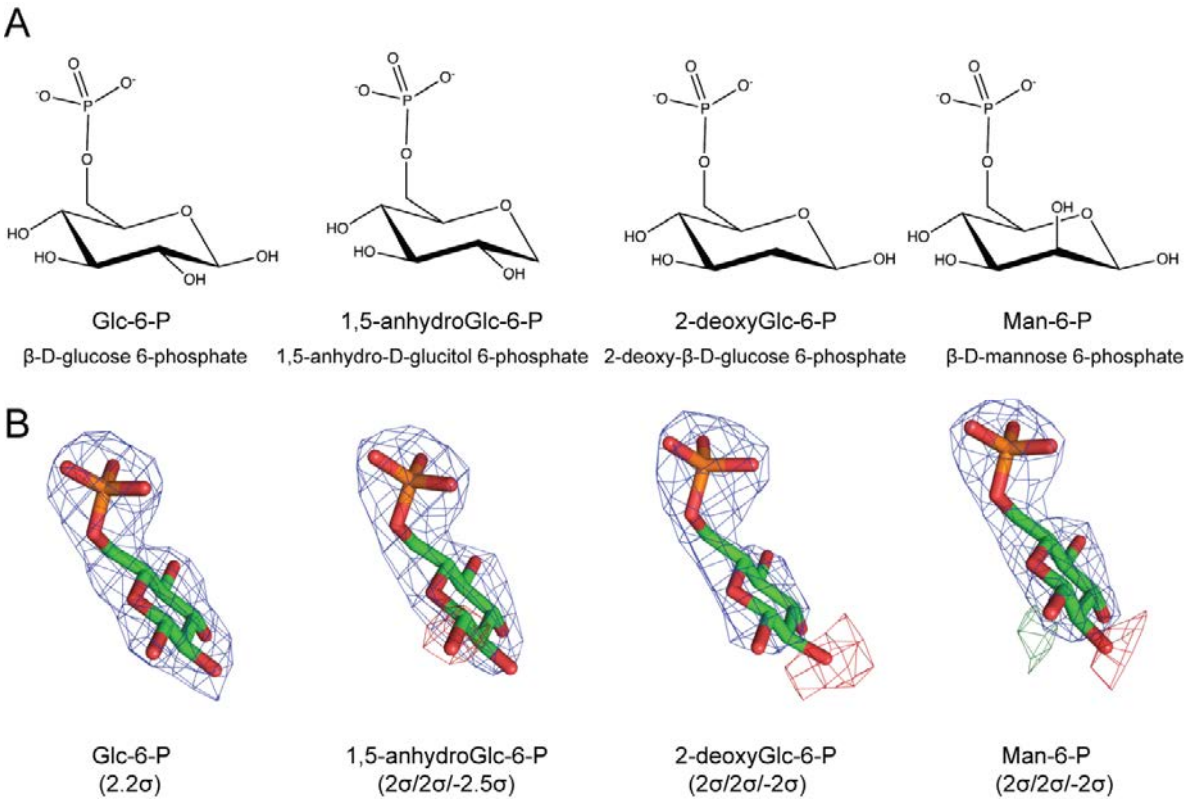

Figure 4. 6-Phosphoryl ligands and associated electron densities. A. Phosphoryl ligands. B. Electron density for each complex with Glc-6-P as the modeled ligand. Density levels are for 2Fo-Fc (blue), positive Fo-Fc (green))and negative Fo-Fc (red) at contour levels indicated for data collected from complexes of enzyme with Glc-6-P, 1,5-anhydroGlc-6-P, 2-deoxyGlc-6-P and Man-6-P. Illustration generated with Chemdraw (*panel A*) and PyMOL (*panel B*).

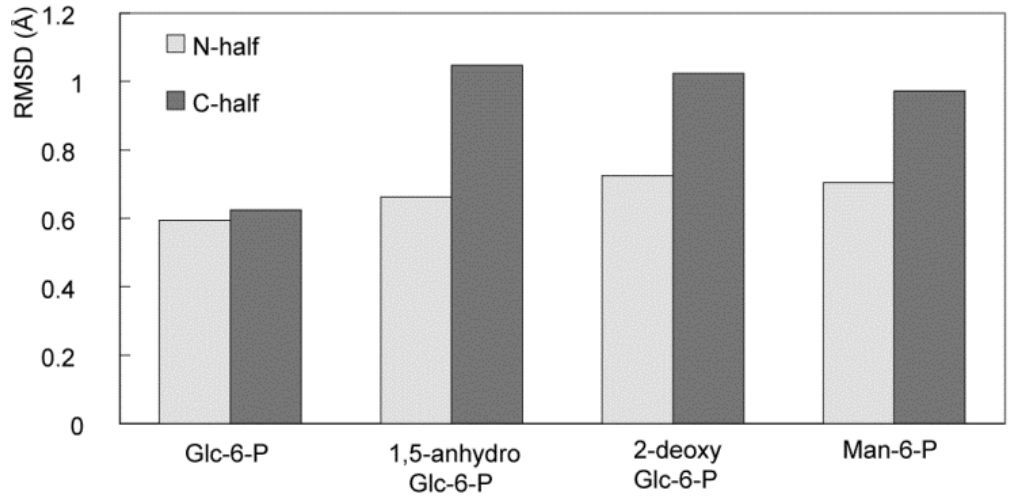

Figure 5. RMSD of phosphoryl ligand from MD simulations for N- and C-terminal halves of each complex.

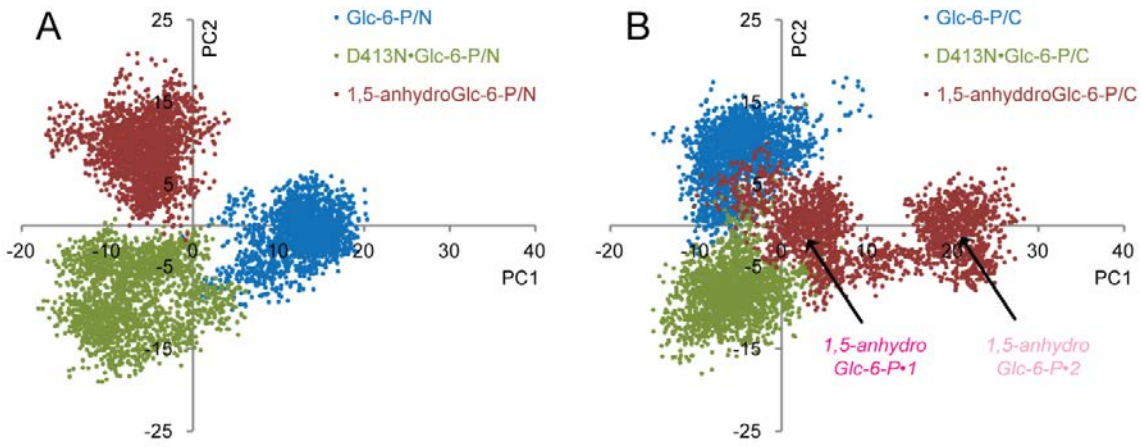

Figure 6. Principal component analysis of HKI. First two components of PCA based on all N-terminal half (A) or C-terminal half (B) structures from wild-type•Glc-6-P, wild-type•1,5-anhydroGlc-6-P and D413N•Glc-6-P MD simulations. Mode 1 and mode 2 for the C-terminal half of the wild-type•1,5-anhydroGlc-6-P simulation are marked by arrows.

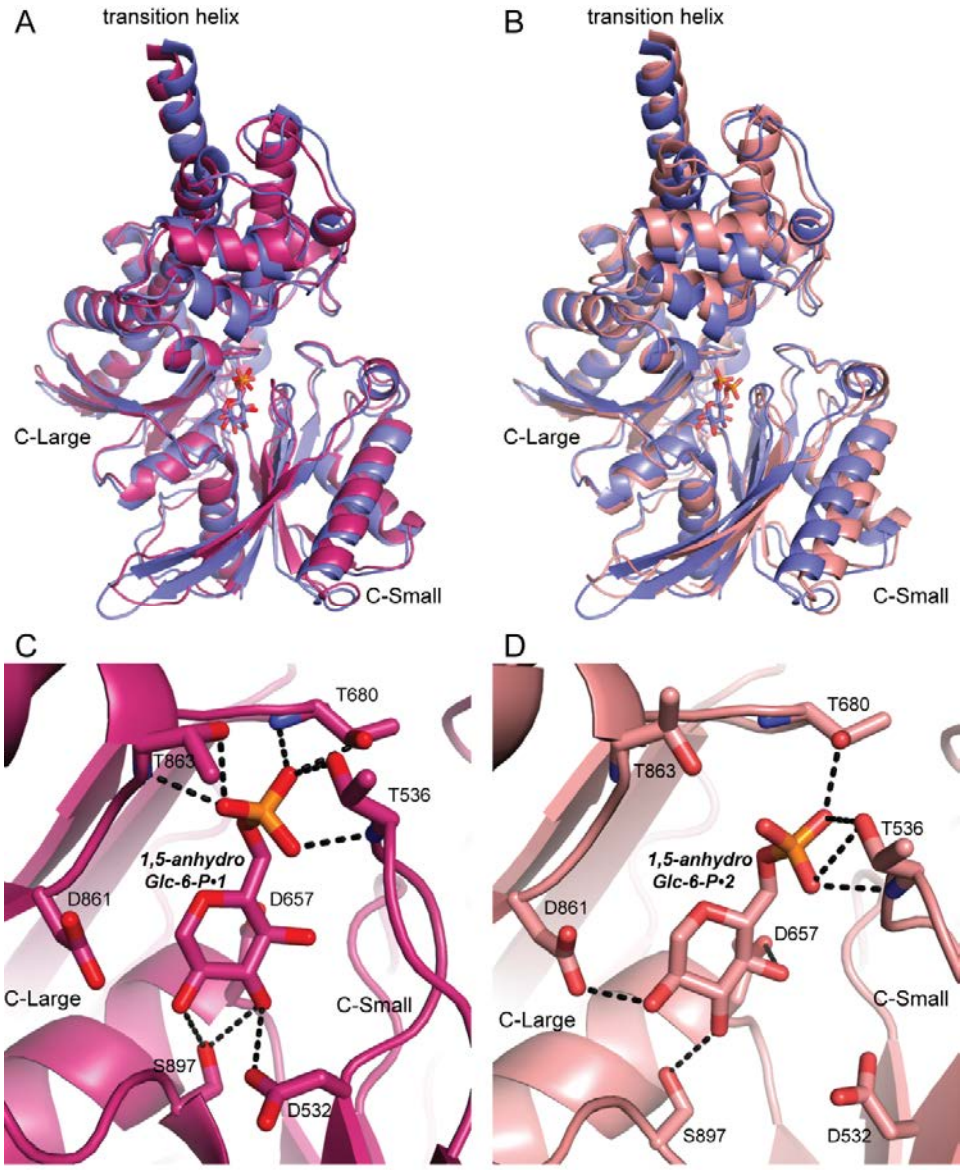

Figure 7. Representative structures from PCA distributions of C-terminal half HKI. Panels A and B are C-terminal halves from simulations of Glc-6-P with wild-type HKI (blue), mode 1 of 1,5-anhydroGlc-6-P and wild-type HKI (magenta) and mode 2 of 1,5-anhydroGlc-6-P and wild-type HKI (pink). Mode 1 and 2 are defined in Figure 6. The large domain of the C-terminal half, excluding residues 766–812 (flexible subdomain), is the basis of superpositions. The C-terminal half in mode 2 is more open relative to that of the C-terminal half with Glc-6-P. Panels C and D show hydrogen bond networks for 1,5-anhydroGlc-6-P in mode 1 (magenta) and mode 2 (pink), respectively.

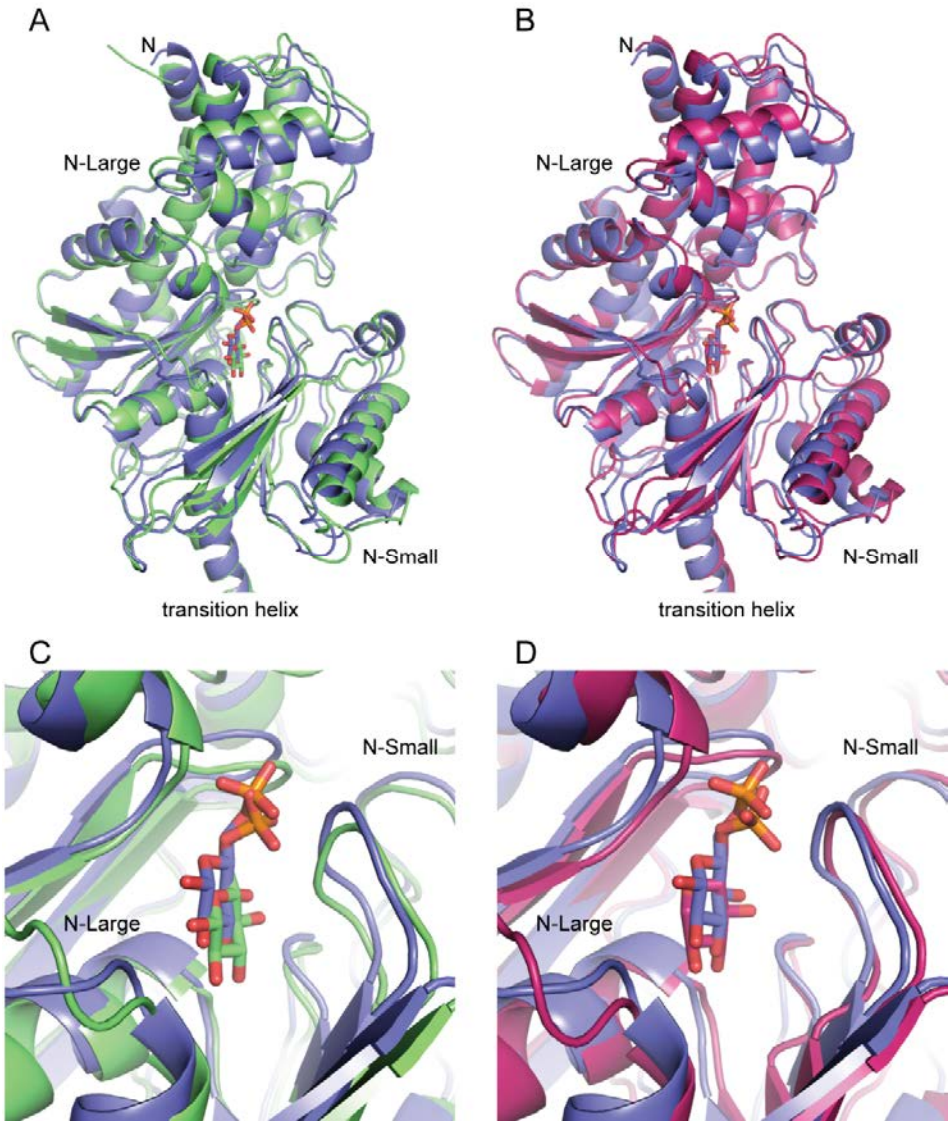

Figure 8. Representative structures from PCA distributions for the N-terminal half of HKI. The N-terminal half large domain, excluding residues 318–364 (residues corresponding to the flexible subdomain of the C-terminal half), is the basis of superposition. *Panels A* and *C* are views of the N-terminal half and its inhibitor binding pocket, respectively, of wild-type•Glc-6-P (blue) and D413N•Glc-6-P (green) complexes. The wild-type•Glc-6-P complex is more closed relative to the D413N•Glc-6-P complex (*panel A*), and the inhibitor occupies different locations within the pocket (*panel C*). *Panels B* and *D* are views of the N-terminal half and its inhibitor binding pocket, respectively, of wild-type•Glc-6-P (blue) and wild-type•1,5-anhydroGlc-6-P (magenta) complexes. The wild-type•1,5-anhydroGlc-6-P complex (magenta) is similar to the D413N•Glc-6-P complex (green), but different from the wild-type•Glc-6-P complex (blue).

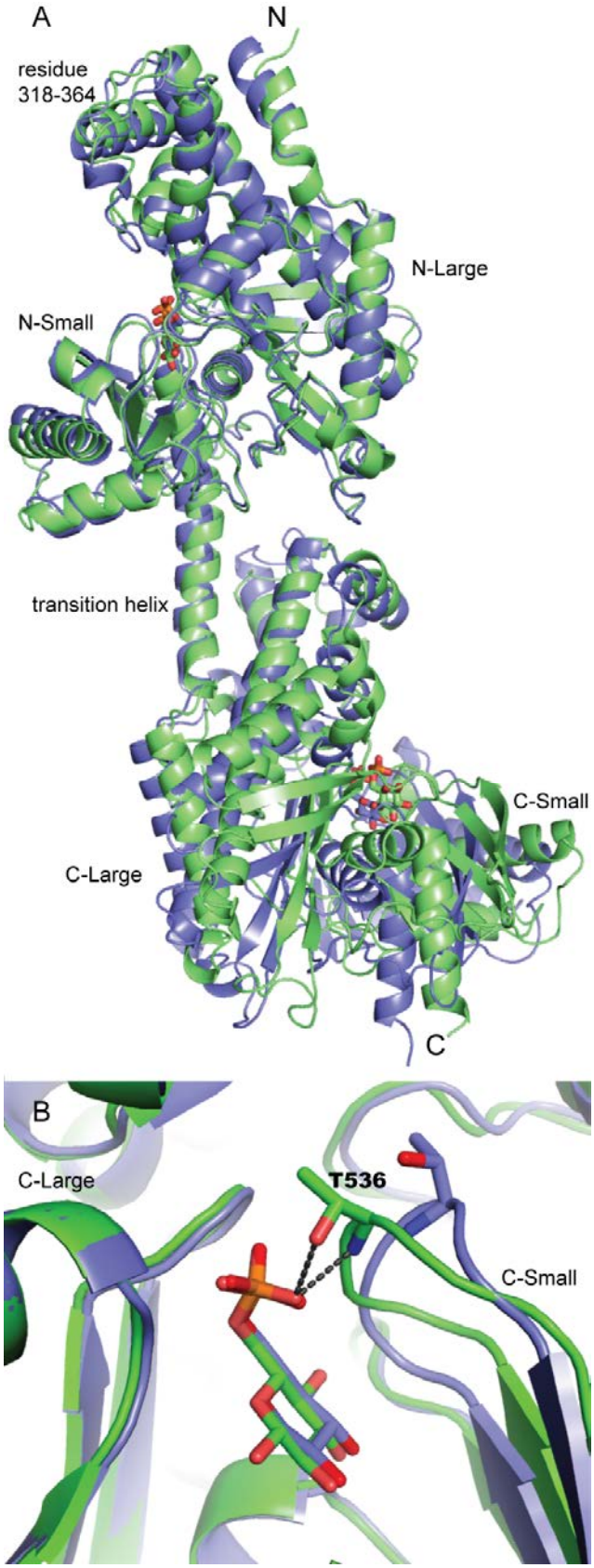

Figure 9. Superposition of representative HKI structures from PCA distributions for the N-terminal half. N-terminal half large domains, excluding residues 318–364 (residues corresponding to the flexible subdomain of the C-terminal half) are the basis of superposition of wild-type (blue) and D413N (green) complexes with Glc-6-P (*panel A*). The transition helix leverages the slight opening of the N-terminal half of D413N HKI into large rigid-body movements in the C- relative to the N-terminal half. These movements ultimately enhance interactions involving the 6-phosphoryl group of Glc-6-P and Thr536 of the C-terminal half (*panel B*).

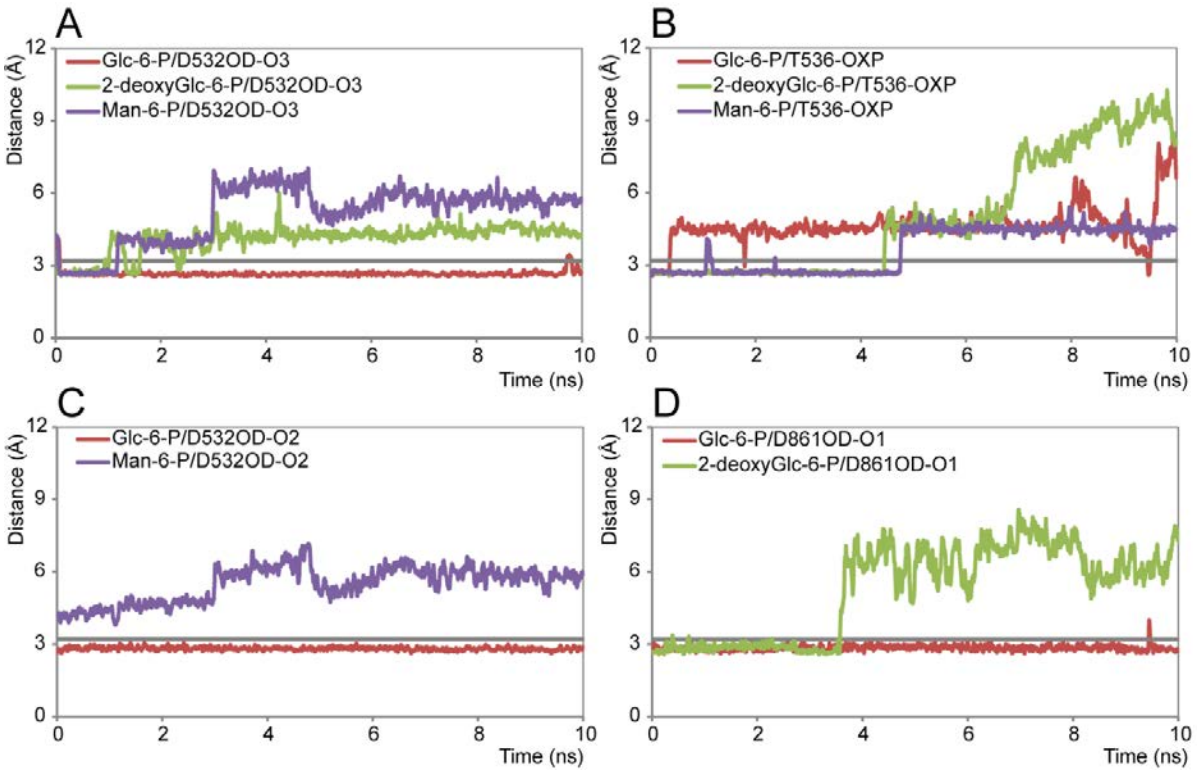

Figure 10. Distance between selected polar atoms from ligand and protein over time. The lines are smoothed by taking averaging five successive frames. OXP and OD represent the closest pair of oxygen atoms between the 6-phosphoryl group and indicated residue.

References

1. Gonzalez, C., Ureta, T., Sánchez, R., and Niemeyer, H. (1964) Multiple molecular forms of ATP: hexose 6-phosphotransferase from rat liver. *Biochem. Biophys. Res. Commun.* **16**, 347-352
2. Grossbard, L., and Schimke, R.T. (1966) Multiple hexokinases of rat tissues. Purification and comparison of soluble forms. *J. Biol. Chem*. **241**, 3546-3560
3. Katzen, H.M. (1967) The multiple forms of mammalian hexokinase and their significance to the action of insulin. *Adv. Enzyme Regul*. **5**, 335-356
4. Katzen, H.M., and Schimke, R.T. (1965) Multiple forms of hexokinase in the rat: tissue distribution, age dependency, and properties. *Proc. Natl. Acad. Sci. U.S.A.* **54**, 1218-1225
5. Wilson, J.E. (1995) Hexokinase. *Rev. Physiol. Biochem. Pharmacol*. **126**, 65-198
6. Easterby, J.S, and O'Brien, M.J. (1973) Purification and properties of pig-heart hexokinase. *Eur. J. Biochem*. **38**, 201-211
7. Holroyde, M.J., and Trayer, I.P. (1976) Purification and properties of skeletal muscle hexokinase. *FEBS Lett*. **62**, 215-219
8. Ureta, T. (1982) The comparative isozymology of vertebrate hexokinases. *Comp. Biochem. Physiol*. **71B**, 549-555
9. Manning, T.A., and Wilson, J.E. (1984) Inhibition of brain hexokinase by a multisubstrate analog results from binding to a discrete regulatory site. *Biochem. Biophys. Res. Commun.* **118**, 90-96
10. Tsai, H.J. and Wilson, J.E. (1996) Functional organization of mammalian hexokinases: both N- and C-terminal halves of the rat type II isozyme possess catalytic sites. *Arch. Biochem. Biophys.* **329**, 17-23
11. White, T.K., and Wilson, J.E. (1989) Isolation and characterization of the discrete N- and C-terminal halves of rat brain hexokinase: retention of full catalytic activity in the isolated C-terminal half. *Arch. Biochem. Biophys*. **274**, 375-393
12. Arora, K.K., Filburn, C.R., and Pedersen, P.L. (1993) Structure/function relationships in hexokinase. Site-directed mutational analyses and characterization of overexpressed fragments implicate different functions for the N- and C-terminal halves of the enzyme. *J. Biol. Chem*. **266**, 5359-5362
13. Aleshin, A.E., Zeng, C., Bourenkov, G.P., Bartunik, H.D., Fromm, H.J., and Honzatko, R.B. (1998) The mechanism of regulation of hexokinase: new insights from the crystal structure of recombinant human brain hexokinase complexed with glucose and glucose-6-phosphate. *Structure.* **6**, 39-50
14. Mulichak, A.M., Wilson, J.E., Padmanabhan, K., and Garavito, R.M. (1998) The structure of mammalian hexokinase-1. *Nat. Struct. Biol*. **5**, 555-560

15. Aleshin, A.E., Fromm, H.J., and Honzatko, R.B. (1998) Multiple crystal forms of hexokinase I: new insights regarding conformational dynamics, subunit interactions, and membrane association. *FEBS Lett*. **434**, 42-46

16. Zeng, C., and Fromm, H.J. (1995) Active site residues of human brain hexokinase as studied by site-specific mutagenesis. *J. Biol. Chem*. **270**, 10509-10513

17. Fang, T.Y., Alechina, O., Aleshin, A.E., Fromm, H.J., and Honzatko, R.B. (1998) Identification of a Phosphate Regulatory Site and a Low Affinity Binding Site for Glucose 6-Phosphate in the N-terminal Half of Human Brain Hexokinase. *J. Biol. Chem*. **273**, 19548-19553

18. Liu, X., Kim, C.S., Kurbanov, F.T., Honzatko, R.B., and Fromm, H.J. (1999) Dual Mechanisms for Glucose 6-Phosphate Inhibition of Human Brain Hexokinase. *J. Biol. Chem.* **274**, 31155-31159

19. Skaff, D.A., Kim, C.S., Tsai, H.J., Honzatko, R.B., and Fromm, H.J. (2005) Glucose 6-phosphate release of wild-type and mutant human brain hexokinases from mitochondria. *J. Biol. Chem*. **280**, 38403-38409

20. Ellison, W.R., Lueck, J.D., and Fromm, H.J. (1974) Studies on the kinetics and mechanism of orthophosphate activation of bovine brain hexokinase. *Biochem. Biophys. Res. Commun*. **57**, 1214-1220

21. Ellison, W.R., Lueck, J.D., and Fromm, H.J. (1975) Studies on the mechanism of orthophosphate regulation of bovine brain hexokinase. *J. Biol. Chem*. **250**, 1864-1871

22. Chou, A.C., and Wilson, J.E. (1974) Rat brain hexokinase: glucose and glucose-6-phosphate binding sites and C-terminal amino acid of the purified enzyme. *Arch. Biochem. Biophys.* **165**, 628-633

23. Crane, R.K., and Sols, A. (1954) The non-competitive inhibition of brain hexokinase by glucose-6-phosphate and related compounds. *J. Biol. Chem*. **210**, 597-606

24. Magnani, M., Stocchi, V., Serafini, G., and Chiarantini, L. (1988) The interaction of phosphorylated sugars with human hexokinase I. *Biochim. Biophys. Acta*. **954**, 336-342

25. Zeng, C., Aleshin, A.E., Hardie, J.B., Harrison, R.W., and Fromm, H.J. (1996) ATP-binding site of human brain hexokinase as studied by molecular modeling and site-directed mutagenesis. *Biochemistry*. **35**, 13157-13164

26. Liu, F., Dong, Q., Myers, A.M., and Fromm, H.J. (1991) Expression of human brain hexokinase in Escherichia coli: purification and characterization of the expressed enzyme. *Biochem. Biophys. Res. Commun.* **177**, 305-311

27. Laemmli, U.K. (1970) Cleavage of structural proteins during the assembly of the head of bacteriophage T4. *Nature.* **227**, 680-685

28. Bradford, M.M. (1976) A rapid sensitive method for the quantitation of microgram quantities of protein utilizing the principle of protein-dye binding. *Anal. Biochem.* **72**, 248-252

29. Faller, L.D. (1990) Binding of the fluorescent substrate analogue 2',3'-O-(2,4,6-trinitrophenylcyclohexadienylidene)adenosine 5'-triphosphate to the gastric H+, K(+)-ATPase: evidence for cofactor-induced conformational changes in the enzyme. *Biochemistry.* **29**, 3179-3186

30. Nimer, M., Watanabe, M., Shen, L., Skaff, D.A., and Honzatko R.B. (2012) Mechanism of ATP-dependent release of wild-type and mutant human brain hexokinases from mitochondria. (to be submitted)

31. Leatherbarrow, R.J. (2010) GraFit Version 7, Erithacus Software Ltd., Horley, U.K.

32. Ferrari, R., and Crane, R. (1959) 1,5-Anhydro-D glucitol 6-phosphate and its use for the specific inhibition of the hexokinase reaction in tissue homogenates. *Arch. Biochem. Biophys.* **80**, 372-377

33. Drueckes, P., Schinzel, R., and Palm, D. (1995) Photometric microtiter assay of inorganic phosphate in the presence of acid-labile organic phosphates. *Anal. Biochem*. **230**, 173-177

34. Pflugrath, J.W. (1999) The finer things in X-ray diffraction data collection. *Acta. Crys.* **D55**, 1718-1725

35. Otwinowski, Z., and Minor, W. (1997) Processing of X-ray diffraction data collected in oscillation mode. *Methods in Enzymology.* **276**, 307-326

36. Aleshin, A.E., Malfois, M., Liu, X., Kim, C.S., Fromm, H.J., Honzatko, R.B., Koch, M.H., and Svergun, D.I. (1999) Nonaggregating mutant of recombinant human hexokinase I exhibits wild-type kinetics and rod-like conformations in solution. *Biochemistry*. **38**, 8359-8366

37. Haritos, A.A, and Rosemeyer, M.A. (1985) Isolation and glucose-6-phosphate-mediated dimerization of hexokinase from human heart. *Biochim. Biophys. Acta.* **830**, 113-119

38. Collaborative Computational Project, Number 4. (1994) The CCP4 suite: programs for protein crystallography. *Acta. Cryst.* **D50**, 760-763

39. Navaza, J. (1994) AMoRe: an automated package for molecular replacement. *Acta Cryst.* **A50**, 157-163

40. Vagin, A.A., Steiner, R.S., Lebedev, A.A., Potterton, L., McNicholas, S., Long, F., and Murshudov, G.N. (2004) REFMAC5 dictionary: organisation of prior chemical knowledge and guidelines for its use. *Acta. Cryst.* **D60**, 2284-2295

41. Brünger, A.T., Adams, P.D., Clore, G.M., DeLano, W.L., Gros, P., Grosse-Kunstleve, R.W., Jiang, J-S., Kuszewski, J., Nilges, M., Pannu, N.S., Read, R.J., Rice, L.M., Simonson, T., and Warren, G.L. (1998) Crystallography & NMR system: a new software suite for macromolecular structure determination. *Acta. Cryst.* **D54**, 905-921

42. McRee, D.E. (1992) A visual protein crystallographic software system for X11/XView. *J. Mol. Graph.* **10**, 44-46

43. Phillips, J.C., Braun, R., Wang, W., Gumbart, J., Tajkhorshid, E., Villa, E., Chipot, C., Skeel, R.D., Kale, L., and Schulten, K. (2005) Scalable molecular dynamics with NAMD. *J. Comput. Chem.* **26**, 1781-1802

44. Jr. MacKerell, A.D., Banavali, N., and Foloppe, N. (2001) Development and current status of the CHARMM force field for nucleic acids. *Biopolymers*. **56**, 257-265

45. Jorgensen, W.L., Chandrasekhar, J., Madura, J.D., Impey, R.W., and Klein, M.L. (1983) Comparison of simple potential functions for simulating liquid water. *J. Chem. Phys*. **79**, 926-935

46. Essmann, U., Perera, L., Berkowitz, M.L., Darden, T., Lee, H., and Pedersen, L.G. (1995) A smooth particle mesh Ewald method. *J. Chem. Phys.* **103**, 8577-8593

47. Glykos, N.M. (2006) Carma: a molecular dynamics analysis program. *J. Comput. Chem*. **27**, 1765-1768

48. Humphrey, W., Dalke, A., and Schulten, K. (1996) VMD - Visual molecular dynamics. *J. Molec. Graphics.* **14**, 33-38

49. Copley, M., and Fromm, H.J. (1967) Kinetic studies of the brain hexokinase reaction. A reinvestigation with the solubilized bovine enzyme. *Biochemistry*. **6**, 3503-3509

50. Aleshin, A.E., Zeng, C., Bartunik, H.D., Fromm, H.J., and Honzatko, R.B. (1998) Regulation of Hexokinase I: Crystal Structure of Recombinant Human Brain Hexokinase Complexed with Glucose and Phosphate. *J. Mol. Biol*. **282**, 345-357

51. Solheim, L.P, and Fromm, H.J. (1983) Effect of inorganic phosphate on the reverse reaction of bovine brain hexokinase. *Biochemistry*. **22**, 2234-2239

52. Mehta, A., Jarori, G.K., and Kenkare, U.W. (1988) Brain hexokinase has no preexisting allosteric site for glucose 6-phosphate. *J Biol Chem*. **263**, 15492-15497

53. Aleshin, A.E., Kirby, C., Liu, X., Bourenkov, G.P., Bartunik H.D., Fromm, H.J., and Honzatko, R.B. (2000) Crystal structures of mutant monomeric hexokinase I reveal multiple ADP binding sites and conformational changes relevant to allosteric regulation. *J. Mol. Biol*. **296**, 1001-1015

54. Petit, P., Antoine, M., Ferry, G., Boutin, J.A., Lagarde, A., Gluais, L., Vincentelli, R., and Vuillard, L. (2011) The active conformation of human glucokinase is not altered by allosteric activators. *Acta. Cryst*. **D67**, 929-935

Chapter III. Determination of Site Affinity Constants for Product Inhibition Wild-type and Mutant forms of Recombinant Human Hexokinase Type I

A paper to be submitted to the Journal of Biological Chemistry

Lu Shen, Yang Gao and Richard B. Honzatko

Department of Biochemistry, Biophysics and Molecular Biology,

Iowa State University, Ames IA 50011

Abstract

Hexokinase I (HKI) is the pacemaker of glycolysis in the red blood cell, being subject to potent feedback inhibition by its product glucose 6-phosphate (Glc-6-P) and the relief of that inhibition by inorganic phosphate (P_i). Presented here are investigations of glucose 1,6-bisphosphate (Glc-1,6-P_2) as an inhibitor of HKI, using kinetics, directed mutation, crystallography and molecular dynamics. The data support the hypothesis of an alternative binding mode for 1,5-anhydroglucitol 6-phosphate (1,5-anhydroGlc-6-P) as the basis for its nonlinear competitive inhibition of HKI. In addition, the investigations identify Lys418 (N-terminal half) and Lys866 (C-terminal half) as critical elements of networks of hydrogen bonds that support potent inhibition of HKI by 1,5-anhydroGlc-6-P. A new approach to the analysis of data from kinetics for the first time provides site dissociation constants for wild-type and mutant forms of HKI. Wild-type and many mutant forms of HKI exhibit binding antagonism between sites of inhibition at the N- and C-terminal halves, with the N-terminal half having the site of high binding affinity. Specific mutations, however, can result in binding synergism and/or change the site of high binding affinity to the C-terminal half. The analysis here is broadly applicable to any form of HKI that exhibits P_i-relief of inhibition.

Introduction

Hexokinase (ATP: D-hexose 6-phosphotransferase, EC2.7.1.1) catalyzes the initial step of glycolysis, the phosphorylation of 6-hydroxyl group of glucose (Glc) using $[ATP\text{-}Mg]^{2-}$ as the phosphoryl donor [1-3]. Four isozymes of hexokinase have been identified in mammalian tissues[4]. Type I, II and III hexokinase isozymes have molecular weights of 100 kDa, and share 70% sequence identity[5]. N- and C-terminal halves of isozymes I–III have ~50%

sequence identity[5], putatively a result of the duplication and fusion of the gene for a primordial hexokinase[6-9]. Hexokinase IV (glucokinase) and yeast hexokinase isoforms A and B have molecular weights of 50 kDa, and exhibit significant sequence similarity to both halves of isozymes I–III[5].

Despite sequence and structural similarities, isozymes I-III differ significantly in functional properties. Both halves of hexokinase II possess catalytic activity[10], whereas the N-terminal halves of hexokinase I and III are inactive[5, 11-12]. The reaction product glucose-6-phosphate (Glc-6-P) potently inhibits isozymes I-III (but not isoform IV) at physiological concentrations[5]. Inorganic phosphate (P_i) is a weak inhibitor of hexokinase II and III[5]; however, P_i antagonizes the inhibition of hexokinase I by 1,5-anhydroglucose 6-phosphate (1,5-anhydroGlc-6-P, an analog of Glc-6-P used in kinetics) at low (micromolar) concentrations, whereas, at millimolar concentrations P_i inhibits catalysis competitively with ATP[5].

Substantial evidence supports a single high-affinity binding site for Glc-6-P. Equilibrium dialysis experiments indicate sub-micromolar dissociation constants for Glc-6-P from HKI, with a binding stoichiometry of one mole of inhibitor per mole of enzyme[13-14]. Fluorescence binding studies are consistent with a single binding site for Glc-6-P with a sub-micromolar dissociation constant (Chapter 2, this thesis). Glc-6-P up to concentrations of 1 mM is a linear competitive inhibitor with respect to ATP[20]. Other observations, however, point to multiple sites of inhibitor action and the possibility of two high-affinity sites. Glc-6-P binds to both halves of HKI in crystal structures, and exhibits essentially identical hydrogen bonding interactions[15-17]. Proteolytic cleavage of HKI produces an active C-terminal half (mini-HKI), inhibited potently by 1,5-anhydroglucose 6-phosphate (1,5-anhydroGlc-6-P, an analog of Glc-6-P used in kinetics) with no P_i-relief of inhibition[12, 18]. The N-terminal half of HKI is inactive, but still binds Glc-6-P tightly[11-12]. 1,5-AnhydroGlc-6-P remains a potent inhibitor of mutant forms of HKI that eliminate inhibitor binding at either the N- or C-terminal half[19-20]. Only mutations at both Glc-6-P binding sites eliminate inhibition[20]. Finally, 1,5-anhydroGlc-6-P is a nonlinear competitive inhibitor with respect to ATP of wild-type HKI[19].

These observations have been the basis for numerous models to explain the functional properties of HKI. Fromm and colleagues favor a single, high-affinity binding site at the C-terminal half that physically overlaps the ATP pocket, but allows glucose to bind to the active site[14, 21-22]. Alternatively, Wilson and colleagues assign the site of high-affinity association of Glc-6-P to the N-terminal half (allosteric mechanism of inhibition)[11, 23]. P_i relieves Glc-6-P inhibition in the Fromm model by binding to the N-terminal half (allosteric mechanism for P_i-relief), and in the Wilson model P_i binds to the 6-phosphoryl site of Glc-6-P[5, 24]. These models have undergone revision over time. The discovery of potent inhibition of mini HKI necessitated an adjustment to the Wilson model, acknowledging the existence of a latent high-affinity site for inhibition at the C-terminal half unmasked by the removal of the N-terminal half[5]. Similarly, the persistence of high-affinity inhibition by 1,5-anhydroGlc-6-P exhibited by T536A HKI is consistent with a mechanism of allosteric inhibition[20]. To reconcile one high-affinity site in equilibrium binding studies and two high affinity sites implied by crystal structures and mutant forms of HKI, Liu *et al.*[20] proposed a model of equal high-affinity sites coupled by negative cooperativity.

Evidence presented in Chapter 2 of this thesis, however, cannot be reconciled with a model of two high-affinity inhibitory sites coupled by negative cooperativity. D413N and/or D861N forms of HKI exhibit nonlinear competitive inhibition by 1,5-anhydroGlc-6-P such that the N- and C-terminal half binding sites must have unequal affinities and be coupled by binding synergism. In this model P_i binds to the N-terminal half, blocking the high-affinity site and elevating the dissociation constant at the C-terminal site through loss of binding synergism. Data from wild-type HKI is consistent with this model as well, further adding to the list of possible mechanisms of inhibition. The mechanism of inhibition is completely determined, however, by assigning values to site dissociation constants and an interaction or coupling parameter, and presented here is a method that accomplishes this goal and quantitatively establishes the mechanism of inhibition of HKI.

Binding synergism of 1,5-anhydroGlc-6-P is ascribed to an alternative binding mode to the C-terminal half of HKI observed in molecular dynamics simulations. Glucose 1,6-bisphosphate (Glc-1,6-P_2) is also an inhibitor of HKI[25-26], but it cannot adopt the alternative binding mode of 1,5-anhydroGlc-6-P because of unfavorable steric interactions

between its 1-phosphoryl group and the enzyme. Glc-1,6-P_2 is a linear competitive inhibitor with respect to ATP (up to 400 μM). At millimolar concentrations, a second molecule of Glc-1,6-P_2 binds to HKI with a dissociation constant of approximately 3 mM, relative to 240 μM for 1,5-anhydroGlc-6-P. Mutations of D413N and/or D861N enhance the binding affinity of Glc-1,6-P_2 to levels near those of 1,5-anhydroGlc-6-P, and still the inhibition mechanism remains linear competitive with respect to ATP. A crystal structure of D413N HKI with Glc-1,6-P_2 and molecular dynamics simulations implicate Lys418 and Lys866 in hydrogen bonding networks that support the recognition of the 1-OH of Glc-6-P. Mutations of K418A and/or K866A increase dissociation constants for 1,5-anhydroGlc-6-P, and K418A (but not K866A) significantly reduces P_i-relief of inhibition. These mutations, along with those in Chapter 2 of this thesis, cover a spectrum of inhibition mechanisms, from binding antagonism to synergism and from N-terminal to C-terminal dominant.

Materials and methods

Materials— A full-length cDNA of human hexokinase I, cloned into vector pET-11a was available from previous studies[18, 27-28]. Oligonucleotides came from IDT-DNA. DNA sequencing was done by the Iowa State University DNA Sequencing and Synthesis Facility. *Escherichia coli* strain DH5a and BL21 were from Invitrogen. DNaseI, phenylmethanesulfonyl fluoride (PMSF), leupeptin, bovine serum albumin (BSA), ATP, NADP, ampicillin, glucose 6-phosphate, and glucose 1,6-bisphosphate were from Sigma. 1,5-Anhydro-D-sorbitol was from Toronto Research Chemicals. Isopropyl-β-D-thiogalactopyranoside (IPTG) was from Bio-World. DEAE sepharose CL-6B and CHT ceramic hydroxyapatite (HA) Type II were from Bio-Rad. DEAE-5PW HPLC media was from Tosohaas. Glusoe-6-phosphate dehydrogenase (G6PDH) was from Roche.

Construction, Expression and Purification of Wild-type and Mutant Hexokinase I— The oligonucleotide primers for directed mutations are as follows: 5'-GAC-GGA-TCT-CTT-TAC-GCG-ACG-CAC-CCA-CAG-3' for K418A and 5'-GG-ACA-CTC-TAC-GCG-CTT-CAT-CCA-CAC-3' for K866A, where the altered codon is underlined.

A 200 ml culture of the transformed *Escherichia coli* BL21 was grown overnight at 37 ºC in LB medium (33mg/L ampicillin) and then 1.5% cell were transferred to 9.6L LB medium (33mg/L ampicillin). The culture was grown at 300 rpm and 37 ºC to A_{600}=1.0. The temperature then was reduced to 16 ºC, isopropyl-β-D-thiogalactopyranoside (IPTG) was added to a final concentration of 0.5 mM and the culture was grown at 200 rpm for 20-22 hr. at 16 ºC. The cells were re-suspended in 25 mM KP_i (pH 7.5), 5 mM glucose, 3 mM $MgCl_2$, 1 mM dithiothreitol (DTT), 1 mM phenylmethanesulfonyl fluoride (PMSF), 50 μg/ml DNaseI and 5 μg/ml leupeptin. The cells were broken by sonication and then centrifuged (33,000*x*g, 1 hr.). The supernatant fluid was adjusted to pH 7.5 and loaded onto a DEAE-anion exchange column, using 25 mM KP_i, 5 mM glucose, 1 mM dithiothreitol DTT (pH 7.5), with a gradient of 0–400 mM NaCl. The fractions containing HKI activity were pooled, concentrated and dialyzed against 50 mM KP_i (pH 7.0), 5 mM glucose, 1 mM dithiothreitol (DTT) and loaded onto a ceramics hydroxyapatite column with a gradient of 0.05–1 M KP_i (pH 7.0). HKI was collected and dialyzed against 25 mM KP_i, 5 mM glucose, 1 mM dithiothreitol (DTT) (pH 7.5), and further purified by DEAE-5PW HPLC chromatography with a gradient of 0–500 mM NaCl. The pure protein was identified by sodium dodecylsulfate polyacrylamide gel electrophoresis (SDS-PAGE)[29]. Protein concentration was determined by the method of Bradford with BSA as a standard[30].

Hexokinase Kinetics— Hexokinase activity was determined by the glucose-6-phosphate dehydrogenase (G6PDH, E.C.1.1.1.49) coupled spectrometric assay[28]. Commercial G6PDH, as precipitate from ammonium sulfate, was dialyzed against 80 mM Tris (pH 8.0) extensively to remove sulfate, which at millimolar concentrations causes relief of 1,5-anhydroGlc-6-P inhibition in the manner of P_i. 1,5-AnhydroGlc-6-P, which is not a substrate for G6PDH, is a surrogate for Glc-6-P in inhibition kinetics of HKI. The dicyclohexylamine salt of 1,5-anhydroGlc-6-P was prepared as described by Ferrari and Crane[31] and its concentration determined by the method of Drueckes *et al.*[32]. The concentration of hexokinase in kinetics assays was 1.2–2.0 μg/ml and the assay volume was 1 ml. The assay buffer was 80 mM Tris (pH 8.0), 0.4 mM NADP, 3 mM $MgCl_2$ and 2 mM Glc.

Crystal Preparation— All the crystals were grown by the hanging drop method. Wild-type or mutant forms of HKI stored in 25 mM KP_i (pH 7.5), 1 mM glucose, 1mM dithiothreitol (DTT) was concentrated to 20–30 mg/ml in 50-kDa cut-off centrifugational filtration tube, then subject to 12–15 cycles of wash at 4 ºC with 2–3 volumes of a ligand buffer. The ligand buffers are 40 mM α-Glc-1,6-P_2 or 20 mM Glc-6-P, all pH 7.5, with 1 mM Glc. 3 μl of the resulting solutions, containing 15–20 mg/ml protein in the ligand buffer, was combined with an equal volume of precipitant solution containing 4.5-6.5% (w/v) polyethylene glycol 4000 or polyethylene glycol 8000, 0.1 M sodium acetate and 0.1 M sodium citrate, pH 6.0. The drops equilibrated against 0.5 ml of the precipitant solution. Prismatic needles of length 0.5–0.8 mm and width 0.2–0.3 mm grew in two to three weeks at 4 ºC. Crystals were transferred sequentially to a solution containing 1:1 ratio of the corresponding precipitant solution and 20% glycerol, and then to 1:1 ratio of the corresponding precipitant solution and 40% glycerol before flash freezing in liquid nitrogen.

X-ray Diffraction Data— X-ray diffraction data for D413N•Glc-6-P and D413N•Glc-1,6-P_2 were collected at APS SBC-sec19. Diffraction data were processed with HKL-3000[33].

Structure Determination, Model Building and Refinement— All crystals has unit cell parameters isomorphous to those of the $P2_1$ crystal form published previously[15-17, 34]. In these crystal forms, HKI is a homodimer consistent with the results of ultracentrifugation studies[37], which reports the dimer prevails at concentrations of protein above 1 mg/ml in the presence of saturating concentrations of Glc and Glc-6-P. Crystal structures were solved by molecular replacement using the HKI•Glc-6-P•Glc complex (PDB entry 1HKB)[15], less ligands and water molecules. The program AMoRe or Molrep from CCP4 suite was used in calculation of rotation and translation functions, based on data to 3 Å resolution[35, 36]. The program RefMac from CCP4 suite was used to refine the structures[37]. Further refinement employed CNS with hydrogen bond restraints[38]. Manual adjustments in the conformation of specific residues employed the program XTALVIEW[39].

Molecular Dynamics Simulations— NAMD package with the CHARMM 27 force field was used for molecular dynamics simulations on hexokinase I[40, 41]. The initial coordinates came from chain A of each of the crystalline complexes. TIP3P water molecules were

added into a rectangular water box surrounding the single molecule of HKI with a buffering distance of 15 Å[42]. To balance the net charge of system, sodium and chloride ions were added. Periodic boundary conditions were applied and the Particle mesh Ewald algorithm was used for the calculation of long-range electrostatic interactions[43]. Non-bonded *Van der Waals* interactions were applied with a cutoff of 12 Å. The integration time step was 2.0 fs. All models were energy-minimized for 100 ps and gradually heated to 300 K to relax unfavorable contacts (if any), followed by another 100 ps simulation to equilibrate the system. Finally, simulations of 10 ns were carried out at constant pressure and temperature (1.01325 bar and 300 K).

Principal Component Analysis (PCA)— Principal component analysis was applied to extract functionally important motions from simulations. Rigid-body translations and rotations of the tetramer were removed before PCA by aligning trajectory structures onto the starting structure. Principle components were calculated by decomposing the covariance matrix *C* which was calculated from the molecular dynamics trajectory as:

$$C_{ij} = \left\langle \left(r_i - \left\langle r_i \right\rangle\right) \bullet \left(r_j - \left\langle r_j \right\rangle\right) \right\rangle,$$

where $i,j = 1,...3N$, N is the total number of C_α atoms in the structure, r is the Cartesian coordinates of i^{th} C_α atom, and the angle brackets denote an average over the entire trajectory. The Carma package was used in PCA analysis and VMD was used to visualize the principal motions[47,48].

Results

Kinetics of wild-type and mutant hexokinases— Asp413 and Asp861 hydrogen bond with the 1-OH group of Glc-6-P (bound as the β-anomer in crystal structures), so mutations here were not expected to have a substantial effect on inhibition of HKI by 1,5-anhydroGlc-6-P or Glc-1,6-P_2 as the former lacks the 1-OH group altogether and the latter is a phosphoryl-linked α-anomer. Parameters (Table I) for 1,5-anhydroGlc-6-P are reproduced from Chapter 2 to facilitate the comparison to those for Glc-1,6-P_2. The effects of the same series of mutations as probed by the two inhibitors differ significantly. 1,5-AnhydroGlc-6-P

is a nonlinear competitive inhibitor of all four enzymes, whereas Glc-1,6-P_2 is a linear competitive inhibitor at concentrations up to 400 μM. A second molecule of Glc-1,6-P_2 binds to HKI with a dissociation constant of approximately 3 mM, approximately 10-fold higher than K_{II} (240 μM) reported for 1,5-anhydroGlc-6-P (Figure 1). The effect of single mutations at position 413 and 861 is a uniform decrease in the K_I of Glc-1,6-P_2, whether the mutation is at the N-terminal or C-terminal half. The effect of the double mutation (D413/861N) appears additive, its K_I approaching that of 1,5-anhydroGlc-6-P for the wild-type enzyme. Same mutations cause K_I of 1,5-anhydroGlc-6-P to increase and K_{II} to decrease.

Motivation for the mutation of Lys418 and Lys866 come from crystallographic structures and molecular dynamics simulations (details of which follow in the results section) which indicate an important role for the side chains at positions 418 and 866 in stabilizing hydrogen bonds between inhibitor and protein. Parameters from kinetics of K418A and/or K866A verify the significance of lysines at positions 418 and/or 866 (Table II). Inhibition by 1,5-anhydroGlc-6-P is 2- to 8-fold weaker for mutant enzymes relative to wild-type or mini HKI. P_i-relief of 1,5-anhydroGlc-6-P inhibition is greatly reduced in constructs that include K418A, even though position 418 is relatively far from the binding site for P_i at the N-terminal half.

Crystalline Complex of D413N HKI with Glc-1,6-P_2— Wild-type HKI did not form quality crystals in the presence of Glc-1,6-P_2, even though control crystallization experiments produced good crystals with Glc-6-P. Glc-1,6-P_2, however, binds with higher affinity to D413N HKI than to wild-type enzyme, and this mutant enzyme produced crystals (Table III) isomorphous to those of the Glc/Glc-6-P complex of the wild-type enzyme[15] (Figure 2). Superpositions of single chains from the Glc/Glc-1,6-P_2 complex with D413N HKI give root-mean-square deviations of less than 0.5 Å. Each asymmetric unit contains a homodimer with observable electron density for residues 16–914. The polypeptide chain crosses three times between large and small domains; residues 16–74 and 210–447 belong to the large domain and residues 75–209 and 448–466 to the small domain of the N-terminal half and residues 467–522 and 658–895 belong to the large domain and residues 523–657 and 896–914 to the small domain of C-terminal half. The two halves of each subunit

contain molecules of Glc and Glc-1,6-P_2 bound to a crevice between large and small domains.

Glc-1,6-P_2 is associated with strong electron density in the C-terminal half and relatively weak density at the N-terminal half, as has been recognized in previously reported crystal structures of 6-phosphoryl ligand complexes of wild-type HKI. Nonetheless, hydrogen bonds between Glc-1,6-P_2 and the N- and C-terminal halves are comparable, and aside from differences due to the α-1-phosphoryl group, are similar to those of Glc-6-P (Table IV). Hydrogen bonds evidently peculiar to the Glc-1,6-P_2 complex involve R91/539 and 1-phosphoryl group (Figure 3). In addition, the structure reveals a hydrogen bond between Lys866 and the backbone carbonyl of Ser893 that draws residues 893-897 closer to the ligand and stabilizes the interaction between 2-hydroxyl group of the inhibitor and Ser897 (Figure 4).

Molecular Dynamics Simulation of the D413N HKI with Glc-1,6-P_2— All simulations presented here begin with the equilibration of a crystallographic structure of the ligated complex of HKI. Root-mean-square deviations (RMSD) of Glc-1,6-P_2 at the C-terminal half are higher than those at the N-terminal half (Figure 5), and comparable to the difference observed for Glc-6-P in previous work (Chapter 2, this thesis). The systematic difference in RMSD values is due primarily to the movement of loop 533–538 away from the 6-phosphoryl group of the ligand (Figure 3), allowing additional space in the binding pocket. Elevated movement of Glc-1,6-P_2 at the C-terminal half, however, does not lead to ligand dissociation or a bimodal distribution in principal component analysis. The distribution of conformational states as represent by the two principal components in the simulation of D413N HKI with Glc-1,6-P_2 is unimodal and much like that observed for Glc-6-P (Figure 6).

Thr536 forms hydrogen bonds with the 6-phosphoryl group of the Glc-1,6-P_2 in the crystal structure, but hydrogen bonds are virtually nonexistent over the simulation (Tables V & VI). In contrast, hydrogen bonds between Ser88 and the 6-phosphoryl group of Glc-1,6-P_2 are present at levels of 100%. The simulation of Glc-6-P in the D413N HKI reveals a different outcome: hydrogen bonds are established between Thr536 (as well as Ser88) and the 6-phosphoryl group (Table VI). The 1-phosphoryl group of Glc-1,6-P_2

group makes hydrogen bonds with Arg91 (N-terminal half) and Arg539 (C-terminal half) over the entire simulation, as observed in the crystal structure (Figure 3). Furthermore, the 1-phosphoryl group of Glc-1,6-P_2 group makes hydrogen bonds with Lys418 (N-terminal half) and Lys866 (C-terminal half) over the entire simulation; and this is not seen in the crystal structures (Figure 3).

The simulation of D413N or wild-type enzyme with Glc-6-P reveals a stable hydrogen bond between Asn413 or Asp413 (N-terminal half) and Asp 861 (C-terminal half) with 1-hydroxyl group of Glc-6-P. In the simulation of D413N HKI with Glc-1,6-P_2, however, no such hydrogen bonds exist because of the substitution of 1-α-phosphoryl for the 1-β-hydroxyl group. Instead, Asn413 forms a hydrogen bond with the backbone carbonyl of Gly448 (in 25% of frames), and Asp861 forms a hydrogen bond with side chain of Ser893 (in 61% of frames). A stable hydrogen bond exists between Asp861 and Lys866 (90% of frames) during the simulation of D413N HKI with Glc-1,6-P_2, but its counterpart (hydrogen bond between Asn413 and Lys418) at the N-terminal half is nearly absent (present in 5% of frames). By comparison, Asn413 and Lys418 from a hydrogen bond (52% of frames), and so too do Asp861 and Ly866 (99% of frames), in the simulation of D413N HKI with Glc-6-P. The simulation of wild type enzyme with Glc-6-P exhibited stable hydrogen bonds at both halves (99% of frames).

Discussion

Wild-type, D413N and/or D861N forms of HKI exhibit nonlinear competitive inhibition by 1,5-anhydroGlc-6-P with respect to ATP[19]. Moreover, the stoichiometric constants for the dissociation of 1,5-anhydroGlc-6-P from singly-ligated HKI and doubly-ligated HKI, were so close in value as to require a model of synergistic binding to sites of unequal affinity (Chapter 2, this thesis). Synergism in binding hypothetically comes from an alternative binding mode for 1,5-anhydroGlc-6-P to the C-terminal half as revealed by a molecular dynamics simulation. Glc-1,6-P_2, however, should not favor this alternative binding mode because of unfavorable steric effects between its α-1-phosphoryl group and the protein. Hence, wild-type, D413N and/or D861N should exhibit only linear competitive inhibition

with respect to ATP, as is indeed the case (Table I) and principal component analysis should exhibit a unimodal distribution indicative of a single binding mode, which is evident from Figure 6.

Asp413 and Asp861 in the wild-type enzyme would have unfavorable electrostatic interactions with the 1-phosphoryl group of Glc-1,6-P_2, and hence mutations of these residues to asparagines could enhance binding affinity by the reduction of negative charge. On the other hand, the loss of charge at positions 413 and 861 could destabilize hydrogen bonding networks involving Lys418 and Lys866 (Asp413 and Asp861 interact directly with Lys418 and Lys866, respectively), and as a consequence weaken interactions with the 2-OH group of the inhibitor. 1,5-AnhydroGlc-6-P derives no benefit in the reduction of negative electrostatic charge, hence its K_I rises due to mutations at 418 and 861 (Table I). Evidently, the reduction of negative charge more than compensates for the weakening of hydrogen bonds causing K_I values of Glc-1,6-P_2 to decrease.

Simulations with 1,5-anhydroGlc-6-P and Glc-6-P put the high affinity site at the N-terminal half (Chapter 2, this thesis), and here a simulation of the Glc-1,6-P_2 complex with D413N HKI indicates a loss of interaction with Thr536 (C-terminal half) while hydrogen bonds persist between protein and ligand at the N-terminal half (Table VI). Again, as for Glc-6-P and 1,5-anhydroGlc-6-P, RMSD values for Glc-1,6-P_2 are consistent with tighter interactions at the N-terminal half relative to the C-terminal half. These observations favor the model of inhibition proposed by Wilson.

Partial relief of inhibition exhibited by K418A is not consistent with the Wilson model in which P_i and inhibitor are mutually exclusive in binding to a single site. Indeed, although Lys418 is in the N-terminal half, its location is removed from the binding site for P_i, and more likely to weaken interactions with inhibitor without loss of binding affinity for P_i. Although P_i-relief of 85% is not 100%, the prevailing belief has been one of mutually exclusive binding of P_i and inhibitor[5]. The existence of K418A HKI with 50% P_i-relief forces reexamination of existing models of allosteric regulation, leading directly to Scheme I:

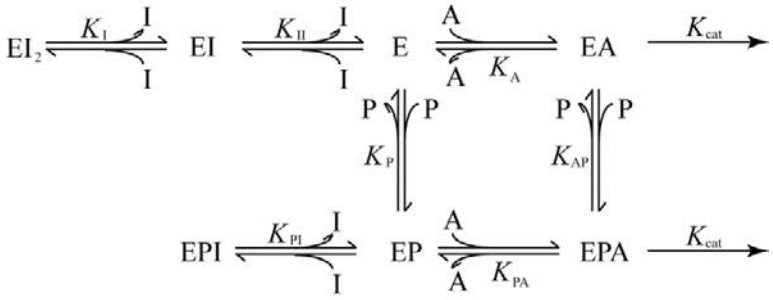

Scheme I

As glucose is saturating in Scheme I, all enzyme states have bound glucose, [*A*] represents the concentration of $[ATP\text{-}Mg]^{2-}$, [*P*] the concentration of P_i, and [*I*] the concentration of 1,5-anhydroGlc-6-P. Scheme I differs from past models in allowing 1,5-anhydroGlc-6-P (*I*) and P_i (*P*) to form an *EPI* complex. This complex has P_i bound to the N-terminal half, eliminating the high-affinity site for inhibitor (by direct displacement or allostery), and in addition a molecule of inhibitor bound to the C-terminal half with relative low affinity. The relationship of reciprocal velocity to [*A*], [*I*], [*P*] and V_{max} (maximum velocity) is given by Eqn. 1 as follows:

$$\frac{1}{V} = \frac{1}{V_{max}}\left(\frac{1+\frac{[A]}{K_A}+\frac{[P]}{K_P}+\frac{[I]}{K_I}+\frac{[A][P]}{K_A K_{AP}}+\frac{[I]^2}{K_I K_{II}}+\frac{[P][I]}{K_P K_{PI}}}{\frac{[A]}{K_A}+\frac{[A][P]}{K_A K_{AP}}}\right) \qquad \text{Eqn. 1}$$

Eqn. 1 can be simplified by letting [*P*] to go to infinity, and having $[A] = K_A$ (conditions of assay) and $K_P = K_{AP}$ (Michaelis constants for ATP are independent of P_i levels). The resulting equation is as follows:

$$\frac{1}{V} = \frac{1}{V_{max}}\left(\frac{\frac{1}{K_P}+\frac{1}{K_{AP}}+\frac{[I]}{K_P K_{PI}}}{\frac{1}{K_{AP}}}\right) = \frac{1}{V_{max}}\left(2+\frac{[I]}{K_{PI}}\right) \qquad \text{Eqn. 2}$$

A plot of 1/*V* versus [I] at saturating concentrations of P_i is linear (as observed), and K_{PI} is one-half of the intercept divided by the slope.

K_{PI} values run from 45–100 μM for 1,5-anhydroGlc-6-P and 210–520 μM for Glc-1,6-P_2 (Table VIII). In the presence of saturating P_i, inhibition by Glc-1,6-P_2 is weaker (K_{PI} higher) than that caused by 1,5-anhydroGlc-6-P, and yet P_i-relief is consistently greater

for 1,5-anhydroGlc-6-P than Glc-1,6-P_2. Moreover, K418A has 50% P_i-relief, but its K_{PI} with respect to 1,5-anhydroGlc-6-P is identical to that of wild-type enzyme which exhibits 85% P_i-relief (Table VI). These apparent discrepancies stem from the dependence of P_i-relief on K_I. In fact if K_{II} is large, then P_i relief $= 100 \times (1-K_I/K_{PI})$. In the case of K418A, K_I increases twofold, but K_{PI} remains unchanged. Hence, the decrease in P_i-relief due to the K418A mutation results from an increase in K_I with no change in K_{PI}. For the mutation K866A, K_{PI} increases 6-fold, but K_I also increases so that P_i-relief is unchanged from that of the wild-type enzyme.

The K_{PI} parameter here offers several advantages and potential insights heretofore not appreciated. Firstly, K_{PI} is a more reliable parameter than K_I or K_{II}. K_I (and hence K_{II}) is sensitive to uncontrolled levels of P_i (contaminants of substrates and/or inhibitors) or sulfate (incomplete dialysis of coupling enzymes), whereas the determination of K_{PI} occurs in the presence of saturating P_i. Secondly, K_{PI} is a direct measure of a site affinity constant, the dissociation of inhibitor from a P_i-HKI complex that has only a single binding site for inhibitor. That binding site, given the overwhelming evidence for the binding of P_i to the N-terminal half, must be at the C-terminal half. Indeed, mutations in the C-terminal half cause significant changes in K_{PI} (Table VIII), whereas most mutations to the N-terminal half have little effect. Thirdly, a mutation in the N-terminal half that changes K_{PI} could result from a perturbation to the allosteric machinery linking the N- and C-terminal halves of HKI.

The second attribute of K_{PI} listed in the foregoing is of particular interest. K_{PI} as a site-dissociation constant for inhibitor at the C-terminal half is a possible measure of the site-affinity constant ${}^0M_2$ introduced in Chapter 2 of this thesis. Given numerical values for K_I, K_{II} and ${}^0M_2$, one can calculate a value for α and ${}^0M_1$ for any HKI construct as follows:

$$\alpha = \left({}^0M_2\right)^2 \Big/ \left\{K_{II}\left({}^0M_2 - K_I\right)\right\} \quad \text{and} \quad {}^0M_1 = \alpha K_{II} - {}^0M_2 \qquad \text{Eqn. 3}$$

Values of α, ${}^0M_2$ and ${}^0M_1$ for each HKI construct studied here are in Table VIII. Values for α vary over a relatively narrow range. The addition of ± 2σ to values of K_{II} change α,

but values for $^0M_1$ are not altered. (As α is proportional to $1/K_{II}$ in Eqn. 3, fixed values of K_I and $^0M_2$ require the product αK_{II} to be constant. Hence, $^0M_1 = \alpha K_{II} - {}^0M_2$ must also be constant). We see from Table VIII that the mutation of Lys418 to alanine causes a 5-fold increase in $^0M_1$ and redefines the high-affinity binding site as $^0M_2$ (which remains unchanged from that of the wild-type enzyme), that is the C-terminal half has now the site of high-affinity, and not surprisingly, P_i-relief has fallen to 44% (Table II). The mutation of Lys866 to alanine on the other hand, increases $^0M_2$ by 6-fold, but causes only a twofold increase in $^0M_1$. Hence, the site of high affinity remains at the N-terminal half. Finally K418/866A causes a 7.6-fold increase in $^0M_2$ (C-terminal half) and a 9-fold increase in $^0M_1$ (N-terminal half) relative to the wild-type enzyme. By teasing out site-dissociation constants from the data, the effects of single and double mutations are consistent and clear. Values for K_I and K_{II} alone, however, do not reveal the impact of a specific mutation on inhibitor binding to a specific site.

The mechanism of inhibition due to Glc-1,6-P_2 stands in contrast to that 1,5-anhydroGlc-6-P for all but the wild-type enzyme. Two inhibitor molecules bind with antagonism to the wild-type enzyme (α significantly below unity); however, for the D413N and/or D861N mutant enzymes, two molecules of 1,5-anhydroGlc-6-P bind with synergism, whereas two molecules of Glc-1,6-P_2 bind with antagonism. Although the value of K_{II} for Glc-1,6-P_2 is uncertain, values as low as 500 μM (clearly not observed from the kinetics data) would still require α less than unity. Hence, the mechanism of inhibition of HKI is not only sensitive to single mutations, but also dependent on the molecular structure of the inhibitor. In fact, Glc-1,6-P_2 might better approximate the properties of Glc-6-P than does 1,5-anhydroGlc-6-P on the basis of molecular dynamics simulation presented here and in Chapter 2 of this thesis.

In the brain cell, intracellular concentrations of Glc are close to 5 μM, hence the concentration of Glc-6-P may never rise to a level that directly inhibits the C-terminal half. P_i-relief then is adequate by itself in countering product inhibition. The situation in the red blood cell, however, may be different as serum levels of Glc are millimolar, and Glc-6-P concentrations are substantial relative to K_{PI}. Logically one would anticipate an additional

mechanism to relieve product inhibition, and indeed the effect of Glc on product inhibition seems a likely place to look for such a mechanism[46]. In the next Chapter of this thesis we show that the weak inhibition of HKI by 1,5-anhydroGlc-6-P is sensitive to the concentration of Glc.

Table I. Kinetics parameters for wild-type and mutant forms of HKI.[#]

HKI	k_{cat} s^{-1}	K_m^{Glc} μM	K_m^{ATP} mM	K_I[a] μM	K_{II}[a] μM	P_i-Relief/ 1,5-anhydroGlc-6-P %	K_i[b] μM	P_i-Relief/ Glc-1,6-P_2 %
WT	92 ± 1	45 ± 3	1.03 ± 0.02	20 ± 3	240 ± 50	85	169 ± 4	65
D413N	82 ± 1	57 ± 2	0.98 ± 0.06	23 ± 4	80 ± 20	80	106 ± 6	78
D861N	9.4 ± 0.1	37 ± 1	2.02 ± 0.09	30 ± 4	80 ± 20	86	67 ± 2	71
D413N/D861N	10.0 ± 0.1	32 ± 2	1.59 ± 0.06	35 ± 5	110 ± 40	78	44 ± 2	72

[#]Assays were in 80mM Tris, pH8.0, 1mM DTT, 0.4mM NADP, 3 mM $MgCl_2$ along with varying amounts of $[ATP\text{-}Mg]^{2-}$, Glc, P_i and/or 1,5-anhydroGlc-6-P. In the determination of K_m^{Glc}, the concentration of Glc varied from 1/ 6 K_m^{Glc} to 10 K_m^{Glc} and that of $[ATP\text{-}Mg]^{2-}$ was fixed at 9mM. In the determination of K_m^{ATP}, the concentration of $[ATP\text{-}Mg]^{2-}$ varied from 1/6 K_m^{ATP} to 6 K_m^{ATP} and that of Glc was fixed at 2 mM. In the determination of inhibition constants K_I and K_{II} for 1,5-anhydroGlc-6-P, the concentration of $[ATP\text{-}Mg]^{2-}$ varied from 1/2 K_m^{ATP} to 4 K_m^{ATP}, that of 1,5-anhydroGlc-6-P from 20 to 100 μM and that of Glc was fixed at 2 mM. Values for K_I and K_{II} were obtained by fitting data to a model of nonlinear competitive inhibition, the equation for which is as follows:

$$V = {V_{max}}\Big/\left[1 + (K_m^{ATP}) \times {1}/{S} + \left({K_m^{ATP}}/{K_I}\right) \times {I}/{S} + \left({K_m^{ATP}}/{K_I \times K_{II}}\right) \times {I^2}/{S}\right]$$

where S and I are concentrations of $[ATP\text{-}Mg]^{2-}$ and 1,5-anhydroGlc-6-P, respectively. In the determination of inhibition constant K_i for Glc-1,6-P_2, the concentration of $[ATP\text{-}Mg]^{2-}$ varied from 1/2 K_m^{ATP} to 6 K_m^{ATP}, that of Glc was fixed at 2 mM, and that of Glc-1,6-P_2 from 40 to 400 μM for wild-type HKI, 40 to 240 μM for D413N, 40 to 160 μM for D861N and D413N/D861N. Values for K_i were obtained by fitting data to a model of linear competitive inhibition, the equation for which is as follows:

$$V = {V_{max}}\Big/\left[1 + (K_m^{ATP}) \times {1}/{S} + \left({K_m^{ATP}}/{K_I}\right) \times {I}/{S}\right]$$

P_i-relief of inhibition is defined as 100×(A-B)/A, where A is the slope from plots of reciprocal relative velocity *versus* the concentration of 1,5-anhydroGlc-6-P or Glc-1,6-P_2 in the absence of P_i, and B is the slope from plot of reciprocal relative velocity *versus* inhibitor concentration in the presence of 3 or 6 mM P_i. Relative velocity is the ratio of velocity at a specific concentration of inhibitor to the velocity in the absence of inhibitor. The $[ATP\text{-}Mg]^{2-}$ concentration is fixed at K_m^{ATP}.

[a]Inhibition constants with respect to 1,5-anhydroGlc-6-P.

[b]Inhibition constants with respect to Glc-1,6-P_2.

Table II. Kinetics parameters for wild-type and mutant forms of HKI.[#]

HKI	k_{at} s^{-1}	K_m^{Glc} μM	K_m^{ATP} mM	K_I μM	K_{II} μM	P_i-Relief %
Wild-type	92 ± 1	45 ± 3	1.03 ± 0.02	20 ± 3 [a]	240 ± 50	85
Mini-HKI	40 ± 1	30 ± 3	0.95 ± 0.05	12.5 ± 0.6 [b]	NA[c]	NR[c]
K418A	63 ± 1	88 ± 4	0.93 ± 0.05	44 ± 4	1100 ± 500	44
K866A	66 ± 2	63 ± 4	1.48 ± 0.09	70 ± 10	400 ± 300	89
K418A/K866A	71 ± 1	56 ± 2	1.1 ± 0.1	170 ± 20	1500 ± 700	52
mini-K866A	41 ± 1	43 ± 3	2.9 ± 0.2	60 ± 3 [b]	NA[c]	NR[c]

[#]Assays were in 80mM Tris, pH8.0, 1mM DTT, 0.4mM NADP, 3 mM $MgCl_2$ along with varying amounts of $[ATP\text{-}Mg]^{2-}$, Glc, P_i and/or 1,5-anhydroGlc-6-P. In the determination of K_m^{Glc}, the concentration of Glc varied from 1/ 6 K_m^{Glc} to 10 K_m^{Glc} and that of $[ATP\text{-}Mg]^{2-}$ was fixed at 9 mM. In the determination of K_m^{ATP}, the concentration of $[ATP\text{-}Mg]^{2-}$ varied from 1/6 K_m^{ATP} to 6 K_m^{ATP} and that of Glc was fixed at 2 mM.

[a]In the determination of K_I and K_{II} for 1,5-anhydroGlc-6-P the concentration of Glc was fixed at 2 mM, that of $[ATP\text{-}Mg]^{2-}$ varied from 1/2 K_m^{ATP} to 4 K_m^{ATP}, that of 1,5-anhydroGlc-6-P from 12 to 200 μM for wild-type, K418A and K866A, from 25 to 400 μM for K418A/K866A double mutant. Values for K_I and K_{II} were obtained by fitting data to a model of nonlinear competitive inhibition, the equation for which is as follows:

$$V = {V_{max}}\Big/\left[1 + (K_m^{ATP}) \times {1}/{S} + \left({K_m^{ATP}}/{K_I}\right) \times {I}/{S} + \left({K_m^{ATP}}/{K_I \times K_{II}}\right) \times {I^2}/{S}\right]$$

where S and I are concentrations of $[ATP\text{-}Mg]^{2-}$ and 1,5-anhydroGlc-6-P, respectively. P_i-relief of inhibition is defined as 100×(A-B)/A, where A is the slope from plots of reciprocal relative velocity *versus* the concentration of 1,5-anhydroGlc-6-P or Glc-1,6-P_2 in the absence of P_i, and B is the slope from plot of reciprocal relative velocity *versus* inhibitor concentration in the presence of 3 or 6 mM P_i. Relative velocity is the ratio of velocity at a specific concentration of inhibitor to the velocity in the absence of inhibitor. The $[ATP\text{-}Mg]^{2-}$ concentration is fixed at K_m^{ATP}.

[b]In the determination of K_I for 1,5-anhydroGlc-6-P, the concentration of $[ATP\text{-}Mg]^{2-}$ varied from 1/2 K_m^{ATP} to 6 K_m^{ATP}, that of Glc was fixed at 2 mM, that of 1,5-anhydroGlc-6-P from 20 to 100 μM for mini-HKI, 30 to 160 μM for mini-K866A. Values for K_I were obtained by fitting data to a model of linear competitive inhibition, the equation for which is as follows:

$$V = {V_{max}}\Big/\left[1 + (K_m^{ATP}) \times {1}/{S} + \left({K_m^{ATP}}/{K_I}\right) \times {I}/{S}\right]$$

[c]N.A.: Not Applicable; N.R.: No Relief.

Table III. Statistics of data collection and refinement Statistics for HKI complex with Glc-6-P or Glc-1,6-P_2.

Protein	**Wild-type**[#]	**D413N**[#]	**D413N**
Ligand	**Glc-6-P**	**Glc-6-P**	**Glc-1,6-P_2**
Space group	P2(1)	P2(1)	P2(1)
Unit cell parameters			
a (Å)	82.63	82.607	82.255
b (Å)	121.53	121.140	120.748
c (Å)	119.83	119.888	120.556
α (°)	90	90	90
β (°)	92.82	92.69	92.62
γ (°)	90	90	90
Resolution limits (Å)	37.90-2.65	44.15-2.48	35.41-2.40
No. of reflections	245322	3458364	1901444
No. of unique reflections	68327	83067	92019
% Completeness (overall)	99.22	98.47	98.52
% Completeness (last shell)	98.99	84.92	95.11
R_{sym} [a]	0.061	0.070	0.046
R-factor [b]	0.2421	0.2391	0.2472
R_{free} [c]	0.2565	0.2527	0.2729
No. of atoms in refinement	14481	14394	14497
No. of water molecules	273	186	275
Mean B parameters (Å^2)			
Main chain	55	61	53
Side chain	57	63	55
Glucose, N-half	45	52	45
Glucose, C-half	35	40	36
Phosphoryl ligand, N-half	51	78	52
Phosphoryl ligand, C-half	35	42	32
Root mean square deviations			
Bond lengths (Å)	0.004	0.004	0.004
Bond angles (°)	0.907	0.889	1.070

[#]Data reproduced from Chapter 2 to facilitate the comparison to those for Glc-1,6-P_2.

[a]$R_{sys} = \Sigma_j \Sigma_i |I_{ij} - \langle I_j \rangle| / \Sigma_i \Sigma_j I_{ij}$, where *i* runs over multiple observations of the same intensity and *j* runs over crystallographically unique intensities.

[b]*R*-factor = $\Sigma \| F_{obs} - F_{calc} \| / \Sigma |F_{obs}|$, $F_{obs} > 0$.

[c]R_{free}- is based upon 10% of the data randomly culled and not used in the refinement.

Table IV. Donor-acceptor distances between phosphoryl ligand and protein in crystal structures[#]

(Two chains are listed separately with at least one donor-acceptor distance ≤ 3.2 Å.)

Phosphoryl Ligand	Residue	Wild-type/Glc-6-P				D413N/Glc-6-P				D413N/Glc-1,6-P_2			
		NA	**NB**	**CA**	**CB**	**NA**	**NB**	**CA**	**CB**	**NA**	**NB**	**CA**	**CB**
O1	D/N413/861[$]:OD1	2.9	3.1			3.5	3.2						
	D/N413/861[$]:O/ND2	2.7	2.5	2.6	3.1	2.5	3.0	2.5	3.3				
O2	D84/532:OD2	2.5	2.9	2.8	2.8	2.5	2.8	2.8	2.7	2.9	3.1	2.9	3.0
	R91/539:NH1					2.7	4.9						
	S449/897:N	3.7	3.1	2.9	2.8	3.3	3.2	2.8	3.0	3.5	3.2	3.0	3.1
	S449/897:OG			3.2	3.6								
O3	D84/532:OD1	2.5	2.8	2.7	2.9	3.2	3.0	2.8	3.0	2.9	3.1	2.7	2.8
	D84/532:OD2	2.7	3.3			2.7	3.2			2.5	3.1		
	S449/897:OG	2.9	2.7	2.5	2.7	2.8	2.8	2.5	2.8	3.5	2.9	2.6	3.1
O4	D209/657:OD2	2.8	2.7	2.9	2.6	2.7	2.7	2.9	2.5	2.8	2.9	3.0	2.6
O1P	S88/T536:N	3.1	3.6			3.1	3.6						
	S88/T536:OG(1)												
	T232/680:N	3.1	2.9	2.8	2.9	3.4	2.8	2.9	2.9	2.9	3.0	2.7	2.9
	T232/680:OG	2.5	2.5	2.7	2.8	2.6	2.6	2.7	2.9	2.5	2.6	2.8	2.8
O2P	S88/T536:OG(1)	2.7	4.2			3.2	3.5						
	T232/680:N	3.3	3.2			3.1	3.8						
	S415/T863:N	2.8	2.9	2.9	2.9	2.8	3.1	2.8	2.8	2.8	3.0	2.9	3.0
	S415/T863:OG(1)	2.6	2.7	2.6	2.5	3.2	2.5	2.8	2.5	2.8	2.7	2.6	2.5
O3P	S88/T536:N	2.8	2.9	2.9	2.9	3.3	2.7	2.8	3.0	2.9	3.1	3.1	3.1
	S88/T536:OG(1)	2.5	2.5	2.7	2.7	2.5	2.6	2.9	2.8	2.7	2.8	2.9	2.9
O1P[*]	N537:OD2											3.1	3.4
	R91/539:NH1									3.7	2.9	3.0	5.2
	R91/539:NH2									3.2	3.3	3.3	2.9

[#]O1P, O2P and O3P are the oxygen atoms from 6-phosphoryl group. O1P[*] is an oxygen atom from 1-phosphoryl group of Glc-1,6-P_2.

[$]D/N413/861 means either D or N 413 from N-terminal half and D861 from C-terminal half.

Table V. Fraction of frames from molecular dynamics simulations with hydrogen bonds between protein residues and 6-phosphoryl ligands[$].

Phosphoryl Ligand	Residue	Wild-type/Glc-6-P		D413N/Glc-6-P		D413N/Glc-1,6-P_2	
		N	C	N	C	N	C
O1	D/N413/861:OD1	0.62	0.90	0.09	0.91	---	---
	D/N413/861:O/ND2	0.52	0.69	0.68	0.62	---	---
	K418/866:NZ	0.47	0.14	0.03	0.61	---	---
	R91/539:NH2	---	---	---	---	0.07	0.29
O2	D84/532:OD1	0.22	0.91	0.41	0.12	---	---
	D84/532:OD2	0.79	0.87	0.73	0.86	---	---
	R91/539:NH1	0.04	---	0.02	0.07	0.06	---
	R91/539:NH2	0.08	0.06	---	---	0.07	0.33
	S449/897:N	0.45	0.15	0.26	0.56	0.26	0.13
	S449/897:OG	0.01	---	0.01	0.03	0.02	0.02
O3	D84/532:OD1	0.85	0.98	0.81	0.81	0.33	0.10
	D84/532:OD2	0.70	---	0.64	0.33	0.43	0.83
	D209/657:OD2	---	---	---	0.05	---	---
	S449/897:OG	0.90	0.96	0.86	0.98	0.89	0.79
O4	G87/535:N	---	0.54	---	0.06	0.10	0.13
	D209/657:OD2	1.00	1.00	1.00	0.99	0.98	0.93
	Glc:O6	---	---	---	---	---	---
O1P	S88/T536:N	0.48	---	0.08	0.07	0.12	---
	S88/T536:OG(1)	0.45	---	0.20	---	---	---
	T232/680:N	0.25	0.42	0.46	0.98	0.87	0.68
	T232/680:OG1	0.25	0.43	0.44	1.00	0.98	0.98
	S415/T863:N	0.20	---	0.48	---	---	---
	S415/T863:OG(1)	0.30	---	0.58	---	---	---
O2P	S88/T536:N	0.33	---	0.56	---	---	---
	S88/T536:OG(1)	0.46	---	0.70	---	0.02	---
	T232/680:N	0.45	0.54	0.00	0.05	0.27	0.43
	T232/680:OG1	0.47	0.57	0.00	---	0.05	0.15
	S415/T863:N	0.19	0.39	0.37	0.86	0.75	0.46
	S415/T863:OG(1)	0.25	0.43	0.43	1.00	1.00	1.00
O3P	S88/T536:N	0.27	0.04	0.42	0.99	0.99	0.04
	S88/T536:OG(1)	0.27	0.04	0.29	1.00	1.00	0.03
	T232/680:N	0.27	0.05	0.56	---	---	---
	T232/680:OG1	0.29	---	0.57	---	---	0.03
	S415/T863:N	0.38	0.50	0.00	---	---	---
	S415/T863:OG(1)	0.48	0.57	0.00	---	---	---
O1P*	R91/539:NH1	---	---	---	---	0.46	0.49
	R91/539:NH2	---	---	---	---	0.39	0.32
O2P*	R91/539:NH1	---	---	---	---	---	0.16
	K418/866:NZ	---	---	---	---	0.92	0.44
O3P*	R91/539:NH1	---	---	---	---	0.72	0.46
	R91/539:NH2	---	---	---	---	0.24	0.30
	K418/866:NZ	---	---	---	---	0.43	0.45

[$]Donor-acceptor distance $\leq$ 3.2 Å between pairs of polar atoms infers the presence of a hydrogen bond. The absence of a value indicates less than 0.01 of frames exhibited a hydrogen bond. O1P, O2P and O3P are oxygen atoms of 6-phosphoryl group and O1P*, O2P*, O3P* are those of the 1-phosphoryl group of Glc-1,6-P_2

Table VI. Fraction of frames from molecular dynamics simulations with hydrogen bonds between protein residues and the 6-phosphoryl groups of ligands[$].

Residue	Wild-type/Glc-6-P		D413N/Glc-6-P		D413N/Glc-1,6-P_2	
	N	C	N	C	N	C
S88/T536:N[$]	0.99	0.04	0.98	0.99	0.99	0.04
S88/T536:OG(1)[$]	0.92	0.04	0.96	1.00	1.00	0.03
S88/T536[#]	1.00	0.04	1.00	1.00	1.00	0.04
T232/680:N[$]	0.96	0.97	0.99	0.98	0.95	0.90
T232/680:OG1[$]	1.00	1.00	1.00	1.00	1.00	1.00
T232/680[#]	1.00	1.00	1.00	1.00	1.00	1.00
S415/T863:N[$]	0.76	0.89	0.85	0.86	0.75	0.46
S415/T863:OG(1)[$]	1.00	1.00	1.00	1.00	1.00	1.00
S415/T863[#]	1.00	1.00	1.00	1.00	1.00	1.00

[$]A pair of polar atoms define a hydrogen bond if the corresponding donor-acceptor distance is less than or equal to 3.2 Å.

[#]Represents the fraction of frames with hydrogen bonds between any polar atom of the indicated protein residue and any atom of the 6-phosphoryl group.

Table VII. Fraction of frames from molecular dynamics simulations with hydrogen bonds between oxygen atoms of the 6-phosphoryl group and any polar atom from the protein[$].

	Wild-type/Glc-6-P		D413N/Glc-6-P		D413N/Glc-1,6-P_2	
	N	C	N	C	N	C
O1P[$]	0.99	0.44	1.00	1.00	0.99	0.99
O2P[$]	0.99	1.00	1.00	1.00	1.00	1.00
O3P[$]	1.00	0.61	0.99	1.00	1.00	0.06
O1P*[#]	---	---	---	---	0.67	0.56
O2P*[#]	---	---	---	---	0.94	0.63
O3P*[#]	---	---	---	---	0.97	0.91

[$]A pair of polar atoms define a hydrogen bond if the corresponding donor-acceptor distance is less than or equal to 3.2 Å.

Table VIII. Kinetics parameters and site affinity constants with respect to 1,5-anhydroGlc-6-P for wild-type HKI and mutants[#]
(α unitless, others in μM)

Inhibitor &construct	K_I	K_{II}	α	${}^0M_1$	${}^0M_2(K_{PI})$	${}^2M_1$	${}^1M_2$
1,5-AnhydroGlc-6-P:							
WT	20 ± 3	240 ± 50	0.38	30	62 ± 2	77	163
D413N	23 ± 4	80 ± 20	1.15	47	45 ± 2	41	39
D861N	30 ± 4	80 ± 20	1.77	43	98 ± 3	24	56
D413/861N	35 ± 5	110 ± 40	1.37	55	95 ± 4	41	69
K418A	44 ± 4	1100 ± 500	0.19	146	63 ± 7	768	332
K866A	70 ± 10	400 ± 300	1.14	86	369 ± 34	76	324
K418/866A	170 ± 20	1500 ± 700	0.49	270	460 ± 14	554	946
Glc-1,6-P_2:							
WT	169 ± 4	2900 ± 400	0.24	313	368 ± 15	1324	1560
D413N	106 ± 6	2900 ± 400	0.23	133	518 ± 19	590	2294
D861N	67 ± 2	2900 ± 400	0.11	98	211 ± 19	916	1968
D413/861N	44 ± 2	2900 ± 400	0.10	54	233 ± 3	545	2339

[#]K_I, and K_{II} are reproduce from Tables I & II. ${}^0M_2(K_{PI})$ is determined experimentally as described in the discussion section. The following equations determine the coupling parameter α and the remaining site dissociation constants:

$$\alpha = {(K_{PI})^2}/{K_{II}(K_{PI} - K_I)};\quad {}^0M_1 = \alpha K_{II} - K_{PI};\quad {}^0M_2 = K_{PI};\qquad {}^2M_1 = {}^0M_1/\alpha;\quad {}^1M_2 = {}^0M_2/\alpha$$

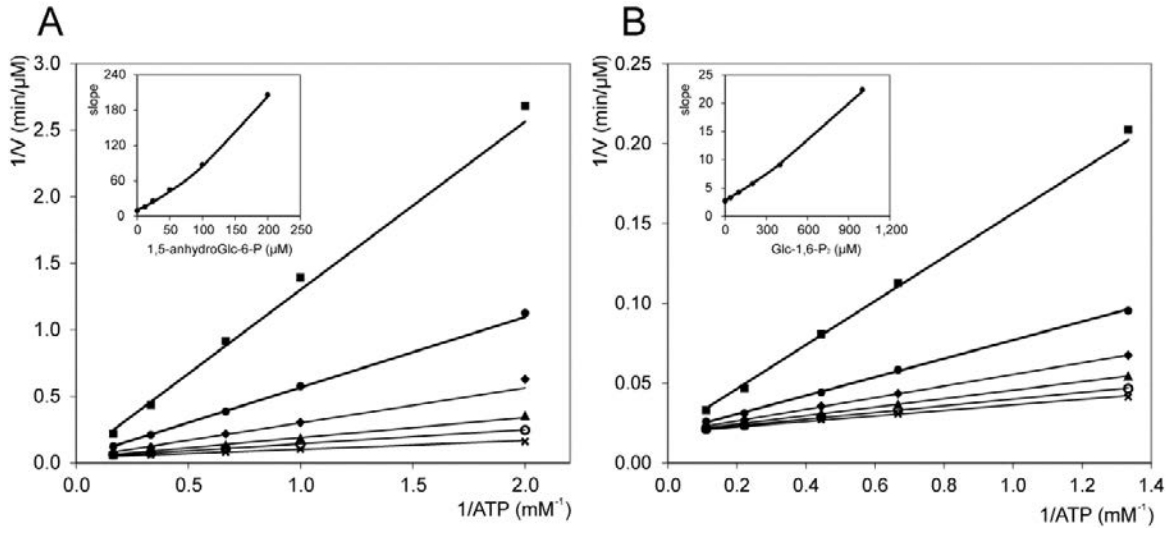

Figure 1. **Inhibition of wild-type HKI by 1,5-anhydroGlc-6-P (*panel A*) and Glc-1,6-P_2 (*panel B*).** In the determination of K_I and K_{II}, the concentration of Glc was fixed at 2 mM, that of $[ATP\text{-}Mg]^{2-}$ varied from 1/2 K_m^{ATP} to 4 K_m^{ATP}, that of 1,5-anhydroGlc-6-P from 12 to 200 μM, and that of Glc-1,6-P_2 from 40 to 1000 μM. Values for K_I and K_{II} were obtained by fitting data to a model of nonlinear competitive inhibition, the equation for which is as follows:

$$V = {V_{max}}\Big/\left[1 + (K_m^{ATP}) \times {1}/{S} + \left({K_m^{ATP}}/{K_I}\right) \times {I}/{S} + \left({K_m^{ATP}}/{K_I \times K_{II}}\right) \times {I^2}/{S}\right]$$

where S and I are concentrations of $[ATP\text{-}Mg]^{2-}$ and 1,5-anhydroGlc-6-P or Glc-1,6-P_2, respectively. Values for the stoichiometric dissociation constants K_I and K_{II} for 1,5-anhydroGlc-6-P are 20±3 and 240±50 μM, respectively, and for G1c-1,6-P_2 195 ± 10 and 2900±400 μM, respectively.

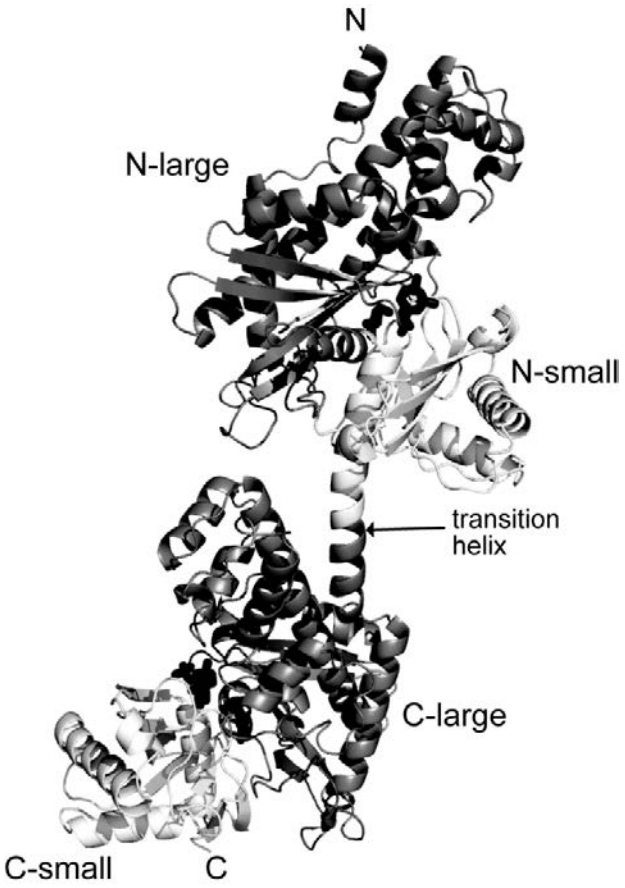

Figure 2. **Overview of the D413N/Glc-1,6-P_2/Glc complex.** Large domains are gray and small domains white. Glc-1,6-P_2 and Glc are black as sticks. (The illustration was generated with PyMOL).

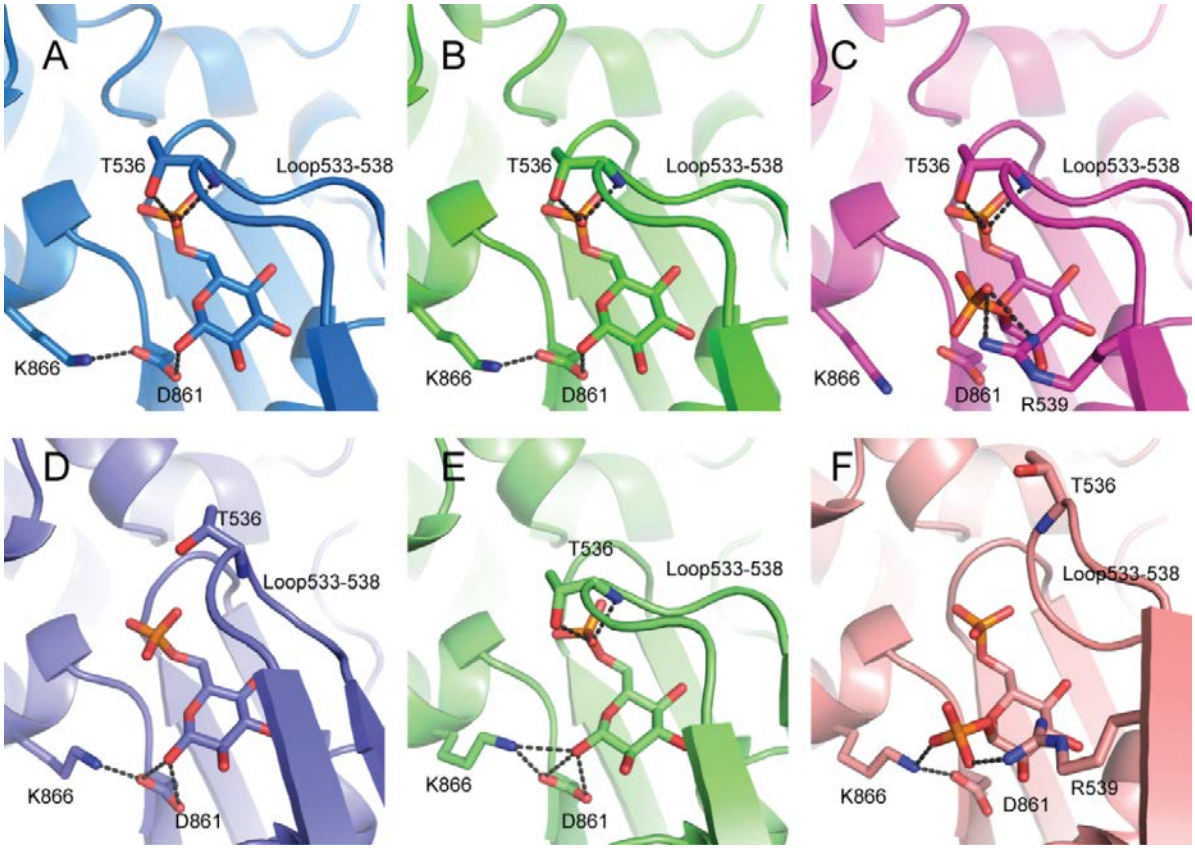

Figure 3. **The binding pocket of ligands from crystal structures (A, B, C) and MD simulations structures (D, E, F).** A, D, wild-type/Glc-6-P structures; B, E, D413N/Glc-6-P structures; C, F, D413N/Glc-1,6-P_2 structures. (The illustration was generated with PyMOL).

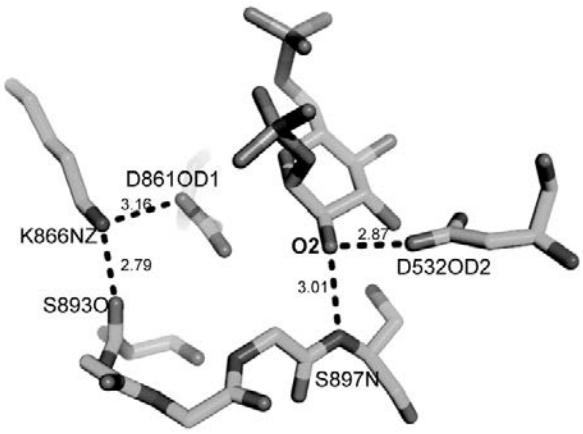

Figure 4. Loop 893–897 with related residues in D413N Glc-1,6-P_2 crystal complex. Donor-acceptor distances are in unit of Å. (The illustration was generated with PyMOL).

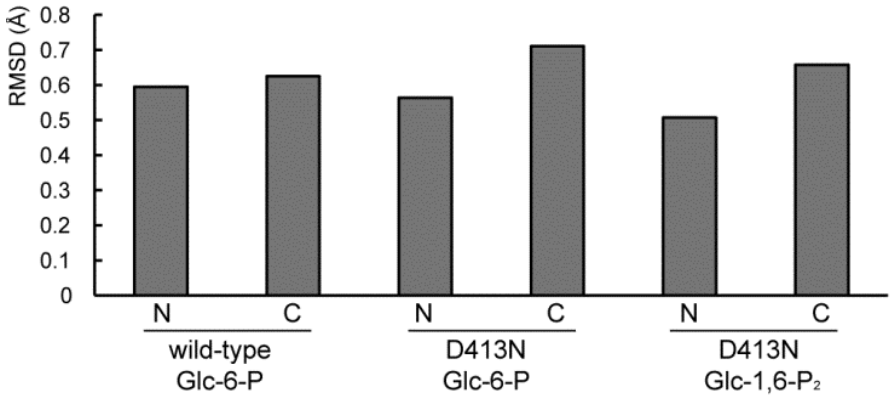

Figure 5. Root-mean-square deviation (RMSD) of atoms of phosphoryl ligands. Deviations are calculated from superimposed N- or C-terminal halves taken over 10 nsec simulations of a single molecule of HKI, ligated at the N and C-terminal halves.

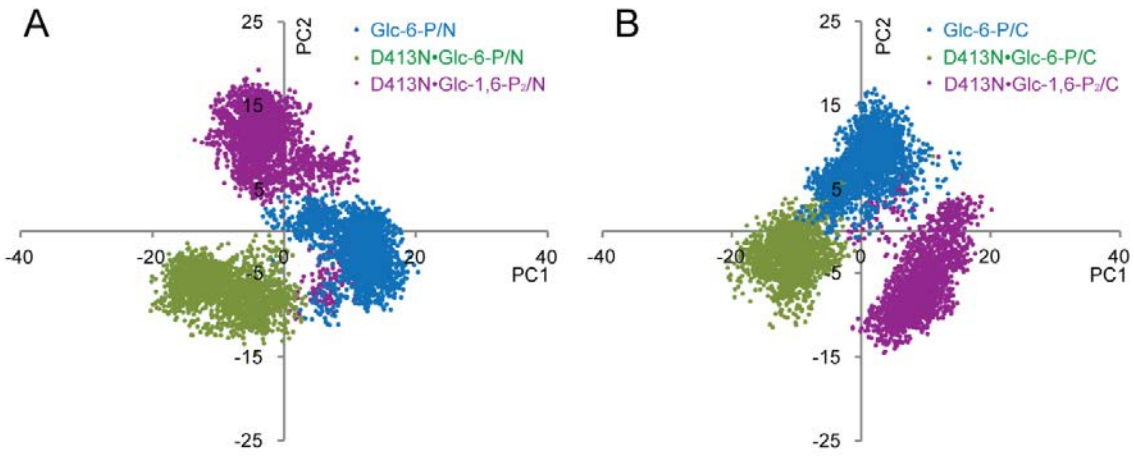

Figure 6. Principal component analysis of HKI. First two components of PCA based on all N-terminal half (A) or C-terminal half (B) structures from wild-type•Glc-6-P, D413N•Glc-6-P and D413N•Glc-1,6-P_2 molecular dynamics simulations.

References

1. Gonzalez, C., Ureta, T., Sánchez, R., and Niemeyer, H. (1964) Multiple molecular forms of ATP: hexose 6-phosphotransferase from rat liver. *Biochem. Biophys. Res. Commun.* **16**, 347-352
2. Grossbard, L., and Schimke, R.T. (1966) Multiple hexokinases of rat tissues. Purification and comparison of soluble forms. *J. Biol. Chem*. **241**, 3546-3560
3. Katzen, H.M. (1967) The multiple forms of mammalian hexokinase and their significance to the action of insulin. *Adv. Enzyme Regul*. **5**, 335-356
4. Katzen, H.M., and Schimke, R.T. (1965) Multiple forms of hexokinase in the rat: tissue distribution, age dependency, and properties. *Proc. Natl. Acad. Sci. U.S.A.* **54**, 1218-1225
5. Wilson, J.E. (1995) Hexokinase. *Rev. Physiol. Biochem. Pharmacol*. **126**, 65-198
6. Easterby, J.S, and O'Brien, M.J. (1973) Purification and properties of pig-heart hexokinase. *Eur. J. Biochem*. **38**, 201-211
7. Holroyde, M.J., and Trayer, I.P. (1976) Purification and properties of skeletal muscle hexokinase. *FEBS Lett*. **62**, 215-219
8. Ureta, T. (1982) The comparative isozymology of vertebrate hexokinases. *Comp. Biochem. Physiol*. **71B**, 549-555
9. Manning, T.A., and Wilson, J.E. (1984) Inhibition of brain hexokinase by a multisubstrate analog results from binding to a discrete regulatory site. *Biochem. Biophys. Res. Commun.* **118**, 90-96
10. Tsai, H.J. and Wilson, J.E. (1996) Functional organization of mammalian hexokinases: both N- and C-terminal halves of the rat type II isozyme possess catalytic sites. *Arch. Biochem. Biophys.* **329**, 17-23
11. White, T.K., and Wilson, J.E. (1989) Isolation and characterization of the discrete N- and C-terminal halves of rat brain hexokinase: retention of full catalytic activity in the isolated C-terminal half. *Arch. Biochem. Biophys*. **274**, 375-393
12. Arora, K.K., Filburn, C.R., and Pedersen, P.L. (1993) Structure/function relationships in hexokinase. Site-directed mutational analyses and characterization of overexpressed fragments implicate different functions for the N- and C-terminal halves of the enzyme. *J. Biol. Chem*. **266**, 5359-5362
13. Mehta, A., Jarori, G.K., and Kenkare, U.W. (1988) Brain hexokinase has no preexisting allosteric site for glucose 6-phosphate. *J Biol Chem*. **263**, 15492-15497
14. Ellison, W.R., Lueck, J.D., and Fromm, H.J. (1975) Studies on the mechanism of orthophosphate regulation of bovine brain hexokinase. *J. Biol. Chem*. **250**, 1864-1871
15. Aleshin, A.E., Zeng, C., Bourenkov, G.P., Bartunik, H.D., Fromm, H.J., and Honzatko, R.B. (1998) The mechanism of regulation of hexokinase: new insights from the crystal

structure of recombinant human brain hexokinase complexed with glucose and glucose-6-phosphate. *Structure*. **6**, 39-50

16. Mulichak, A.M., Wilson, J.E., Padmanabhan, K., and Garavito, R.M. (1998) The structure of mammalian hexokinase-1. *Nat. Struct. Biol*. **5**, 555-560
17. Aleshin, A.E., Fromm, H.J., and Honzatko, R.B. (1998) Multiple crystal forms of hexokinase I: new insights regarding conformational dynamics, subunit interactions, and membrane association. *FEBS Lett*. **434**, 42-46
18. Zeng, C., and Fromm, H.J. (1995) Active site residues of human brain hexokinase as studied by site-specific mutagenesis. *J. Biol. Chem*. **270**, 10509-10513
19. Fang, T.Y., Alechina, O., Aleshin, A.E., Fromm, H.J., and Honzatko, R.B. (1998) Identification of a Phosphate Regulatory Site and a Low Affinity Binding Site for Glucose 6-Phosphate in the N-terminal Half of Human Brain Hexokinase. *J. Biol. Chem*. **273**, 19548-19553
20. Liu, X., Kim, C.S., Kurbanov, F.T., Honzatko, R.B., and Fromm, H.J. (1999) Dual Mechanisms for Glucose 6-Phosphate Inhibition of Human Brain Hexokinase. *J. Biol. Chem.* **274**, 31155-31159
21. Solheim, L.P, and Fromm, H.J. (1981) Kinetic evidence that the high-affinity glucose 6-phosphate site on hexokinase I is the active site. *Arch. Biochem. Biophys.* **211**, 92-99
22. Solheim, L.P, and Fromm, H.J. (1983) Effect of inorganic phosphate on the reverse reaction of bovine brain hexokinase. *Biochemistry*. **22**, 2234-2239
23. White, T.K., and Wilson, J.E. (1987) Rat brain hexokinase: location of the allosteric regulatory site in a structural domain at the N-terminus of the enzyme. *Arch. Biochem. Biophys.* **259**, 402-411
24. Aleshin, A.E., Zeng, C., Bartunik, H.D., Fromm, H.J., and Honzatko, R.B. (1998) Regulation of Hexokinase I: Crystal Structure of Recombinant Human Brain Hexokinase Complexed with Glucose and Phosphate. *J. Mol. Biol*. **282**, 345-357
25. Beitner, R., Klein, S., and Nordenberg, J. (1982) The participation of glucose-1,6-diphosphate in the regulation of hexokinase and phosphoglucomutase activities in brains of young and adult rats. *Int. J. Biochem.* **14**, 195-199
26. Beitner, R., and Lilling, G. (1984) Inhibition of mitochondrial and soluble hexokinase from various rat tissues by glucose 1,6-bisphosphate. *Int. J. Biochem*. **16**, 991-996
27. Zeng, C., Aleshin, A.E., Hardie, J.B., Harrison, R.W., and Fromm, H.J. (1996) ATP-binding site of human brain hexokinase as studied by molecular modeling and site-directed mutagenesis. *Biochemistry*. **35**, 13157-13164
28. Liu, F., Dong, Q., Myers, A.M., and Fromm, H.J. (1991) Expression of human brain hexokinase in Escherichia coli: purification and characterization of the expressed enzyme. *Biochem. Biophys. Res. Commun.* **177**, 305-311
29. Laemmli, U.K. (1970) Cleavage of structural proteins during the assembly of the head of bacteriophage T4. *Nature.* **227**, 680-685

30. Bradford, M.M. (1976) A rapid sensitive method for the quantitation of microgram quantities of protein utilizing the principle of protein-dye binding. *Anal. Biochem.* **72**, 248-252

31. Ferrari, R., and Crane, R. (1959) 1,5-Anhydro-D glucitol 6-phosphate and its use for the specific inhibition of the hexokinase reaction in tissue homogenates. *Arch. Biochem. Biophys.* **80**, 372-377

32. Drueckes, P., Schinzel, R., and Palm, D. (1995) Photometric microtiter assay of inorganic phosphate in the presence of acid-labile organic phosphates. *Anal. Biochem*. **230**, 173-177

33. Otwinowski, Z., and Minor, W. (1997) Processing of X-ray diffraction data collected in oscillation mode. *Methods in Enzymology.* **276**, 307-326

34. Aleshin, A.E., Malfois, M., Liu, X., Kim, C.S., Fromm, H.J., Honzatko, R.B., Koch, M.H., and Svergun, D.I. (1999) Nonaggregating mutant of recombinant human hexokinase I exhibits wild-type kinetics and rod-like conformations in solution. *Biochemistry*. **38**, 8359-8366

35. Collaborative Computational Project, Number 4. (1994) The CCP4 suite: programs for protein crystallography. *Acta. Cryst.* **D50**, 760-763

36. Navaza, J. (1994) AMoRe: an automated package for molecular replacement. *Acta Cryst.* **A50**, 157-163

37. Vagin, A.A., Steiner, R.S., Lebedev, A.A., Potterton, L., McNicholas, S., Long, F., and Murshudov, G.N. (2004) REFMAC5 dictionary: organisation of prior chemical knowledge and guidelines for its use. *Acta. Cryst.* **D60**, 2284-2295

38. Brünger, A.T., Adams, P.D., Clore, G.M., DeLano, W.L., Gros, P., Grosse-Kunstleve, R.W., Jiang, J-S., Kuszewski, J., Nilges, M., Pannu, N.S., Read, R.J., Rice, L.M., Simonson, T., and Warren, G.L. (1998) Crystallography & NMR system: a new software suite for macromolecular structure determination. *Acta. Cryst.* **D54**, 905-921

39. McRee, D.E. (1992) A visual protein crystallographic software system for X11/XView. *J. Mol. Graph.* **10**, 44-46

40. Phillips, J.C., Braun, R., Wang, W., Gumbart, J., Tajkhorshid, E., Villa, E., Chipot, C., Skeel, R.D., Kale, L., and Schulten, K. (2005) Scalable molecular dynamics with NAMD. *J. Comput. Chem.* **26**, 1781-1802

41. Jr. MacKerell, A.D., Banavali, N., and Foloppe, N. (2001) Development and current status of the CHARMM force field for nucleic acids. *Biopolymers*. **56**, 257-265

42. Jorgensen, W.L., Chandrasekhar, J., Madura, J.D., Impey, R.W., and Klein, M.L. (1983) Comparison of simple potential functions for simulating liquid water. *J. Chem. Phys*. **79**, 926-935

43. Essmann, U., Perera, L., Berkowitz, M.L., Darden, T., Lee, H., and Pedersen, L.G. (1995) A smooth particle mesh Ewald method. *J. Chem. Phys.* **103**, 8577-8593

44. Glykos, N.M. (2006) Carma: a molecular dynamics analysis program. *J. Comput. Chem*. **27**, 1765-1768

45. Humphrey, W., Dalke, A., and Schulten, K. (1996) VMD - Visual molecular dynamics. *J. Molec. Graphics.* **14**, 33-38

46. Fujii, S., and Beutler, E. (1985) High glucose concentrations partially release hexokinase from inhibition by glucose 6-phosphate. *Proc. Natl. Acad. Sci. U.S.A.* **82**, 1552-1554

Chapter IV. Glucose as a Modulator of Inhibition in Recombinant Human Hexokinase Type I

Lu Shen and Richard B. Honzatko

Department of Biochemistry, Biophysics and Molecular Biology,

Iowa State University, Ames IA 50011

Abstract

Hexokinase I (HKI) catalyzes the initial step of glycolysis in brain and red blood cells. 1,5-Anhydroglucitol 6-phosphate (1,5-anhydroGlc-6-P), an analog of the product glucose 6-phosphate (Glc-6-P), inhibits by binding antagonistically to sites of unequal affinity at the N- and C-terminal halves of HKI. P_i displaces 1,5-anhydroglucitol 6-phosphate from the N-terminal half, but is unable to displace inhibitor from the C-terminal half. Presented here are the effects of glucose (Glc) on the inhibition of HKI. Consistent with findings of multiple binding sites for Glc and Glc-6-P in crystal structures, the kinetics of HKI are nonlinear as a function of Glc and 1,5-anhydroGlc-6-P concentrations. For wild-type HKI and mutant forms of HKI that eliminate the binding of inhibitor to either the N- or C-terminal half, two molecules of Glc must bind before the occurrence of potent inhibition. High concentrations of Glc eliminate inhibition due to the binding of a second molecule of inhibitor to the wild-type enzyme, but mutant forms of HKI that have but one inhibitor binding site exhibit no Glc-relief of inhibition. The relevance of these findings to the physiological function of HKI are as follows: at low concentrations of Glc typically found in brain cells, HKI may not be subject to strong product inhibition. At normal levels of glucose in red blood cells, HKI can be potently inhibited by product. At elevated levels of glucose common in hyperglycemia, product inhibition is potent but partial.

Introduction

Glucose (Glc) is the main energy source for all mammalian cells and the sole energy source for brain[1]. In fact, approximately 40-50% of all circulating glucose in humans supports energy metabolism of the brain[2]. Only a short period of hypoglycemia causes permanent damage to brain[3]. Hexokinase (ATP: D-hexose 6-phosphotransferase, EC2.7.1.1) is the crucial enzyme in regulation of glucose metabolism and catalyzes the initial step of glucose phosphorylation using $[ATP\text{-}Mg]^{2-}$ as the phosphoryl donor[4-6]. In mammalian tissues, four isozymes of hexokinase have been identified[7]. Types I, II and III hexokinases, all with molecular weights of approximately 100 kDa, share 70% sequence identity[8]. N- and C-terminal halves of isozymes I–III show ~50% sequence identity, putatively a consequence of duplication and fusion of a primordial hexokinase gene[9-12]. Hexokinase IV (glucokinase) and yeast hexokinase isoforms A and B have molecular weights of 50 kDa, and exhibit significant sequence similarity to both halves of isozymes I–III[8].

Different isozyme of hexokinase has different tissue distributions and kinetic properties. Hexokinase I is found in all mammalian tissues and is highly or even exclusively expressed in brain and red blood cells[4-6]. Hexokinase II is mainly expressed in insulin-sensitive tissues such as skeletal muscle and adipose tissue[13]. Hexokinase III is expressed at very low levels, and is associated with the cell nucleus[13]. Hexokinase IV is mainly present in liver, but also found in nuoroendocrine cells[13]. Both hexokinase I and II are overexpressed in many cancer cells[14-15]. The overexpression leads to protection against apoptotic cell death[14-15].

Both halves of hexokinase II possess catalytic activity, whereas the N-halves of hexokinase I and III are devoid of activity [8, 16-18]. The reaction product, glucose-6-phosphate (Glc-6-P), potently inhibits isozymes I-III (but not isoform IV) at physiologically concentrations[8]. Inorganic phosphate (P_i) is an inhibitor for hexokinase II and III[8]. However, P_i specifically antagonizes the inhibition of hexokinase I by

1,5-anhydroglucitol 6-phosphate (1,5-anhydroGlc-6-P, an analog of Glc-6-P used in kinetics) at relatively low concentrations, whereas at higher concentrations it acts as an inhibitor competitive with ATP[8].

Substantial evidence supports a single high-affinity binding site for Glc-6-P. Both equilibrium dialysis experiments and fluorescence binding studies (Chapter 2, this thesis) indicate a single binding site for Glc-6-P with a submicromolar dissociation constant[19-20]. Glc-6-P up to concentrations of 1 mM is a linear competitive inhibitor with respect to ATP[20]. Other observations, however, point to multiple sites of inhibitor action and even two high-affinity sites. Glc-6-P binds to both halves of HKI in crystal structures (Figure 1), and exhibit essentially identical hydrogen bonding interactions[2, 21-22]. Proteolytic cleavage of HKI produces an active C-terminal half (mini-HKI) and inactive N-terminal half[17, 23]. A high-affinity site for Glc-6-P exists in the N-terminal half and in mini-HKI, and inhibition of mini-HKI by 1,5-anhydroGlc-6-P is comparable to that of the intact enzyme, save for the loss of P_i-relief[17, 23-24]. 1,5-anhydroGlc-6-P is a nonlinear competitive inhibitor with respect to ATP of wild-type HKI[25]. Separate mutations of the binding pocket for Glc-6-P at each half does not abolish 1,5-anhydroGlc-6-P inhibition, only the combined mutations at both N- and C-terminal halves eliminate inhibition[25-26].

These observations historically provide the basis for two models for HKI inhibition. Fromm and colleagues suggest that Glc-6-P inhibits the enzyme by binding to the C-terminal half, with the 6-phosphoryl group overlapping the γ-phosphate site for ATP and the glucopyranose moiety binding to a site distinct from the glucose pocket[20, 27-28]. Wilson and colleagues assigned Glc-6-P inhibition to an allosteric site at the N-terminal half[17, 23]. Both models have P_i as an antagonist of Glc-6-P inhibition, binding to a high-affinity site at the N-terminal half[8, 29]. These models have undergone revision over time. The discovery of potent inhibition of mini-HKI necessitated an adjustment to the Wilson model, acknowledging the existence of a latent high-affinity site for inhibition at the C-terminal half

unmasked by the removal of the N-terminal half[8]. Similarly, the persistence of high-affinity inhibition by 1,5-anhydroGlc-6-P exhibited by T536A HKI is consistent only with a mechanism of allosteric inhibition[26]. To reconcile one high-affinity site in equilibrium binding studies and two sites indicate by crystal structures and mutant forms of HKI, Liu *et al.* proposed a model of equal high-affinity sites coupled by negative cooperativity[26]. Results of Chapters 2 and 3 of this thesis, however, clearly show binding sites for 1,5-anhydroGlc-6-P must have unequal affinity for inhibitor, with antagonistic coupling of inhibitor binding sites for the wild-type enzyme. Moreover, P_i only displaces 1,5-anhydroGlc-6-P from the N-terminal high-affinity site, leaving unchanged the residual inhibition due to the binding of inhibitor to the C-terminal half.

Glucose binds tightly to both halves of HKI[2] (to the active site of the C-terminal half and to the vestigial active site of the N-terminal half) interacting with residues of identical or comparable type. The effect of glucose on HKI is not entirely clear. The binding of Glc-6-P or P_i to HKI is synergistic with glucose[17]. Nonetheless, Glc-6-P still binds with high affinity to HKI in the absence of glucose[19-20], and Wilson has assigned this glucose-independent binding site to the N-terminal half[23]. Synergistic interactions between glucose and Glc-6-P are also observed with mini-HKI but not the N-terminal half[17]. The observation of synergism between P_i and glucose in HKI is puzzling given the absence of synergism between glucose and Glc-6-P in the separate N-terminal half. Even more perplexing is the partial relief of Glc-6-P inhibition due to high concentrations of Glc[30].

These results suggest important roles for glucose in Glc-6-P inhibition. Presented here are studies of the effect of Glc and Glc-6-P on the fluorescence emission of TNP-ADP, a competitive inhibitor of HKI with respect to ATP. In addition, the nonlinear response of the wild-type enzyme to the concentration of Glc divides into zones of low, moderate and high Glc concentrations. The results are consistent with synergistic interactions between Glc binding to the active site and inhibitor binding to the C-terminal or N-terminal half of the

enzyme, that in fact the binding of Glc to the active site is necessary for potent inhibition. Glc concentrations in excess of 1 mM, however, antagonize inhibitor binding at the C-terminal half. A kinetic mechanism is proposed here that accounts for 1,5-anhydroGlc-6-P inhibition of HKI at the extraordinarily broad range of Glc concentrations observed in brain tissue and the red blood cell.

Materials and methods

Materials – The plasmids in vector pET11a for wild-type HKI and T232A, G896A and mini-HKI were available from previous studies (chapter 2, this thesis). *Escherichia coli* strain DH5a and BL21 were from Invitrogen. DNaseI, PMSF, leupeptin, bovine serum albumin (BSA), ATP, NADP, Glc-6-P, ampicillin were from Sigma. 1,5-anhydro-D-sorbitol was from Toronto Research Chemicals. isopropyl-D-thiogalactopyranoside (IPTG) was from Bio-World. DEAE sepharose CL-6B and CHT ceramic hydroxyapatite (HA) Type II media were from Bio-Rad. DEAE-5PW HPLC media was from Tosohaas. Glusoe-6-phosphate dehydrogenase (G6PDH) was from Roche. 2'-(or-3')-O-(2,4,6-trinitrophenyl)-adenosine 5'- diphosphate (TNP-ADP) was from Invitrogen.

Expression and Purification of Wild-type and Mutant Hexokinases— Plasmids for wild-type, T232A and G896A enzymes were developed as indicated in Chapters 2 and 5 of this thesis. A 200 ml culture of the transformed *Escherichia coli* BL21 was grown overnight at 37 ºC in LB medium (33 mg/L ampicillin) and then 1.5% cell were transferred to 9.6 L LB medium (33 mg/L ampicillin). The culture was grown at 300 rpm and 37 ºC to A_{600}=1.0. The temperature then was reduced to 16 ºC, isopropyl-β-D-thiogalactopyranoside (IPTG) was added to a final concentration of 0.5 mM and the culture was grown at 200 rpm for 20-22 hr. at 16 ºC. The cells were re-suspended in 25 mM KP_i (pH 7.5), 5 mM glucose, 3 mM $MgCl_2$, 1 mM dithiothreitol (DTT), 1 mM phenylmethanesulfonyl fluoride (PMSF), 50 μg/ml

DNaseI and 5 μg/ml leupeptin. The cells were broken by sonication and then centrifuged (33,000*x*g, 1 hr.). The supernatant fluid was adjusted to pH 7.5 and loaded onto a DEAE-anion exchange column, using 25 mM KP_i, 5 mM glucose, 1 mM dithiothreitol DTT (pH 7.5), with a gradient of 0–400 mM NaCl. The fractions containing HKI activity were pooled, concentrated and dialyzed against 50 mM KP_i (pH 7.0), 5 mM glucose, 1 mM dithiothreitol (DTT) and loaded onto a ceramics hydroxyapatite column with a gradient of 0.05–1 M KP_i (pH 7.0). HKI was collected and dialyzed against 25 mM KP_i, 5 mM glucose, 1 mM dithiothreitol (DTT) (pH 7.5), and further purified by DEAE-5PW HPLC chromatography with a gradient of 0–500 mM NaCl. The pure protein was identified by sodium dodecylsulfate polyacrylamide gel electrophoresis (SDS-PAGE)[31]. Protein concentration was determined by the method of Bradford with BSA as a standard[32].

TNP-ADP Binding and Displacement— Wild-type and mutant enzymes were prepared to a concentration of 40 mg/ml in 50 mM Hepes (pH 7.8) and 1 mM Glc, then diluted to a final concentration of 0.2 mg/ml (2 μM) in 50 mM Hepes (pH7.8) containing 5 μM Glc, 25 μM Glc, 75 μM Glc and 1 mM Glc, respectively before each experiment. In binding experiments, TNP-ADP concentrations range from 0–10 μM, whereas in displacement experiments, the TNP-ADP concentration is 3.66 μM. Fluorescence measurements were made at room temperature using a 1-cm^2 quartz cuvette on a SLM Amico 8000 fluorometer with entrance/exit slits of 4 mm. The excitation wavelength is 409 nm and emission scans are from 530 to 560 nm. Fluorescence intensity (average of three scans for each datum) was integrated over 530–560 nm using 30 increments and an accumulation time of 1 sec per increment. Fluorescence data were analyzed by the method described by Faller[33], as modified by Nimer *et al.*[34].

The observed fluorescence from a mixture of TNP-ADP and HKI comes from free TNP-ADP, TNP-ADP bound to HKI and HKI itself:

$$F_{obs} = F_{free} + F_{bound} + F_{protein}$$

$$F_{free} = a + b[L] - c[L]^2$$

$$F_{bound} = Gb([L_o] - [L])$$

$$F_{obs} = a + b[L] - c[L]^2 + Gm([L_o] - [L]) + S$$

$F_{protein}$ is an adjustable parameter (*S*) that accounts for background fluorescence due to the protein sample. As HKI has no native fluorophore sensitive to an excitation wavelength of 409 nm the parameter *S* should be a small value and nearly constant over the experiment presented here. $[L_o]$ and $[L]$ represent the total and free TNP-ADP concentrations, respectively. G is a fluorescence enhancement factor of the bound fluorescent ligand relative to the free state. Parameters *a*, *b* and *c* are determined by fitting fluorescence versus $[L]$ in the absence of protein, the data for which comes from the addition of TNP-ADP to buffer. The same buffer is used for the binding and displacement experiments.

A single binding-site model adequately accounts for the F_{obs} of the bound state as well as the displacement of TNP-ADP by phosphoryl ligand Glc-6-P, or 2-deoxyGlc-6-P or Man-6-P:

$$P + L = PL \quad , \qquad K_L = \frac{[P][L]}{[PL]}$$

$$P + A = PA \quad , \qquad K_A = \frac{[P][A]}{[PA]}$$

$$[L_o] = [L] + [PL];\ [A_o] = [A] + [PA];\ [P_o] = [P] + [PL] + [PA];$$

$[A_o]$ and $[A]$ are total and free phosphoryl ligand concentrations, respectively; $[P_o]$ and $[P]$ are total and free protein concentrations, respectively. K_L and K_A are constants for the dissociation of TNP-ADP and phosphoryl ligand from protein, respectively. The equilibrium and mass conservation relationships for $[L_o]$ (total fluorophore concentration), $[A_o]$ (total concentration of displacing ligand) and $[P_o]$ (total concentration of protein) lead to a third-order equation in the concentration of free protein [P]. Substitution of the

equilibrium relationships into mass conservation relationships for protein leads to a third-order equation in the concentration of free protein [P]. For circumstances here, K_A >> [P], allowing an approximation that reduces the third-order equation to one of second order:

$$\left(1+\frac{[A_0]}{K_A}\right)[\mathrm{P}]^2+\left(\frac{K_A-[P_0]+[A_0]K_L}{K_L+[L_0]}\right)[\mathrm{P}]^2-\mathrm{P}_0K_L=0$$

The physical root of this quadratic relationship is the concentration of free protein, and determines the concentration of free fluorophore $[L]=[L_o]K_L/(K_L+[P])$ at a given total concentration of fluorophore, $[L_o]$. GraFit software optimizes the fit of the observed fluorescence to the right-hand side of Eqn. 1 at fixed $[P_o]$ and varying $[L_o]$ and $[A_o]$ by adjusting parameters K_A, K_L, G and $F_{protein}$[35].

Hexokinase Kinetics Studies -- Hexokinase activity was determined by the glucose-6-phosphate dehydrogenase (G6PDH, E.C.1.1.1.49) - coupled fluorometric or spectrometric assay [36]. Commercial G6PDH in ammonium sulfate precipitate form was dialyzed extensively against 50mM Hepes (pH7.8) buffer (for fluorometric assay) and 50mM Tris (pH7.8) buffer (for spectrometric assay), repectively, to remove sulfate and eliminate the relief effect on Glc-6-P inhibition by mimicking P_i. 1,5-anhydroGlc-6-P is a surrogate for Glc-6-P to study Glc-6-P inhibition and the dicyclohexylamine salt of AnGlc-6-P was prepared as described by Ferrari R.[37]. The concentration was determined by the method described by Drueckes P.[38]. The concentration of hexokinase was 0.03-0.05 μg/ml for fluorometric assay and 1.2-2.0 μg/ml for spectrometric assay. The Kinetic analysis was done with the computer program GraFit 7.0[35].

Results

Rationale for the Selection of Mutants— Besides the wild-type enzyme, three mutations were employed in this report to study the glucose-dependency of Glc-6-P binding and 1,5-anhydroGlc-6-P inhibition. Mini-HKI is the truncated C-terminal half of full-length

HKI[24, 26, 39-40]. The mutations T232A and G896A eliminate 1,5-anhydroGlc-6-P inhibition originating at the N-terminal half[26] and C-terminal half, respectively (Chapter 5, this thesis). All the above mutants have specific activity no worse than 50% of the wild-type enzyme. Although all the mechanisms of inhibition by 1,5-anhydroGlc-6-P are competitive with respect to ATP, the kinetic mechanisms of inhibition with respect to Glc have not been reported. Preliminary work indicated a complex kinetic mechanism for the wild-type enzyme. In principle, the investigation of mutants with only a single inhibitory mechanism could clarify phenomena exhibited by the wild-type system. Wild-type and mutant hexokinases investigated here are at least 95% pure as determined by SDS-polyacrylamide gel electrophoresis (data not shown).

TNP-ADP Binding and Displacement— As shown in Table I, and Figure 2.A, the parameters for baseline fitting were unaffected by changes in glucose concentrations. TNP-ADP binds to wild-type HKI and all mutants with high affinity (K_L < 0.6 μM). Whereas dissociation constants for wild-type HKI, mini-HKI and T232A are nearly the same within experimental uncertainty, K_L values for G896A are 3–4-fold higher than that of the other HKI forms. All the forms of HKI exhibit 1.2–1.5-fold increase in K_L (dissociation constant for TNP-ADP from the enzyme) and 1.05–1.15 fold increase in G (fluorescence enhancement factor) as glucose concentration increase from 5–1000 μM (Table I & Figure 4.A). $F_{protein}$ (S) values are close for each protein, indicating no unexpected fluorescence from any of the protein preparations. The displacement of TNP-ADP by Glc-6-P becomes more effective as glucose concentrations increase; however, the Glc-dependency of Glc-6-P differs for each enzyme. Relative to K_A at 1 mM Glc, K_A values at 5 μM Glc increase 1.1-, 1.4-, 3.3- and 4.1-fold for G896A, wild-type HKI, T232A and mini-HKI, respectively (Table II, Figure 3 and 4.B). Evidently, wild-type HKI behaves more like G896A, whereas T232A behaves more like mini-HKI.

Kinetics at High Glc Concentrations— Scheme I is a rapid-equilibrium model governing the

kinetics of wild-type HKI for Glc concentrations up to 10 mM, and is relevant to results of Figure 5.

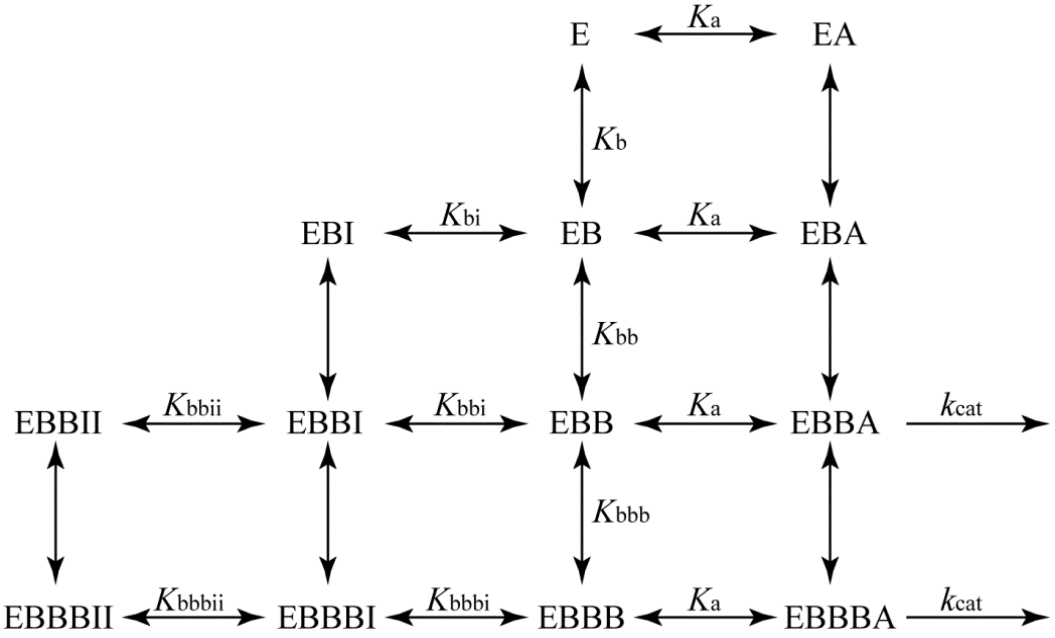

Scheme I

In Scheme I, the association/dissociation of ligands are not shown explicitly, but can be deduced from the different ligation levels of the enzyme. All equilibrium constants are stoichiometric constants of dissociation, with *B*, *A*, *I*, *P* and *E* representing Glc, $[ATP\text{-}Mg]^{2-}$, 1,5-anhydroGlc-6-P, P_i and wild-type HKI, respectively. Scheme I leads to Eqn. 1:

$$V = {}^{N1}/_{D1} \qquad \text{Eqn.1}$$

$$N1 = V_{max}\left(\frac{AB^2}{K_aK_bK_{bb}}\right)\left(\frac{AB^3}{K_aK_bK_{bb}K_{bbb}}\right)$$

$$D1 = 1 + \frac{A}{K_a} + \frac{B}{K_b} + \frac{AB}{K_aK_b} + \frac{BB}{K_bK_{bb}} + \frac{BI}{K_bK_{bi}} + \frac{AB^2}{K_aK_bK_{bb}} + \frac{B^3}{K_bK_{bb}K_{bbb}} + \frac{B^2I}{K_bK_{bb}K_{bbi}} + \frac{AB^3}{K_aK_bK_{bb}K_{bbb}} + \frac{B^2I^2}{K_bK_{bb}K_{bbi}K_{bbii}} + \frac{B^3I}{K_bK_{bb}K_{bbb}K_{bbbi}} + \frac{B^3I^2}{K_bK_{bb}K_{bbb}K_{bbbi}K_{bbbii}}$$

Assumptions well-grounded in experimental data constrain some of the parameters of Eqn 1. On the basis of fluorescence binding data (Table I) the dissociation constant for TNP-ADP is not sensitive to the concentration of Glc. Hence the dissociation of *A* from *EA*, *EBA*, *EBBA* and *EBBBA* is governed by the same constant $K_a = K_m^{ATP}$. As a consequence of thermodynamic cycles in Scheme I, K_b is the constant of dissociation of *B* from *EB* and *EBA*, K_{bb} is the constant of dissociation of *B* from *EBB* and *EBBA*, and K_{bbb} is the constant of dissociation of *B* from *EBBB* and *EBBBA*. Glc is not a substrate inhibitor and k_{cat} values for the conversion of *EBBA* and *EBBBA* into products must equal to within experimental error (linear behavior of reciprocal velocity at high concentrations of Glc in the absence of inhibitor). The *EBA* species is a mixture of ATP-bound C-terminal half with a Glc-bound N-terminal half and ATP-bound C-terminal half with a Glc-bound C-terminal half, of which only the latter is active. The assumption of $k_{cat} = 0$ for the *EBA* species is equivalent to having most of it with Glc bound to the N-terminal half. Indeed several observations support high-affinity binding of Glc to the N-terminal half of HKI[8, 17, 23]. *EB* then must represent Glc bound primarily to the N-terminal half, and the constant for dissociation of Glc from *EBB*, represented by K_{bb}, is the K_m for Glc.

In fitting Eqn.1 to data, values for K_m^{ATP}, K_m^{Glc} and k_{cat} were determined independently by separate experiments in which either Glc or ATP varied over a concentration range from $1/5\times K_m$ to $5\times K_m$. Refinement employed these experimentally determined values for K_m^{ATP}, K_m^{Glc} and k_{cat} as constants in the refinement of initial values for K_{bi}, K_{bbi}, K_{bbbi}, K_{bbii}, K_{bbbii}, K_b and K_{bbb} using Eqn. 1. Optimization followed the protocol of Table III and resulted in reasonable values for parameters with uncertainties no greater than 30%, except for K_b, which refined to a value of 1 μM with substantial relative uncertainty (Table IV).

Fits of data for T232A and G896A HKI employ Scheme II and Eqn. 2, the fundamental difference being the elimination of complexes with two bound inhibitors.

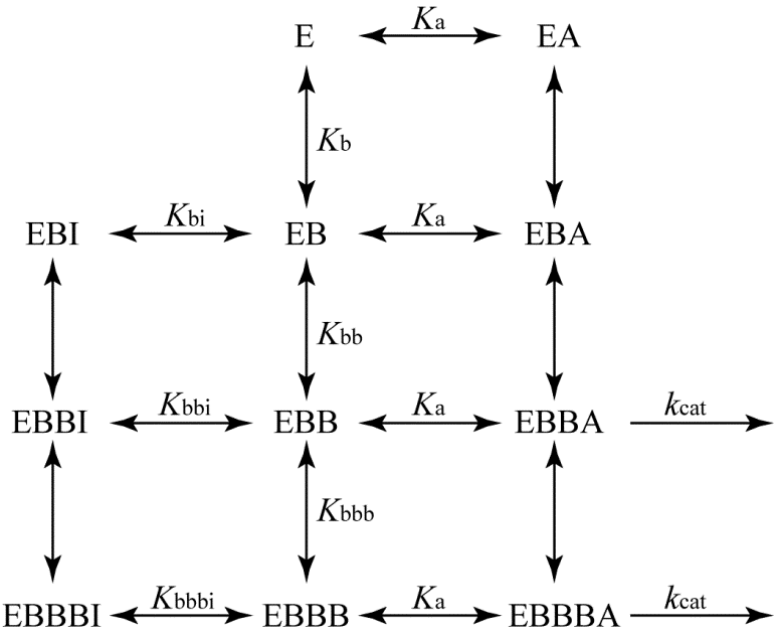

Scheme II

$$V = {}^{N2}/_{D2} \qquad \text{Eqn.2}$$

$$N2 = V_{max}\left(\frac{AB^2}{K_aK_bK_{bb}}\right)\left(\frac{AB^3}{K_aK_bK_{bb}K_{bbb}}\right)$$

$$D2 = 1 + \frac{A}{K_a} + \frac{B}{K_b} + \frac{AB}{K_aK_b} + \frac{BB}{K_bK_{bb}} + \frac{BI}{K_bK_{bi}} + \frac{AB^2}{K_aK_bK_{bb}} + \frac{B^3}{K_bK_{bb}K_{bbb}}$$

$$+ \frac{B^2I}{K_bK_{bb}K_{bbi}} + \frac{AB^3}{K_aK_bK_{bb}K_{bbb}} + \frac{B^3I}{K_bK_{bb}K_{bbb}K_{bbbi}}$$

Species in Scheme II are defined as in Scheme I, and the results of optimization are in Table IV.

Finally fits of data for mini-HKI use Scheme III and Eqn. 3, which eliminates species with three bound molecules of Glc and/or two bound molecules of inhibitor.

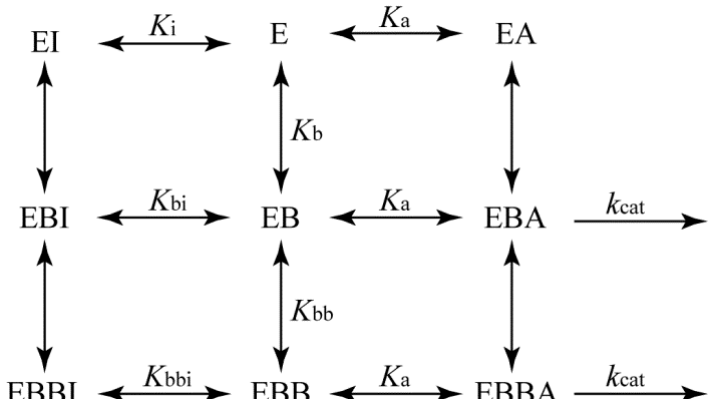

Scheme III

$$V = {}^{N3}/_{D3} \qquad \text{Eqn.3}$$

$$N3 = V_{max}\left(\frac{AB}{K_aK_b}\right)\left(\frac{AB^2}{K_aK_bK_{bb}}\right)$$

$$D3 = 1 + \frac{A}{K_a} + \frac{B}{K_b} + \frac{I}{K_i} + \frac{AB}{K_aK_b} + \frac{BB}{K_bK_{bb}} + \frac{BI}{K_bK_{bi}} + \frac{AB^2}{K_aK_bK_{bb}} + \frac{B^2I}{K_bK_{bb}K_{bbi}}$$

Species in Scheme III are defined as in Scheme I, and the results of optimization are in Table IV.

Discussion

Past efforts to account for observed functional behavior of HKI relied on simple models proscribed by Occam's razor. Models had but one binding site for Glc, Glc-6-P, ATP and P_i[8]. Crystal structures of HKI provided the first concrete basis for more complex interactions between ligands and HKI, defining two sites for Glc, Glc-6-P, and ATP, and one site for P_i[2, 22, 29, 39]. Here we provide evidence for a third binding site for Glc that probably overlaps one of the binding sites for Glc-6-P. Except for the ATP site at the N-terminal half[39], all other sites have well-defined roles in modulating the activity of HKI.

The refined value for K_b (approximately 1 μM) is consistent with the tight binding of

Glc to HKI observed by Kenkare and coworkers[19]. If values of K_b rise significantly above 10 μM, the model-based curves of Figure 5 become convex upward at low concentrations of Glc rather than the observed set of near-parallel lines. In fact, all constructs of HKI presented in Figure 5 approximate a set of parallel lines which is the hallmark of a mechanism of uncompetitive inhibition with respect to Glc. Although the EB complex in Scheme I represents a mixture of ligated states have one bound molecule of Glc, the dominant component of this mixture should have the N-terminal half with Glc.

K_{bi} has high values for wild-type, T232A and G896A hexokinases, which indicates weak binding of 1,5-anhydroGlc-6-P to enzyme with one bound molecule of Glc, presumably to the N-terminal half. This outcome is a surprise, but to have tight binding of inhibitor to say the N-terminal half would be fundamentally inconsistent with the sets of parallel lines in Figure 5. Binding of the first inhibitor molecule becomes tight only after a second molecule of glucose binds, presumably at the active site. Substantial synergism exists in all constructs, as measured by the quotient K_{bi}/K_{bbi} (K_i/K_{bi} for mini-HKI), but synergism is extraordinary for the wild-type and G896A enzymes (10- and 40-fold, respectively). Binding of the second molecule of 1,5-anhydrGlc-6-P to the wild-type enzyme is approximately 20-fold weaker than the first molecule of inhibitor. The effect of binding a third molecule of Glc is negligible on the first-bound inhibitor molecule, but decidedly antagonistic toward the second bound molecule of inhibitor.

Of the observations made in the foregoing paragraph, the requirement for two bound molecules of Glc for potent inhibition by 1,5-anhydrolGlc-6-P is most intriguing. The inhibitor has two possible binding sites (N- and C-terminal halves), but the high-affinity binding of inhibitor must be synergistic with the binding of Glc to the C-terminal half. The easiest explanation for such synergism puts the high-affinity binding site at the C-terminal half, where Glc and 1,5-anhydroGlc-6-P can together leverage a conformational change from an open to a closed half. The kinetics of the wild-type enzyme however, indicate that

inhibitor binds with higher affinity to the N-terminal half (Chapter 3, this thesis). For latter to be consistent with Scheme I and observations here, inhibitor binding to the N-terminal half must be synergistically with Glc binding to the C-terminal half. Indeed, the G896A enzyme (C-terminal inhibitor site impaired) exhibits a higher level of synergism than the T232A enzyme (N-terminal inhibitor site impaired). Hence, conformational change in HKI in response to the binding of Glc at the active site (C-terminal half) greatly enhances the binding of inhibitor to the N-terminal half of the protein. The conformational changes in HKI that leverage this effect are unclear. In essence, Glc is a substrate and a modulator of an allosteric inhibition.

Neither T232A HKI nor G896A HKI, enzymes that have impaired inhibitor binding sites at the N- and C-terminal half, respectively, exhibit Glc-relief of inhibition (Figure 5). High concentrations of Glc also have no effect on the truncated C-terminal half of HKI (mini HKI) (Figure 5). Evidently, the mechanism of Glc-relief of inhibition by 1,5-anhydroGlc-6-P affects the binding of the second inhibitor molecule. Given the property of binding antagonism for 1,5-anhydroGlc-6-P to the wild-type enzyme (Chapter 3, this thesis) the second inhibitor molecule binds to either the N- or C-terminal half with elevated site affinity constants relative to the first molecule of bound inhibitor. At sufficient concentrations, Glc can compete at either the N- or C-terminal half to remove the second molecule of bound inhibitor, but concentrations of Glc never rise sufficiently to compete with the first molecule of bound inhibitor. The Glc-relieved state of inhibition most likely puts a molecule of Glc (the third to bind to HKI) at the glucopyranose locus of the inhibitor pocket (Figure 6). Hence, the *EBBBI* complex is a mixture of two states of ligation: One state has one inhibitor and one Glc molecule bound to the N-terminal half with two Glc molecules bound to the C-terminal half and the other has two Glc molecules bound to the N-terminal half with one inhibitor and one Glc molecule bound to the C-terminal half. The two states may not be equally populated, but in the absence of dissociation constants for Glc from the

inhibitor sites, the dominant state (if any) cannot be determined.

The question also remains as to whether Glc-relief and P_i-relief of inhibition are additive. From the model presented in Chapter 3 of this thesis, one would predict no Glc-relief of inhibition in the presence of P_i. P_i would displace inhibitor from the N-terminal half, causing the site affinity constant for inhibitor at the C-terminal half to decrease from 163 to 62 μM (Chapter 3, Table VIII, this thesis). The effect would be equivalent to the mutation of Thr232 to alanine, which eliminates 1,5-anhydroGlc-6-P inhibition at the N-terminal half. T232A HKI does not exhibit Glc-relief of inhibition, and one would not expect Glc-relief in the presence of millimolar levels of P_i. Given these observations one might anticipate Glc- and Pi-relief mechanisms to overlap, and as a consequence be non-additive.

Tris and Hepes buffers result in significant differences in the kinetics of wild-type HKI. For instance, K_{bbii} almost doubles in Hepes relative to Tris. The doubling effect is consistent with results of Liu[26], which indicate elevated K_{ii} values in the presence of Hepes for the wild-type and engineered monomeric forms of HKI. One cannot rule out the possibility of Hepes at 100 mM competing with the binding of the second molecule of 1,5-anhydroGlc-6-P, but notably such competition is not evidenced by lower K_{bbi} values for potent inhibition. Other differences due to buffer and/or pH seem plausible. The K_L reported here (Hepes, pH 7.8) for the dissociation of TNP-ADP from wild-type HKI at 1 mM Glc is 0.18 ± 0.02 μM, a 3-fold difference from that reported in Chapter 2 (Tris, pH 7.5). K_A (dissociation constant for Glc-6-P) is 0.21 ± 0.01 μM in Hepes versus 0.51 ± 0.02 μM in Tris at 1 mM Glc (Table II). Tris has been the buffer of choice historically for investigations of hexokinase, but at low protein concentrations, the enzyme retains specific activity longer and has lower K_m values for Glc and ATP in Hepes than in Tris.

Fromm and colleagues reported a dissociation constant of 0.124 μM in Tris, pH 7.6, with 0.6 mM Glc and a dissociation constant of 0.50 μM putatively free of glucose[20];

however, complete removal of Glc from HKI is difficult even by means of extensive washing and dialysis[19, 29]. Kenkare and colleagues reported a dissociation constant of 0.9 ± 0.05 μM in NEM acetate buffer, pH 8.0, 0.1 M KCl and 2.5 mM Glc; and a constant of 2.8 ± 0.48 μM in the same buffer with 0.5 μM glucose. Results are consistent with previous reports indicating a decreased dissociation constant for Glc-6-P from HKI as concentrations of Glc increase[17, 19, 20]. This phenomenon reflects synergism between the binding of glucose to the C-terminal half, which in turn enhances inhibitor association at either the C- or N-terminal halves.

Under normal respiration, glycolysis is limited to 3% of capacity in the brain by the supply of glucose. P_i may play only a small role in regulation of HKI under these conditions[42]. Moreover, results here would indicate an absence of potent product inhibition (compare K_{bi} and K_{bbi}). During oxygen deprivation or heightened activity in localized regions of the brain, intracellular Glc concentrations can rise sharply as plasma glucose (at a level of 5 mM) floods into the brain cell through glucose transporters. Under these conditions, HKI is susceptible to potent feedback inhibition by product, and relief of that inhibition by possibly the combined actions of Glc and P_i. In erythrocytes, glucose concentrations are normally 5 mM and blood glucose homeostasis is tightly regulated[1]. Blood glucose levels in the blood cell is slightly elevated relative to the serum glucose concentration[45]. Hence, glucose concentrations inside the red blood cell are high enough to induce Glc-relief of Glc-6-P inhibition of HKI. In the erythrocytes of diabetic patients, Glc-6-P concentrations are elevated[30]. In normal erythrocytes, however, HKI is saturated with glucose. Thus the increase of Glc-6-P concentration under hyperglycemic conditions cannot be due to increased availability of glucose. In fact, high concentrations of Glc-6-P levels of diabetic patients may be evidence of Glc-relief of Glc-6-P inhibition of HKI, enhancing flux through glycolysis as a mechanism to reduce serum glucose levels. Further

relief of HKI from product inhibition in the red blood cell then could offer a means of treatment of the hyperglycemic condition.

Table I. Parameters for TNP-ADP titration experiments at different Glc concentrations [#]

	parameter	[Glc] = 5 μM	[Glc] = 25 μM	[Glc] = 75 μM	[Glc] = 1 mM
Buffer/ Baseline	a	0.27 ± 0.02	0.27 ± 0.01	0.244 ± 0.005	0.240 ± 0.006
	b	4.54 ± 0.09	4.57 ± 0.06	4.66 ± 0.03	4.65 ± 0.04
	c	0.12 ± 0.01	0.132 ± 0.008	0.141 ± 0.004	0.143 ± 0.005
Wild-type	K_L	0.118 ± 0.008	0.13 ± 0.01	0.15 ± 0.01	0.18 ± 0.02
	G	3.65 ± 0.02	3.80 ± 0.02	3.94 ± 0.02	4.09 ± 0.03
	S	1.3 ± 0.1	1.3 ± 0.2	1.2 ± 0.2	1.2 ± 0.2
T232A	K_L	0.095 ± 0.008	0.101 ± 0.009	0.12 ± 0.01	0.128 ± 0.009
	G	4.76 ± 0.03	4.79 ± 0.03	5.03 ± 0.04	5.32 ± 0.03
	S	1.0 ± 0.2	1.1 ± 0.2	0.7 ± 0.3	1.0 ± 0.2
G896A	K_L	0.46 ± 0.07	0.48 ± 0.06	0.53 ± 0.07	0.55 ± 0.06
	G	5.7 ± 0.1	5.8 ± 0.1	5.8 ± 0.1	6.02 ± 0.09
	S	2.0 ± 0.8	2.0 ± 0.6	2.6 ± 0.7	2.2 ± 0.6
Mini-HKI	K_L	0.11 ± 0.03	0.12 ± 0.03	0.13 ± 0.03	0.14 ± 0.02
	G	3.35 ± 0.06	3.41 ± 0.06	3.55 ± 0.06	4.03 ± 0.05
	S	2.2 ± 0.4	2.1 ± 0.4	1.9 ± 0.5	1.8 ± 0.4

[#]Experiments employ 2 μM enzyme in 50 mM Hepes, pH7.8, at indicted Glc concentrations.

Table II. Parameters for displacement of TNP-ADP by Glc-6-P at different Glc concentrations[#]

HKI	Parameter	[Glc] = 5 μM	[Glc] = 25 μM	[Glc] = 75 μM	[Glc] = 1 mM
Wild-type	K_A	0.29 ± 0.01	0.22 ± 0.01	0.21 ± 0.01	0.21 ± 0.01
	G	3.85 ± 0.02	3.99 ± 0.04	4.23 ± 0.04	4.55 ± 0.05
	S	2.6 ± 0.1	2.4 ± 0.2	1.9 ± 0.2	2.2 ± 0.2
T232A	K_A	2.14 ± 0.08	1.14 ± 0.04	0.97 ± 0.05	0.65 ± 0.03
	G	4.41 ± 0.03	4.48 ± 0.03	4.84 ± 0.04	5.11 ± 0.04
	S	3.0 ± 0.2	2.8 ± 0.2	3.3 ± 0.3	4.2 ± 0.3
G896A	K_A	1.07 ± 0.07	1.07 ± 0.05	1.09 ± 0.04	0.96 ± 0.05
	G	4.75 ± 0.06	5.08 ± 0.05	5.17 ± 0.04	5.34 ± 0.05
	S	8.6 ± 0.3	7.6 ± 0.2	7.6 ± 0.2	7.7 ± 0.2
Mini-HKI	K_A	0.60 ± 0.03	0.27 ± 0.02	0.16 ± 0.01	0.15 ± 0.01
	G	2.84 ± 0.02	3.11 ± 0.04	3.38 ± 0.06	3.98 ± 0.05
	S	8.4 ± 0.2	10.1 ± 0.2	9.7 ± 0.3	8.6 ± 0.2

[#]Experiments employ 3.36 μM TNP-ADP and 2 μM enzyme in 50 mM Hepes, pH7.8, at indicated Glc concentrations.

Table III. Fitting process for wild-type HKI in Tris buffer[$].

		Round 1	Round 2	Round 3	Round 4
k_{cat}	(s^{-1})	**83 ± 1**[#]	**83**	**83**	**83**
K_b	(μM)	1 ± 3	**1 ± 3**	**1 ± 3**	**1 ± 3**
K_{bb}	(μM)	**110 ± 5**[#]	**110**	**110**	**110**
K_{bbb}	(μM)	*1000*	*1000*	*1000*	1200 ± 400
K_a	(μM)	**1300 ± 20**[#]	**13000**	**1300**	**1300**
K_{bi}	(μM)	*100*	160 ± 70	**160 ± 70**	**160 ± 70**
K_{bbi}	(μM)	*15*	*15*	15.1 ± 0.3	**15.1 ± 0.3**
K_{bbbi}	(μM)	*15*	*15*	15.2 ± 0.4	**15.2 ± 0.4**
K_{bbii}	(μM)	*300*	280 ± 20	**280 ± 20**	**280 ± 20**
K_{bbbii}	(μM)	*600*	*600*	*600*	580 ± 60

[#]Determined independently.

[$]For each round, the **bold** font represents parameters already determined and fixed in the refinement of other parameters. The *italic* font represents the initial estimated for the parameters input prior to fitting, determined by trial-and-error spection. The underlined font represents parameters determined by Grafit for that round.

Table IV. Inhibition of 1,5-anhydroGlc-6-P with respect to Glc at fixed ATP concentrations[#]

HKI	Wild-type	Wild-type	T232A	G896A		Mini-HKI
Buffer	Hepes, pH7.8	Tris, pH8.0	Tris, pH8.0	Tris, pH8.0	Buffer	Tris, pH8.0
ATP (μM)	6000	6000	9000	600	ATP	9000
k_{cat} (s^{-1})	91	83	60	88	k_{cat} (s^{-1})	50
K_b (μM)	1 ± 3	1 ± 3	2 ± 1	4 ± 2		
K_{bb} [$] (μM)	57	110	81	45	K_b [*] (μM)	37.7
K_{bbb} (μM)	424 ± 113	1200 ± 400	900 ± 500	700 ± 200	K_{bb} (μM)	670 ± 130
K_a [$] (μM)	817	1300	1400	566	K_a [*] (μM)	1001
K_{bi} (μM)	516 ± 963	160 ± 70	220 ± 70	6000 ± 7000	K_i (μM)	43 ± 9
K_{bbi} (μM)	12.6 ± 0.7	15.1 ± 0.3	39 ± 5	152 ± 4	K_{bi} (μM)	5.6 ± 0.1
K_{bbbi} (μM)	11.4 ± 0.4	15.2 ± 0.4	52 ± 9	162 ± 2	K_{bbi} (μM)	4.9 ± 0.1
K_{bbii} (μM)	150 ± 10	280 ± 20	N.A.	N.A.		
K_{bbbii}(μM)	230 ± 10	580 ± 60	N.A.	N.A.		

[#]Data for wild-type enzyme is fitted according to Scheme I and Eqn. 1, T232A and G896A are fitted according to Scheme II and Eqn. 2 and mini-HKI are fitted according to Scheme III and Eqn. 3.

[$]$K_{bb}$ is K_m^{Glc} and K_a is K_m^{ATP} for wild-type HKI, T232A and G896A.

*K_b is K_m^{Glc} and K_a is K_m^{ATP} for mini-HKI.

N.A.: not applicable

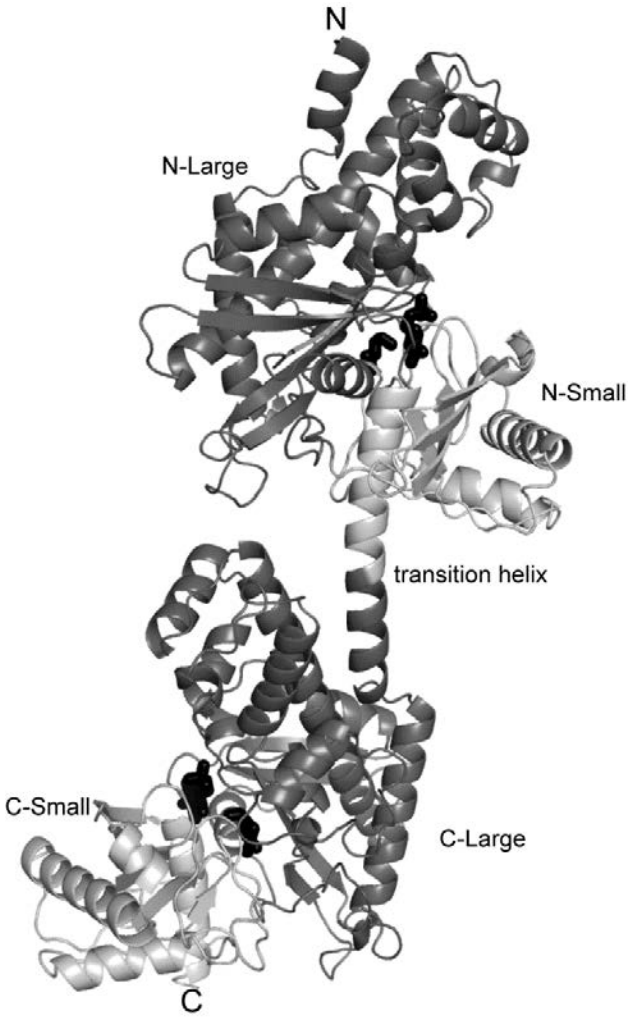

Figure 1. Overview of HKI·Glc-6-P·Glc complex (PDB: 1HKB). The large domains are colored dark grey and small domains colored light grey. Ligands Glc-6-P and Glc are colored black as sticks. (The illustration was generated with PyMOL.)

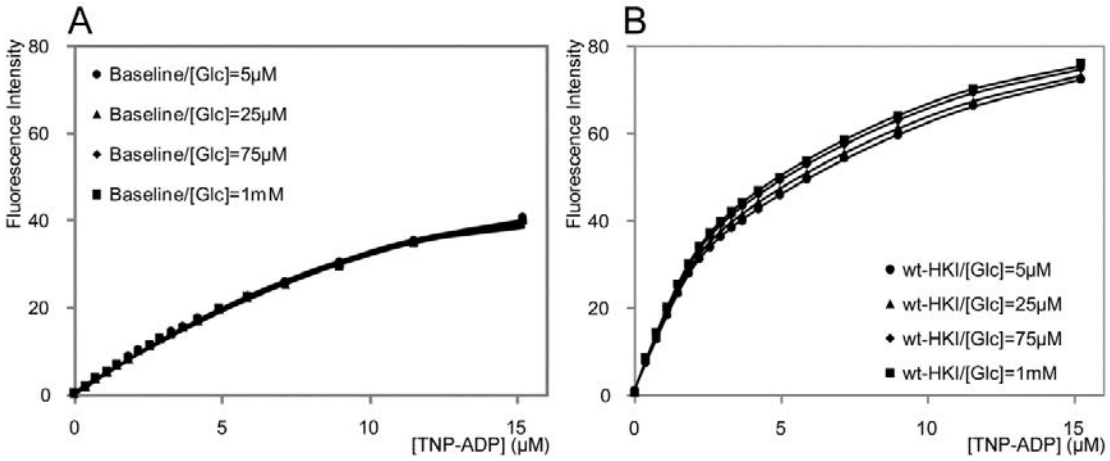

Figure 2. TNP-ADP baseline and binding to wild-type HKI at different concentrations of Glc. A, Addition of TNP-ADP to 50 mM Hepes buffer, pH 7.8. B, Addition of TNP-ADP to 2 μM HKI in 50 mM Hepes, pH 7.8. Glc concentrations are as indicated.

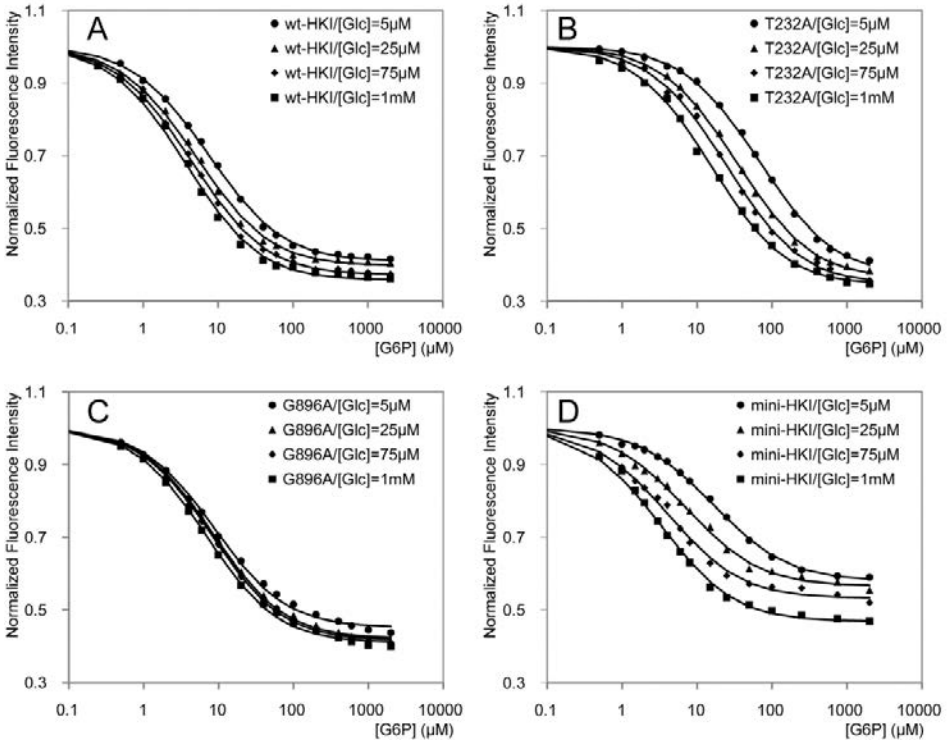

Figure 3. Displacement of TNP-ADP by Glc-6-P at different concentrations of Glc for wild-type and mutant HKI. A, wild-type HKI. B, T232A. C, G896A. D, mini-HKI. Glc concentrations are as indicated ---- Raw data is as following (without vertical axis normalized):

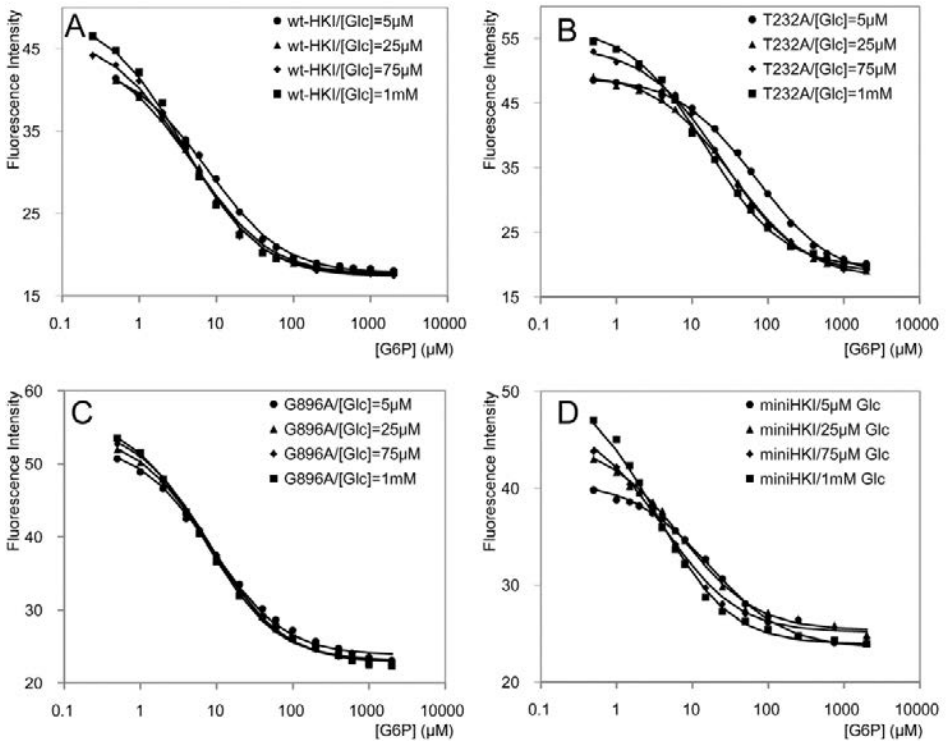

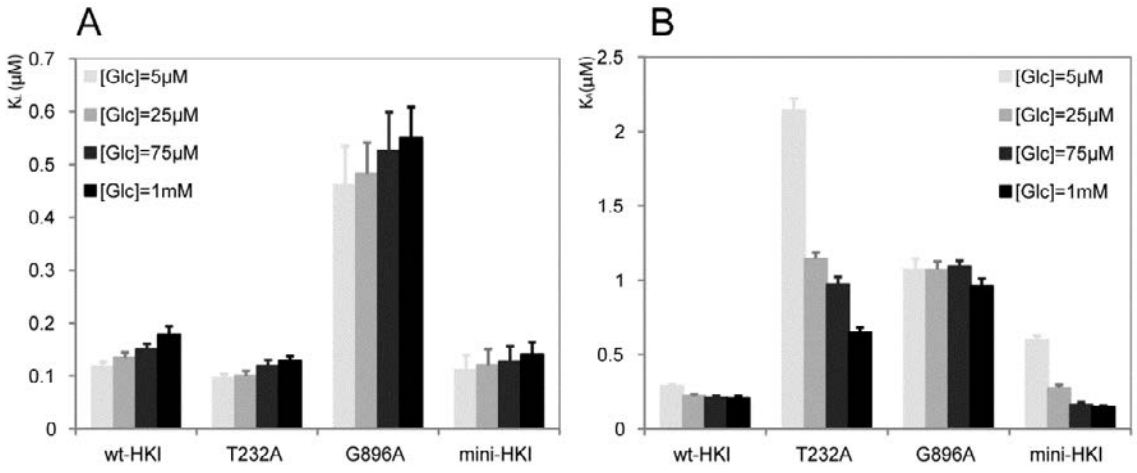

Figure 4. Dissociation constants for TNP-ADP (K_L. *panel A*) and Glc-6-P (K_A, *panel B*) for wild-type and mutant HKI at different concentrations of Glc.

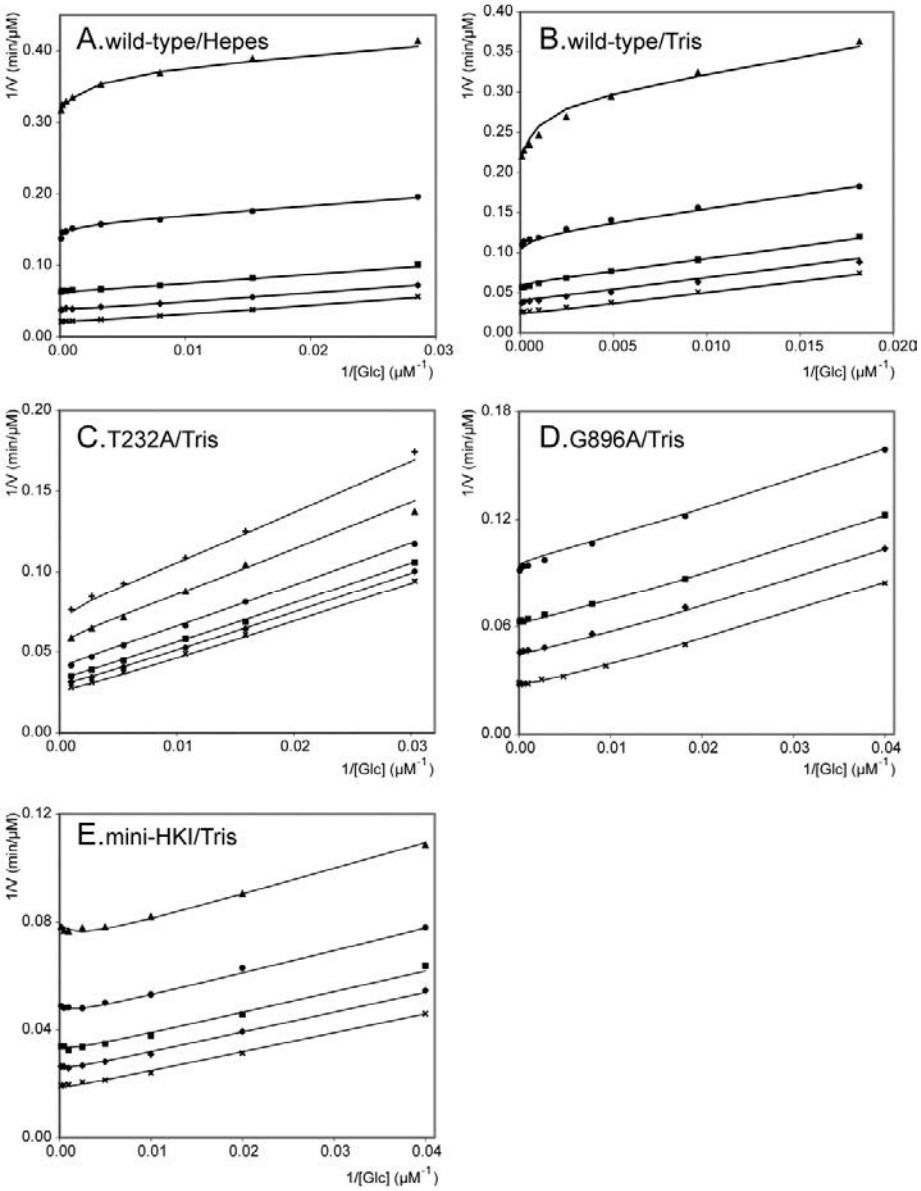

Figure 5. Inhibition of HKI enzymes by 1,5-anhydroGlc-6-P with respect to Glc at fixed ATP concentrations. Assays are in 50 mM Hepes, pH 7.8, 0.2 mM NADP, and 3 mM $MgCl_2$ (*panel A*) or in 80 mM Tris, pH 8.0, 0.4 mM NADP, and 3 mM $MgCl_2$ (*panels B–E*). A. wild-type HKI with [Glc] = 35 μM–10 mM, [1,5-anhydroGlc-6-P] = 50–385μM, and [ATP] = 4.5 mM. The data were fit to Scheme I and Eqn. 1. B. wild-type HKI with [Glc] = 55μM–10mM, [1,5-anhydroGlc-6-P] = 50-385 μM, [ATP] = 6 mM. The data were fit Scheme I and Eqn. 1. C. T232A HKI with [Glc] = 33μM–1mM, [1,5-anhydroGlc-6-P] = 10–600 μM, [ATP] = 9mM. The data were fit to Scheme II and Eqn. 2. D. G896A HKI with [Glc] = 25 μM–10 mM, [1,5-anhydroGlc-6-P] = 200–800 μM, [ATP] = 0.6 mM. The data were fit to Scheme II and Eqn. 2. E. mini-HKI with [Glc] = 25 μM–5 mM, [1,5-anhydroGlc-6-P] = 20-160 μM, [ATP] = 9 mM The data were fit to Scheme III and Eqn. 3.

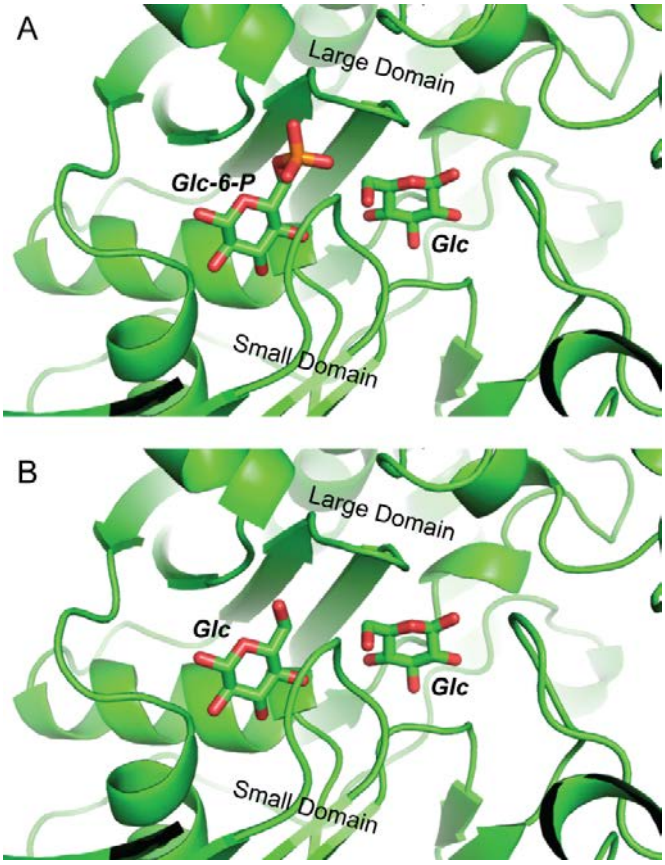

Figure 6. Glucose binding sites observed and implied. A. Glc-6-P and Glc molecules sit in the ligand pocket (from crystal structure of the HKI•Glc-6-P•Glc complex, Chapter 1, this thesis). B. Model for two bound Glc molecules in the ligand pocket. (This illustration was generated with PyMOL).

Reference

1. Berne, R.M., and Levy, M.N. (1992) *Physiology*. Third Edition Mosby Year Book, Chicago
2. Aleshin, A.E., Zeng, C., Bourenkov, G.P., Bartunik, H.D., Fromm, H.J., and Honzatko, R.B. (1998) The mechanism of regulation of hexokinase: new insights from the crystal structure of recombinant human brain hexokinase complexed with glucose and glucose-6-phosphate. *Structure.* **6**, 39-50
3. Hers, H.G., and Hue, L. (1983) Gluconeogenesis and related aspects of glycolysis. *Annu. Rev. Biochem*. **52**, 617-653
4. Gonzalez, C., Ureta, T., Sánchez, R., and Niemeyer, H. (1964) Multiple molecular forms of ATP: hexose 6-phosphotransferase from rat liver. *Biochem. Biophys. Res. Commun.* **16**, 347-352
5. Grossbard, L., and Schimke, R.T. (1966) Multiple hexokinases of rat tissues. Purification and comparison of soluble forms. *J. Biol. Chem*. **241**, 3546-3560
6. Katzen, H.M. (1967) The multiple forms of mammalian hexokinase and their significance to the action of insulin. *Adv. Enzyme Regul*. **5**, 335-356
7. Katzen, H.M., and Schimke, R.T. (1965) Multiple forms of hexokinase in the rat: tissue distribution, age dependency, and properties. *Proc. Natl. Acad. Sci. U.S.A.* **54**, 1218-1225
8. Wilson, J.E. (1995) Hexokinase. *Rev. Physiol. Biochem. Pharmacol*. **126**, 65-198
9. Easterby, J.S, and O'Brien, M.J. (1973) Purification and properties of pig-heart hexokinase. *Eur. J. Biochem*. **38**, 201-211
10. Holroyde, M.J., and Trayer, I.P. (1976) Purification and properties of skeletal muscle hexokinase. *FEBS Lett*. **62**, 215-219
11. Ureta, T. (1982) The comparative isozymology of vertebrate hexokinases. *Comp. Biochem. Physiol*. **71B**, 549-555
12. Manning, T.A., and Wilson, J.E. (1984) Inhibition of brain hexokinase by a multisubstrate analog results from binding to a discrete regulatory site. *Biochem. Biophys. Res. Commun.* **118**, 90-96
13. Wilson, J.E. (2003) Isozymes of mammalian hexokinase: structure, subcellular localization and metabolic function. *J. Exp. Biol.* **206**, 2049-2057
14. Pedersen, P.L., Mathupala, S., Rempel, A., Geschwind, J.F., and Ko, Y.H. (2002) Mitochondrial bound type II hexokinase: a key player in the growth and survival of

many cancers and an ideal prospect for therapeutic intervention. *Biochim. Biophys. Acta*. **1555**, 14-20

15. Bryson, J.M., Coy, P.E., Gottlob, K., Hay, N., and Robey, R.B. (2002) Increased hexokinase activity, of either ectopic or endogenous origin, protects renal epithelial cells against acute oxidant-induced cell death. *J. Biol. Chem.* **277**, 11392-11400
16. Tsai, H.J. and Wilson, J.E. (1996) Functional organization of mammalian hexokinases: both N- and C-terminal halves of the rat type II isozyme possess catalytic sites. *Arch. Biochem. Biophys.* **329**, 17-23
17. White, T.K., and Wilson, J.E. (1989) Isolation and characterization of the discrete N- and C-terminal halves of rat brain hexokinase: retention of full catalytic activity in the isolated C-terminal half. *Arch. Biochem. Biophys*. **274**, 375-393
18. Arora, K.K., Filburn, C.R., and Pedersen, P.L. (1993) Structure/function relationships in hexokinase. Site-directed mutational analyses and characterization of overexpressed fragments implicate different functions for the N- and C-terminal halves of the enzyme. *J. Biol. Chem*. **266**, 5359-5362
19. Mehta, A., Jarori, G.K., and Kenkare, U.W. (1988) Brain hexokinase has no preexisting allosteric site for glucose 6-phosphate. *J Biol Chem*. **263**, 15492-15497
20. Ellison, W.R., Lueck, J.D., and Fromm, H.J. (1975) Studies on the mechanism of orthophosphate regulation of bovine brain hexokinase. *J. Biol. Chem*. **250**, 1864-1871
21. Mulichak, A.M., Wilson, J.E., Padmanabhan, K., and Garavito, R.M. (1998) The structure of mammalian hexokinase-1. *Nat. Struct. Biol*. **5**, 555-560
22. Aleshin, A.E., Fromm, H.J., and Honzatko, R.B. (1998) Multiple crystal forms of hexokinase I: new insights regarding conformational dynamics, subunit interactions, and membrane association. *FEBS Lett*. **434**, 42-46
23. White, T.K., and Wilson, J.E. (1987) Rat brain hexokinase: location of the allosteric regulatory site in a structural domain at the N-terminus of the enzyme. *Arch. Biochem. Biophys.* **259**, 402-411
24. Zeng, C., and Fromm, H.J. (1995) Active site residues of human brain hexokinase as studied by site-specific mutagenesis. *J. Biol. Chem*. **270**, 10509-10513
25. Fang, T.Y., Alechina, O., Aleshin, A.E., Fromm, H.J., and Honzatko, R.B. (1998) Identification of a Phosphate Regulatory Site and a Low Affinity Binding Site for Glucose 6-Phosphate in the N-terminal Half of Human Brain Hexokinase. *J. Biol. Chem*. **273**, 19548-19553

26. Liu, X., Kim, C.S., Kurbanov, F.T., Honzatko, R.B., and Fromm, H.J. (1999) Dual Mechanisms for Glucose 6-Phosphate Inhibition of Human Brain Hexokinase. *J. Biol. Chem.* **274**, 31155-31159

27. Solheim, L.P, and Fromm, H.J. (1981) Kinetic evidence that the high-affinity glucose 6-phosphate site on hexokinase I is the active site. *Arch. Biochem. Biophys.* **211**, 92-99

28. Solheim, L.P, and Fromm, H.J. (1983) Effect of inorganic phosphate on the reverse reaction of bovine brain hexokinase. *Biochemistry*. **22**, 2234-2239

29. Aleshin, A.E., Zeng, C., Bartunik, H.D., Fromm, H.J., and Honzatko, R.B. (1998) Regulation of Hexokinase I: Crystal Structure of Recombinant Human Brain Hexokinase Complexed with Glucose and Phosphate. *J. Mol. Biol*. **282**, 345-357

30. Fujii, S., and Beutler, E. (1985) High glucose concentrations partially release hexokinase from inhibition by glucose 6-phosphate. *Proc. Natl. Acad. Sci. U.S.A.* **82**, 1552-1554

31. Laemmli, U.K. (1970) Cleavage of structural proteins during the assembly of the head of bacteriophage T4. *Nature.* **227**, 680-685

32. Bradford, M.M. (1976) A rapid sensitive method for the quantitation of microgram quantities of protein utilizing the principle of protein-dye binding. *Anal. Biochem.* **72**, 248-252

33. Faller, L.D. (1990) Binding of the fluorescent substrate analogue 2',3'-O-(2,4,6-trinitrophenylcyclohexadienylidene)adenosine 5'-triphosphate to the gastric H+, K(+)-ATPase: evidence for cofactor-induced conformational changes in the enzyme. *Biochemistry.* **29**, 3179-3186

34. Nimer, M., Watanabe, M., Shen, L., Skaff, D.A., and Honzatko R.B. (2012) Mechanism of ATP-dependent release of wild-type and mutant human brain hexokinases from mitochondria. (to be submitted)

35. Leatherbarrow, R.J. (2010) GraFit Version 7, Erithacus Software Ltd., Horley, U.K.

36. Liu, F., Dong, Q., Myers, A.M., and Fromm, H.J. (1991) Expression of human brain hexokinase in Escherichia coli: purification and characterization of the expressed enzyme. *Biochem. Biophys. Res. Commun.* **177**, 305-311

37. Ferrari, R., and Crane, R. (1959) 1,5-Anhydro-D glucitol 6-phosphate and its use for the specific inhibition of the hexokinase reaction in tissue homogenates. *Arch. Biochem. Biophys.* **80**, 372-377

38. Drueckes, P., Schinzel, R., and Palm, D. (1995) Photometric microtiter assay of inorganic phosphate in the presence of acid-labile organic phosphates. *Anal. Biochem*. **230**, 173-177

39. Aleshin, A.E., Kirby, C., Liu, X., Bourenkov, G.P., Bartunik H.D., Fromm, H.J., and Honzatko, R.B. (2000) Crystal structures of mutant monomeric hexokinase I reveal multiple ADP binding sites and conformational changes relevant to allosteric regulation. *J. Mol. Biol*. **296**, 1001-1015

40. Magnani, M., Bianchi, M., Casabianca, A., Stocchi, V., Daniele, A., Altruda, F., Ferrone, M., and Silengo, L. (1992) A recombinant human 'mini'-hexokinase is catalytically active and regulated by hexose 6-phosphates. *Biochem. J*. **285**, 193-199

41. Raskin P. (1994) Risk factors for the development of diabetic complications. *J. Diabetes Complications.* **8**, 195-200

42. Lowry, O.H., and Passonneau, J.V. (1964) The relationships between substrates and enzymes of glycolysis in brain. *J. Biol. Chem.* **239**, 31-42

43. Copley, M., and Fromm, H.J. (1967) Kinetic studies of the brain hexokinase reaction. A reinvestigation with the solubilized bovine enzyme. *Biochemistry*. **6**, 3503-3509

44. Smith, A.D., and Wilson, J.E. (1991) Effect of ligand binding on the tryptic digestion pattern of rat brain hexokinase: relationship of ligand-induced conformational changes to catalytic and regulatory functions. *Arch. Biochem. Biophys*. **291**, 59-68

45. Chawla R. (2003) *Practical Clinical Biochemistry: Methods and Interpretations*. 3rd Edition

Chapter V. Tracking Allosteric Pathways in Human Hexokinase Type I by Directed Mutation

Lu Shen, Yang Gao and Richard B. Honzatko

Department of Biochemistry, Biophysics and Molecular Biology,

Iowa State University, Ames IA 50011

Abstract

Hexokinase I (HKI) catalyzes the first step in glycolysis, the formation of glucose 6-phosphate (Glc-6-P) from glucose (Glc). HKI is subject to potent product inhibition and relief of product inhibition by phosphate P_i. Crystallographic studies reveal paired binding sites for Glc-6-P and Glc at each half of HKI, and a high-affinity binding site for P_i at the N-terminal half. Glc-6-P can inhibit catalysis by binding to the N-terminal half or C-terminal half. P_i partially relieves inhibition by displacing Glc-6-P from the N-terminal half. Here we explore the effect of mutations at putative structural elements of the regulatory machinery of HKI, the ends of the transition helix connecting N- and C-terminal halves and the flexible subdomain of C-terminal half including the contact region between two halves of HKI. Mutations at both the N-terminal end of the transition helix and the flexible subdomain severely disrupt 1,5-anhydroGlc-6-P inhibition and P_i-relief of inhibition. HKI activity and inhibition kinetics with alternative nucleoside triphosphates indicate different functional states for the C-terminal half of HKI relative to truncated HKI lacking the N-terminal half. Results from directed mutation are consistent with a proposed mechanism in which the ligation of the N-terminal half by Glc-6-P induces a rotation of the N-terminal half that alters nonbonded contacts with and within the flexible subdomain of the C-terminal half. Conformational changes in the flexible subdomain, which involve the re-organization of hydrophobic residues within the core of that domain, stabilize an open binding pocket for ATP.

Introduction

Hexokinase (ATP: D-hexose 6-phosphotransferase, EC2.7.1.1) catalyzes the first step of glycolysis, the phosphorylation of 6-hydroxyl group of glucose (Glc) using $[ATP\text{-}Mg]^{2-}$ as

the phosphoryl donor [1-3]. Four isozymes of hexokinase have been identified in mammalian tissues [4]. Type I, II and III hexokinases, all with molecular weights of approximately 100 kDa, share 70% sequence identity[5], whereas isozyme IV (glucokinase) has molecular weights of 50 kDa[5]. N- and C- terminal halves of isozymes I–III, as well as isozyme IV, show extensive sequence and structure similarity but different functional properties [5]. Both halves of hexokinase II possess catalytic activity, whereas the N-halves of hexokinase I and III are inactive [5-8]. The reaction product, glucose-6-phosphate (Glc-6-P), potently inhibits isozymes I-III (but not isoform IV, 50kDa) at physiologically relevant concentrations [5]. Inorganic phosphate (P_i) itself is an inhibitor of hexokinase II and III[5]. However, P_i specifically antagonizes the inhibition of hexokinase I by Glc-6-P at relatively low concentrations; whereas, at higher concentrations it acts as an inhibitor competitive with ATP[5].

Presumably, all members in the hexokinase family derive from a common ancestor, a 30 kDa glucomannokinase-like enzyme which utilized poly(P) as substrate in an age before the appearance of ATP[9]. During evolution, this ancient hexokinase acquired additional attributes, such as flexible subdomain (residues 766–812 in hexokinase I) and became ATP-specific at the cost of losing poly(P) as a substrate[9]. Through gene duplication and fusion, the 100 kDa hexokinase architecture appeared[10-13]. However, whether the product inhibition evolved before or after gene duplication and fusion remains unclear.

Wild-type HKI exists as a head-to-tail dimer in crystals[14-16]. Mutations that disrupt dimerization retain properties in Glc-6-P inhibition and P_i-relief, indicating the allosteric communication must come from crosstalk between the N- and C- terminal halves of a single subunit[17]. The N- and C-terminal halves are connected by a long transition helix which starts from Glc-6-P binding site at the N-terminal half. C-terminal half of HKI is in an open state and the N-terminal half closed when Glc and P_i are present[18]. Glc-6-P induces the closure of C-terminal half as well as a rotation of the N-teminal half relative to the C-terminal half. That rotation alters contacts between segment 241–253 from the N-terminal half and the flexible subdomain from C-terminal half[17]. ADP-bound HKI is in a conformation similar to Glc-6-P-bound HKI, with N- and C- terminal halves closed;

however, the flexible subdomain from C-terminal half is substantially different in two structures[18]. A pocket for the base moiety of ADP is closed when Glc-6-P is bound, and Thr784 exists in different locations and networks of hydrogen bonds in the presence of the adenine nucleotide or Glc-6-P.

In crystal structures, Glc-6-P binds to both halves of hexokinase I (HKI)[14-17]. When HKI is cleaved proteolytically into two halves, the C-terminal half (mini-HKI) is active and inhibited potently by Glc-6-P and this inhibition is not subject to P_i-relief[8, 19]. The N-half of HKI is inactive, but it still binds Glc-6-P tightly[7-8]. Mutational studies have shown that Glc-6-P is capable of inhibiting HKI potently when binding to either of the two binding sites on the enzyme[20-21]. Only mutations at both Glc-6-P binding sites eliminate the inhibition[21]. Data from equilibrium binding and kinetics experiments, however, indicate only one molecule of Glc-6-P binds to HKI with high-affinity, causing potent Glc-6-P inhibition[21-25].

Investigators have differed as to the Glc-6-P inhibition mechanism since the 1970s. According to Fromm, Glc-6-P inhibits the enzyme by binding to the C-terminal half, the 6-phosphoryl group directly competing with the γ-phosphoryl site of ATP[23, 26]. Wilson assigned Glc-6-P inhibition to an allosteric site at the N-terminal half, on the basis of Glc-6-P protection against proteolysis[7, 27]. Both Fromm and Wilson agree, however, that P_i antagonizes Glc-6-P inhibition by binding to a high-affinity site at the N-terminal half[5, 18]. P_i competes with Glc-6-P for the same phosphoryl binding site directly in the Wilson model, whereas P_i competes via an allosteric mechanism with Glc-6-P bound at the C-terminal half in the Fromm model[5, 18]. The existence of a single high-affinity site for Glc-6-P in equilibrium binding experiments can be reconciled with high affinity sites in each of the C- and N-terminal halves by a mechanism of anti-cooperativity in Glc-6-P binding[21]. The most recent variation (Chapters 3 & 4, this thesis) requires Glc to bind at the active site in order to induce potent inhibition at either the N- or C-terminal halves, with inhibitor binding being mutually antagonistic. P_i relieves allosteric inhibition by the displacement of inhibitor from the N-terminal half; however, intrinsically weaker inhibition at the C-terminal half is not relieved by P_i. Regardless of model, allosteric communications between N- and

C-terminal halves of HKI is an expectation.

Presented here are studies that demonstrate an effect of the N-terminal half on the functional properties of the C-terminal half of HKI, that the molecular mechanism of inhibition for the truncated C-terminal half (mini HKI) differ significantly from that of wild-type HKI. In addition, directed mutations at the N-terminal end of the transition helix and the flexible subdomain of the C-terminal half reveal significant effects at inhibitor binding pockets well removed from the sites of mutation. The results are in agreement with the model proposed by Aleshin *et al.*[17]: rigid-body movement of the N-terminal domain induced by the binding of inhibitor stabilizes the flexible subdomain in a conformation unfavorable to the binding of ATP.

Materials and methods

Materials— A full-length cDNA of human hexokinase I, cloned into vector pET-11a was available from previous studies[19, 28-29]. Oligonucleotides came from IDT-DNA. DNA sequencing was done at the Iowa State University DNA Synthesis and Sequencing Facility. *Escherichia coli* strain DH5a and BL21 were from Invitrogen. DNaseI, phenylmethanesulfonyl fluoride (PMSF), leupeptin, bovine serum albumin (BSA), ATP, NADP, ampicillin, glucose 6-phosphate, mannose 6-phosphate and 2-deoxy-D-glucose 6-phosphate were from Sigma. 1,5-anhydro-D-sorbitol was from Toronto Research Chemicals. Isopropyl-D-thiogalactopyranoside (IPTG) was from Bio-World. DEAE sepharose CL-6B and CHT ceramic hydroxyapatite (HA) Type II were from Bio-Rad. DEAE-5PW HPLC media was from Tosohaas. Glucose-6-phosphate dehydrogenase (G6PDH) was from Roche.

Construction, Expression and Purification of Wild-type and Mutant Hexokinase I—
Oligonucleotide primers for directed mutations are as follows:
5’-GGC-ACC-ATG-ATG-GCG-TGT-GGC-TAT-GAC-GAC-3’ for T216A,
5’-C-CTG-ATC-ATC-GGC-GCG-GGC-ACC-AAT-GCT-TGC-3’ for T232A,
5’-CGC-TTC-CTC-CTC-GCG-GAG-AGT-GGC-AGC-3’ for S445A;
5’-CTC-CTC-TCG-GAG-GAT-GGC-AGC-GGC-AAG-G-3’ for S447D;

5’-C-CTC-TCG-GAG-AGT-GCG-AGC-GGC-AAG-G-3’ for G448A;
5’-G-GAG-AGT-GGC-CCG-GGC-AAG-GGG-GCT-G-3’ for S449P;
5’-G-CAG-ATA-GAG-GAG-ACC-GAT-GCT-CAT-TTC-CAC-3’ for L474D;
5’-GAG-ACC-CTG-GCT-CAT-GCG-CAC-CTC-ACC-AAA-GAC3’ for F477A;
5’-G-GAT-GAT-ATC-AGG-ATT-CAC-TAC-GAC-AGA-CTG-3’ for T723I;
5’-CG-ATG-AAG-ACC-CGG-GGC-GCG-TTT-GAG-ACC-AAG -3’ for L781A;
5’-GC-ATC-TTT-GAG-GCG-AAG-TTT-CTC-TCT-C-3’ for T784A;
5’-GC-ATC-TTT-GAG-CTG-AAG-TTT-CTC-TCT-C-3’ for T784L;
5’-GC-ATC-TTT-GAG-ACC-AAG-ATG-CTC-TCT-CAG-ATC-G-3’ for F786M;
5’-GC-ATC-TTT-GAG-ACC-AAG-GAT-CTC-TCT-CAG-ATC-G-3’ for F786D;
5’-GAG-AGT-GAC-CGA-GAA-GCA-CTG-CTC-CAG-GTC-3’ for L795E;
5’-GT-GAC-CGA-TTA-GCA-ACC-CTC-CAG-GTC-CGG-GCT-ATC-3’ for L797T;
5’-C-CGA-TTA-GCA-CTG-GAA-CAG-GTC-CGG-GCT-ATC-3’ for L798E;
5’-CTC-CAG-GTC-CGG-GCT-GCG-CTC-CAG-CAG-CTA-GG-3’ for I803A;
5’-GG-ACA-CTC-TAC-AAG-GCG-CAT-CCA-CAC-TTC-TCC-3’ for L867A;
5’-GG-ACA-CTC-TAC-AAG-TAT-CAT-CCA-CAC-TTC-TCC-3’ for L867Y and
5’-CTC-CTG-TCT-GAG-GAT-GCG-AGC-GGC-AAG-G-3’ for G896A, where in each of the preceding, the altered codon is underlined.

A 200 ml culture of the transformed *Escherichia coli* BL21 was grown overnight at 37 ºC in LB medium (33mg/L ampicillin) and then 1.5% cell were transferred to 9.6L LB medium (33mg/L ampicillin). The culture was grown at 300 rpm and 37 ºC to A_{600}=1.0. The temperature then was reduced to 16 ºC, isopropyl-β-D-thiogalactopyranoside (IPTG) was added to a final concentration of 0.5 mM and the culture was grown at 200 rpm for 20-22 hr. at 16 ºC. The cells were re-suspended in 25 mM KP_i (pH 7.5), 5 mM glucose, 3 mM $MgCl_2$, 1 mM dithiothreitol (DTT), 1 mM phenylmethanesulfonyl fluoride (PMSF), 50 μg/ml DNaseI and 5 μg/ml leupeptin. The cells were broken by sonication and then centrifuged (33,000*x*g, 1 hr.). The supernatant fluid was adjusted to pH 7.5 and loaded onto a DEAE-anion exchange column, using 25 mM KP_i, 5 mM glucose, 1 mM dithiothreitol DTT (pH 7.5), with a gradient of 0–400 mM NaCl. The fractions containing HKI activity were pooled,

concentrated and dialyzed against 50 mM KP_i (pH 7.0), 5 mM glucose, 1 mM dithiothreitol (DTT) and loaded onto a ceramics hydroxyapatite column with a gradient of 0.05–1 M KP_i (pH 7.0). HKI was collected and dialyzed against 25 mM KP_i, 5 mM glucose, 1 mM dithiothreitol (DTT) (pH 7.5), and further purified by DEAE-5PW HPLC chromatography with a gradient of 0–500 mM NaCl. The pure protein was identified by sodium dodecylsulfate polyacrylamide gel electrophoresis (SDS-PAGE)[30]. Protein concentration was determined by the method of Bradford with BSA as a standard[31].

Hexokinase I Kinetics Studies— Hexokinase activity was determined by the glucose-6-phosphate dehydrogenase (G6PDH, E.C.1.1.1.49) coupled spectrometric assay[29]. Commercial G6PDHas an ammonium sulfate precipitate was dialyzed against 80 mM Tris (pH 8.0) to remove sulfate, that mimics P_i in relief of 1,5-anhydroGlc-6-P inhibition. 1,5-anhydroGlc-6-P is a surrogate for Glc-6-P in the kinetics of Glc-6-P inhibition. The dicyclohexylamine salt of 1,5-anhydroGlc-6-P was prepared as described by Ferrari & Crane.[32] and it concentration determined by the method described by Drueckes *et al.*[33]. The concentration of hexokinase in kinetics assay was 1.2–2.0 μg/ml. The assay buffer for wild-type and mutant enzymes has 80 mM Tris, pH 8.0, 0.4 mM NADP, 3 mM $MgCl_2$ and 2 mM Glc. For the determination of K_m^{Glc}, the assay buffer contained 80 mM Tris, pH 8.0, 0.4 mM NADP, 3 mM $MgCl_2$, 9 mM $[ATP\text{-}Mg]^{2-}$ with concentrations of Glc over the range of 1/5 K_m^{Glc} to 5 K_m^{Glc}. For the determination of K_m^{ATP}, the assay buffer contained 80 mM Tris, pH 8.0, 0.4 mM NADP, 3 mM $MgCl_2$ and 2 mM Glc with concentrations of $[ATP\text{-}Mg]^{2-}$ ranging from 1/5 K_m^{ATP} to 5 K_m^{ATP}. Determination of KI and KII employed a concentration of Glc of 2 mM, concentrations of 1,5-anhydroGlc-6-P from 0–400 μM and those of $[ATP\text{-}Mg]^{2-}$ from 1/2 K_m^{ATP} to 4 K_m^{ATP}. P_i-relief of inhibition (%) is defined as $100\times(A\text{-}B)/A$, where A is the slope from (relative velocity of HKI)$^{-1}$ *versus* inhibitor concentration in the absence of P_i, and B is the slope from plot of (relative velocity of HKI)$^{-1}$ *versus* inhibitor concentration in the presence of 6 mM P_i[21]. The relative velocity of HKI in the absence of inhibitor and P_i is unity[21]. The $[ATP\text{-}Mg]^{2-}$ concentration is fixed at K_m^{ATP} in P_i-relief assays. Determination of K_{PI} and site dissociation constants is as described in Chapter 3 of this thesis. Data-fitting was done with the computer program GraFit 7.0[34].

Results

Rationale for Directed Mutations— In the model of allostery proposed by Aleshin *et al*.[17], the binding of Glc-6-P leverages a rotation of the N-terminal half about the end of the transition helix, which in turn induces conformational change in the flexible subdomain of the C-terminal half (Figure 1). The flexible subdomain can have two conformations, one of which prefers bound ATP and the other bound Glc-6-P. In fact, glucokinase, which is insensitive to Glc-6-P inhibition, adopts an arrangement of residues (including the critical threonine) consistent with that observed for the ADP complex of HKI. If the Aleshin mechanism is correct, then mutations to specific residues in the core of the flexible subdomain and near the N-terminus of the transition helix (pivot for the rotation of the N-terminal half) should greatly affect inhibition.

Mutations in the vicinity of the pivot focus on the glucopyranose pocket of Glc-6-P, which includes a segment (loop 445–449) that exhibits conformational differences in crystal structures of P_i- and Glc-6-P-complexes of wild-type HKI[14, 18] (Figure 2). Not only do main-chain angles of loop 445–449 differ, Ser499 hydrogen bonds with the 2-OH group of Glc-6-P, making a direct connection between inhibitor and the N-terminal end of the transition helix (Figure 3). The mutation G448A is incompatible with observed main-chain angles and/or packing interactions observed in both the P_i- and Glc-6-P-complexes (Figure 4). S449P restrains the motion of the loop and disrupts hydrogen bonds between loop and inhibitor. Thr216 forms a hydrogen bond with the carbonyl group of Gly448 in the P_i complex, but not in the Glc-6-P complex.

The flexible subdomain combines a loop (residues 766–783) and two helices (α9, residues 784–791, and α10, residues 797–807)[14]. The base of ADP occupies a crevice between helix α9 and helix α11' (residues 862–868)[17]. Asp861 is important for catalysis and the inhibition at the C-terminal half (Chapter 2, this thesis), and Lys866 is important to inhibition (Chapter 3, this thesis). Hydrogen bonds between the base of ADP and residues of helix α9 (Figure 5) indicate a direct role for the flexible subdomain in the recognition of ATP. In the ADP complex structure, Thr784 from helix α9 forms a hydrogen bond with the backbone carbonyl group of Gly747[17]. The backbone carbonyl Gly747 also hydrogen

bonds with 2'-hydroxyl group of the adenine nucleotide[17]. Thr784 in the Glc-6-P complex, blocks the base binding pocket of ADP (Figure 5). Leu867, from helix α11', makes non-bonded contacts with the base of ADP[17] (Figure 5). Electron density is present for two conformations of Phe786. One conformer puts the side chain into the hydrophobic core of the flexible domain, whereas the other exposes the side chain to solvent. Non-bonded contacts involving the side chains of Ile781 and Ile803 (Figure 5) also exhibit significant differences in the ADP and Glc-6-P-complexes of HKI. The residues in the N-terminal half corresponding to Phe786 and Ile781 are Asp338 and Lys333, respectively. Similarly, hydrophobic residues Leu795, Leu797 and Leu798 have residues with polar side chain in the N-terminal half (Figure 5).

The last locus for sites of mutations (Leu474, Phe477 and T723) explored whether a point of articulation exists as the C-terminal end of the helix (Figure 3).

Finally, in the instance of G448A, the effect on function was so significant, that the corresponding mutation to the C-terminal half (G896A) was simply done out of curiosity, and provided the best construct known in eliminating C-terminal half inhibition by 1,5-anhydroGlc-6-P without greatly affecting catalytic activity.

The type of mutation was often the substitution of alanine, but in several cases residue types observed in the N-terminal half were substituted for corresponding residues of the C-terminal half.

Kinetics Results for Wild-type and Mutant Hexokinases— Wild-type and mutant hexokinases are at least 95% pure as determined by SDS-polyacrylamide gel electrophoresis (data not shown). Shown in Table I are kinetic parameters for all mutant enzymes. Mutant enzymes for which the analytical methods of Chapter 3 are possible (data available for K_i, K_{ii} and K_{PI}), have site dissociation constants and cooperativity parameters listed in Table II. As the amount of tabular information is overwhelming, histograms of site dissociation constants and cooperativity parameters are available to allow quick visualization of mutations having significant effects on allosteric interactions (Figure 6).

Mutations which have little effect on properties are S445A, S447D, L474D, F477A and T723I. The list includes all the mutations at the C-terminal end of the transition helix.

T216A near the N-terminal pivot, and F786D, F786M and I803A in the flexible subdomain enhance site binding affinities for inhibitor at both the N- and C-terminal halves. I781A has the most significant effect on inhibition for those enzyme forms amenable to the analysis of Chapter 3, causing 3-fold and 17-fold changes in site dissociation constants at the C- and N-terminal half, respectively. Others mutant enzymes listed in Table II have been presented and discussed in Chapters 2 and 3 of this thesis.

Mutant enzymes not listed in Table II are missing information, the mutant forms having been characterized prior to the development of analytical methods in Chapter 3 of this thesis. If K_{ii} is too high to measure, then K_i is a site-dissociation constant. If K_{PI} is known and K_i equals K_{PI}, then no P_i-relief is observed and inhibition is due to the direct binding of 1,5-anhydroGlc-6-P to the C-terminal half. If K_{PI} is extremely high, then P_i-relief is complete and inhibition is due to the binding of inhibitor to the N-terminal half. Hence, G448A HKI has no inhibition from the N-terminal half and no P_i-relief, whereas G896A HKI has no inhibition from the C-terminal half and complete P_i-relief. These two mutant forms of HKI represent opposite extremes in HKI inhibition (Figure 7). The double mutation G896A/T232A eliminates measureable inhibition, as expected.

Results of other mutations of residues in the flexible subdomain cause significant changes in properties of HKI. T784A and L867A exhibit no inhibition, but the mutant enzymes have low activity. L795E and L797T have no measurable K_{ii} value. Data are not available for these to mutant enzymes to unequivocally assign the mechanism of inhibition, but the low values for P_i-relief suggest inhibition by way of the C-terminal half.

The situation for Phe786 is complicated. F786D and F786M HKI exhibit enhanced inhibition as noted above; however F786D-mini HKI exhibits no measurable inhibition. Data for T232A/F786D HKI confirms inhibition comes from the C-terminal half.

Kinetics of Wild-type and Mini Hexokinases with Different Substrates— As shown in Table III, both full-length and mini HKI use ATP, ITP, GTP, UTP and CTP as substrates; however, 1,5-anhydroGlc-6-P does not inhibit catalysis of wild-type HKI supported by GTP, UTP or CTP, and exhibits a five-fold increase in IC_{50} in catalysis supported by ITP. In contrast, 1,5-anhydroGlc-6-P inhibits mini HKI potently regardless of the nucleoside triphosphate

used in support catalysis.

Discussion

HKI in most crystal structures is a dimer; whereas, in solution under conditions of assay (<1 mg/ml protein concentration) it is a monomer[5, 14-16, 18, 36]. The lone example of a monomeric HKI in crystal structures is the triple mutant (E280A, R283A and G284Y), which eliminates subunit interactions of the crystalline dimer[17]. The triple mutant exhibits wild-type functional responses to 1,5anhydroGlc-6-P, P_i and substrates, and adopts a rod-like conformation of a single subunit in the crystallographic dimer[14-18]. Hence, HKI in solution should maintain a global conformation similar to that observed in crystallographic structures[36]. Interactions between the N- and C-terminal halves then occur only by way of the transition helix and a few polar contacts involving residues 242–251 of the N-terminal half and the flexible subdomain of the C-terminal half.

Crystal structures reveal two binding sites for Glc-6-P, paired with binding sites for Glc. In solution one molecule of Glc-6-P binds to HKI with high affinity, and a second molecule of inhibitor binds with low-affinity[14-17, 21-25]. Fromm suggested that Glc-6-P potently inhibits the enzyme by binding to the C-terminal half, whereas Wilson assigned Glc-6-P inhibition to a site at the N-terminal half[7, 23, 26-27]. The Fromm and Wilson models agree, however, that P_i antagonizes Glc-6-P inhibition by binding to a high-affinity site at the N-terminal half[5, 18]. P_i replaces Glc-6-P directly in the Wilson model, whereas P_i competes via an allosteric mechanism with Glc-6-P bound at the C-terminal half in the Fromm model[5, 18].

Results from numerous investigations from the laboratories of Fromm and Wilson clearly indicate that each model individually cannot account for all observed phenomena. The Glc-6-P analog 1,5-anhydroGlc-6-P is a nonlinear competitive inhibitor of HKI with respect to ATP[20] and that Glc-6-P can bind to either N- or C-terminal halves causing potent inhibition[7-8, 19-21]. Moreover, several mutant forms of HKI (D84A, HKI^+, HKI^+-D84A, S88A, K418A, R801A, S415A, HKI-α+2) the sites of mutation all distant from the P_i binding site, exhibit reduced P_i-relief of 1,5-anhydroGlc-6-P inhibition and are inconsistent with the Wilson's model [20, 25, 35, 37, 38], which make inhibitor and P_i binding inseparable.

Recent findings (Chapters 2, 3 and 4, this thesis) indicate inhibition arises by interactions of 1,5-anhydroGlc-6-P at both N- and C-terminal halves of HKI, that binding affinity of the inhibitor is higher at the N- relative to the C-terminal half, that inhibitor binding sites interact antagonistically in the wild-type enzyme, that P_i displaces inhibitor from the N-terminal half, but not the C-terminal half, and that Glc must bind to the active site in order to engender potent product inhibition.

In developing a model for allostery in HKI, one cannot rely on the properties of the truncated C-terminal half to represent the properties of the C-terminal half in the wild-type enzyme. Properties of catalysis and inhibition of mini-HKI differ from those of wild-type HKI, and identical mutations in each system do not always cause identical changes in properties. 1,5-AnhydGlc-6-P inhibits catalysis regardless of the nucleoside triphosphate employed as a substrate of mini HKI (Table III). On the other hand, 1,5-anhydroGlc-6-P potently inhibits wild-type HKI activity only when ATP is the substrate. Mutations (T747A and L867A) eliminate or greatly reduce 1,5-anhydroGlc-6-P inhibition of wild-type HKI, but have little effect on 1,5-anhydroGlc-6-P inhibition of mini HKI (Table I). In contrast F786D exhibits enhanced inhibition at both the N- and C-terminal domains in the full-length enzyme and no inhibition in mini HKI. The conclusion is inescapable: the molecular mechanisms of inhibition for mini HKI and wild-type HKI differ.

1,5-AnhydroGlc-6-P must bind directly to the active site of mini HKI, whereas inhibitor acts on wild-type HKI primarily through an allosteric mechanism (Chapters 2 and 3, this thesis). In the direct binding mechanism, the 6-phosphoryl group of the inhibitor occupies the binding site for the α-phosphoryl group of adenine nucleotides[17]. If an alternative nucleotide binds productively to mini HKI, its phosphoryl group must overlap the binding pocket for inhibitor. The situation differs markedly for wild-type HKI. 1,5-AnhydroGlc-6-P closes the base binding pocket for the adenine nucleotide through an allosteric mechanism (to be described in detail below). The triphosphoryl locus of the nucleotide binding pocket remains accessible, however, and as a consequence a range of nucleoside triphosphates can bind productively, albeit weakly, to phosphorylate Glc.

An alternative binding mode for triphosphate nucleosides has indirect support from *Toyoshima et al.*, who have observed different binding modes for ATP and TNP-ATP

(2'-(or-3')-*O*-(trinitrophenyl) adenosine 5'-triphosphate) to Ca^{2+}-ATPase[39]. Although TNP-ADP binds with high affinity to wild-type HKI (Chapters 2 and 3, this thesis), steric collisions between the TNP moiety and residues 746–747 disallows the canonical binding mode (Figure 8). TNP-ADP, however, can adopt an alternative binding mode analogous to that observed for Ca^{2+}-ATPase. In this alternative mode, the base moiety of the nucleotide does not occupy the base-binding pocket, but rather occupies the glucopyranosyl pocket for Glc-6-P. Hence, a productive binding mode that sidesteps the proposed allosteric inhibition mechanism of wild-type HKI is plausible.

Mapping locations of mutations (those presented here and in the literature) that significantly reduce P_i-relief, eliminate a measureable K_{ii} and/or eliminate inhibition altogether results in Figure 9. The locations of mutations are consistent with the model proposed by Aleshin *et al.*[17], namely mutations cluster in the region of the pivot and in the flexible subdomain. The vast majority of mutant enzymes and the wild-type enzyme exhibit antagonistic coupling of inhibitor binding sites, but some mutant enzymes that have synergistic coupling. Mutations that cause inhibition entirely through the N- or C-terminal half are known (G448A and G896A) and distinguishable from the mixed-inhibition mechanism of the wild-type enzyme.

Table I. Kinetics parameters for mutant and wild-type HKI.[#]

Group	HKI	K_{cat} S^{-1}	K_m^{Glc} μM	K_m^{ATP} mM	K_I^c μM	K_{II}^c μM	K_{PI}^c μM	P_i-Relief[d] %
	Wild-type	92 ± 1	45 ± 3	1.03 ± 0.02	19 ± 2 [a]	240 ± 50 [a]	62 ± 2	85
	Mini-HKI	40 ± 1	30 ± 3	0.95 ± 0.05	12.5 ± 0.6 [b]	N.A	N.A	N.R
Transition helix N and the Glc-6-P pocket	D413N	82 ± 1	57 ± 2	0.98 ±0.06	23 ± 4	80 ± 20	45 ± 2	80
	D861N	9.4 ± 0.1	37 ± 1	2.02 ± 0.09	30 ± 4	80 ± 20	98 ± 3	86
	D413N/D861N	10.0 ± 0.1	32 ± 2	1.59 ± 0.06	35 ± 5	110 ± 40	95 ± 4	78
	K418A	63 ± 1	88 ± 4	0.93 ± 0.05	44 ± 4	1100 ± 500	63 ± 7	44
	K866A	66 ± 2	63 ± 4	1.48 ± 0.09	70 ± 10	400 ± 300	369 ± 34	89
	K418A/K866A	71 ± 1	56 ± 2	1.1 ± 0.1	170 ± 20	1500 ± 700	460 ± 14	52
	mini-K866A	41 ± 1	43 ± 3	2.9 ± 0.2	60 ± 3 [b]	N.A	N.A	N.R
	T216A	58 ± 1	70 ± 3	0.93 ± 0.03	8.1 ± 0.5 [a]	400 ± 90 [a]	36 ± 3	81
	T232A	60 ± 1	77 ± 3	0.73 ± 0.05	40 ± 1	N.A	60± 5	3
	S445A	69 ± 1	74 ± 3	0.69 ± 0.03	20 ± 2 [a]	290 ± 80 [a]	53 ± 1	76
	S447D	72 ± 1	113 ± 5	1.16 ± 0.03	23 ± 1 [a]	300 ± 60 [a]	57 ± 2	76
	S449P	84 ± 2	75 ± 2	0.88 ± 0.05	36 ± 2 [b]	N.A	57 ± 4	48
	G448A	79 ± 1	107 ± 4	0.97 ± 0.06	64 ± 2 [b]	N.A	61 ± 2	7
	G896A	86 ± 2	113 ± 2	0.45 ± 0.02	112 ± 6 [b]	N.A	2300 ± 300	95
	T232A/G896A	68 ± 1	81 ± 2	0.30 ± 0.01	N.I	N.A	1800 ± 300	N.A
	Mini-G896A	64 ± 1	74 ± 3	0.73 ± 0.05	400 ± 10 [b]	N.A	N.A	N.R
	L867A	0.92 ± 0.08	55 ± 4	0.91 ± 0.05	N.I	N.A	N.A	N.A
	L867Y	1.60 ± 0.03	28 ± 3	1.8 ± 0.1	N.I	N.A	N.A	N.A
	Mini-L867A	0.72 ± 0.02	40 ± 3	0.64 ± 0.05	74 ± 5 [b]	N.A	N.A	N.T
Transition helix C	L474D	70 ± 1	65 ± 3	1.23 ± 0.04	14.9 ± 0.9 [a]	110 ± 20 [a]	35 ± 2	76
	F477A	70 ± 1	80 ± 3	0.62 ± 0.03	22 ± 2 [a]	230 ± 60 [a]	93 ± 2	92
	T723I	66 ± 1	110 ± 4	0.84 ± 0.03	18 ± 1 [a]	150 ± 30 [a]	42 ± 3	80

--To be continued

Table I. Continued

Group	HKI	K_{cat} S^{-1}	K_m^{Glc} μM	K_m^{ATP} mM	K_I[c] μM	K_{II}[c] μM	K_{PI}[c] μM	P_i-Relief[d] %
	Wild-type	92 ± 1	45 ± 3	1.03 ± 0.02	19 ± 2 [a]	240 ± 50 [a]	62 ± 2	85
	Mini-HKI	40 ± 1	30 ± 3	0.95 ± 0.05	12.5 ± 0.6 [b]	N.A	N.A	N.R
Flexible Subdomain	I781A	163 ± 4	76 ± 2	1.23 ± 0.03	130 ± 10 [a]	1100 ± 300 [a]	169 ± 4	51.35
	Mini-I781A	55 ± 1	87 ± 4	1.3 ± 0.09	77 ± 3 [b]	N.A	N.A	N.R
	T784A	1.35 ± 0.09	110 ± 20	0.90 ± 0.08	N.I	N.A	N.A	N.A
	T784L	1.1 ± 0.1	28 ± 2	1.14 ± 0.07	N.I	N.A	N.A	N.A
	Mini-T784A	0.90 ± 0.08	33 ± 1	1.2 ± 0.1	40 ± 2 [b]	N.A	N.A	N.T
	F786M	42 ± 3	43 ± 5	1.08 ± 0.04	9 ± 1 [a]	80 ± 30 [a]	22.5 ± 0.3	81
	F786D	16.1 ± 0.2	31 ± 3	3.1 ± 0.1	7 ± 1 [a]	100 ± 30 [a]	14.9 ± 0.5	76
	T232A/F786D	17 ± 1	48 ± 2	3.1 ± 0.3	12.9 ± 0.5 [b]	N.A	16.9 ± 0.2	10
	Mini-F786M	8.2 ± 0.3	19 ± 2	1.16 ± 0.05	6.5 ± 0.2 [b]	N.A	N.A	N.R
	Mini-F786D	30.9 ± 0.4	142 ± 3	0.60 ± 0.04	N.I	N.A	N.A	N.A
	L795E	121 ± 1	68 ± 5	0.35 ± 0.02	45 ± 3	N.A	N.A	23
	L797T	12.2 ± 0.2	23 ± 1	2.24 ± 0.06	39 ± 3	N.A	N.A	28
	L798E	74 ± 2	45 ± 2	0.90 ± 0.07	47 ± 3	220 ± 20	N.T	78
	I803A	34 ± 1	49 ± 1	2.7 ± 0.1	7.0 ± 0.7 [a]	50 ± 10 [a]	14.8 ± 0.3	80

[#]Data for wild-type, D413N, D861N, D413N/D861N, K418A, K866A, K418A/K866A are reproduced from Chapter 3, this thesis.
[a]Data fit a non-linear competitive model.
[b]Data fit linear competitive model.
[c]K_I and K_{II} are stoichiometric dissociation constants for 1,5-anhydroGlc-6-P from singly- and doubly-ligated enzymes and K_{PI} is the stoichiometric dissociation constant for 1,5-anhydroGlc-6-P from the enzyme-Pi complex.
[d]P_i-relief of inhibition is defined as 100×(A-B)/A, where A is the slope from plots of reciprocal relative velocity *versus* 1,5-anhydroGlc-6-P concentration in the absence of P_i, and B is the slope from plot of reciprocal relative velocity *versus* inhibitor concentration in the presence of 6 mM P_i. Relative velocity is the ratio of velocity at a specific concentration of inhibitor to the velocity in the absence of inhibitor. The ATP concentration is fixed at K_m^{ATP} for each enzyme.
N.I., no inhibition observed up to 1 mM 1,5-anhydroGlc-6-P; N.T., not tested; N.R., no relief; N.A., not applicable.

Table II. Kinetics parameters and site affinity constants with respect to 1,5-anhydroGlc-6-P for wild-type HKI and mutants[#]

(all units except α are μM)

Group	HKI	K_I	K_{II}	α	${}^0M_1$	${}^0M_2$	${}^2M_1$	${}^1M_2$
	Wild-type	20	240	0.37	30	62	77	163
Glc-6-P Proximity	T216A	8.1	400	0.12	10	36	90	310
	D413N	23	80	1.15	47	45	41	39
	D861N	30	80	1.77	43	98	24	56
	D413N/D861N	35	110	1.37	55	95	41	69
	K418A	44	1100	0.19	146	63	768	332
	K866A	70	400	1.14	86	369	76	324
	K418A/K866A	170	1500	0.49	270	460	554	946
	S445A	20	290	0.29	32	53	109	181
	S447D	23	300	0.32	39	57	121	179
Hinge	L474D	14.9	110	0.55	26	35	47	63
	F477A	22	230	0.53	29	93	54	176
	T723I	18	150	0.49	32	42	64	86
Flexible Sub-domain	I781A	130	1100	0.67	563	169	846	254
	F786D	7	100	0.28	13	14.9	47	53
	F786M	9	80	0.47	15	22.5	32	48
	I803A	7	50	0.56	13	14.8	24	26

[#]Results for wild-type, D413N, D861N, D413N/D861N, K418A, K866A, K418A/K866A are reproduced from Chapter 3, this thesis. The following equations are used in the calculation of site dissociation constants:

$$\alpha = {(K_{PI})^2}\Big/{K_{II}(K_{PI} - K_I)}; \quad {}^0M_1 = \alpha K_{II} - K_{PI}; \quad {}^0M_2 = K_{PI}; \quad {}^2M_1 = {}^0M_2\Big/\alpha; \quad {}^1M_2 = {}^0M_1\Big/\alpha$$

Table III. Kinetics parameters of full-length HKI and mini-HKI with common nucleoside triphosphates

Nucleoside Triphosphate	Full-length HKI			Mini-HKI		
	k_{cat}[a] (s^{-1})	K_m^{NTP}[a] (mM)	IC_{50}[b] (μM)	k_{cat}[a] (s^{-1})	K_m^{NTP}[a] (mM)	IC_{50}[b] (μM)
ATP	91 ± 2	0.53 ± 0.04	20 ± 1	36.7 ± 0.5	0.47 ± 0.02	28 ± 1
ITP	3.0 ± 0.2	2.9 ± 0.7	94 ± 4	1.83 ± 0,04	1.95 ± 0.09	38 ± 1
GTP	4 ± 2	2.9 ± 0.5	----[c]	1.66 ± 0.03	4.5 ± 2	12.8 ± 0.7
UTP	3.8 ± 0.1	5.9 ± 0.4	----[c]	0.8 ± 0.1	7.8 ± 2	28.4 ± 0.3
CTP	2.68 ± 0..06	3.3 ± 0.2	----[c]	1.14 ± 0.04	4.6 ± 0.2	6.2 ± 0.9

[a]Assays were in 100 mM Tris, pH7.4, and 2 mM Glc, and Mg^{2+} 2 mM in excess of nucleotide. The nucleoside triphosphates varied from 1/3 to 3 K_m^{NTP} .

[b]IC_{50} means the concentration of 1,5-anhydroGlc-6-P that cause 50% inhibition with NTP concentrations fixed at K_m^{NTP} and glucose concentration fixed at 2 mM.

[c]No detectable inhibition up to 1 mM 1,5-anhydroGlc-6-P.

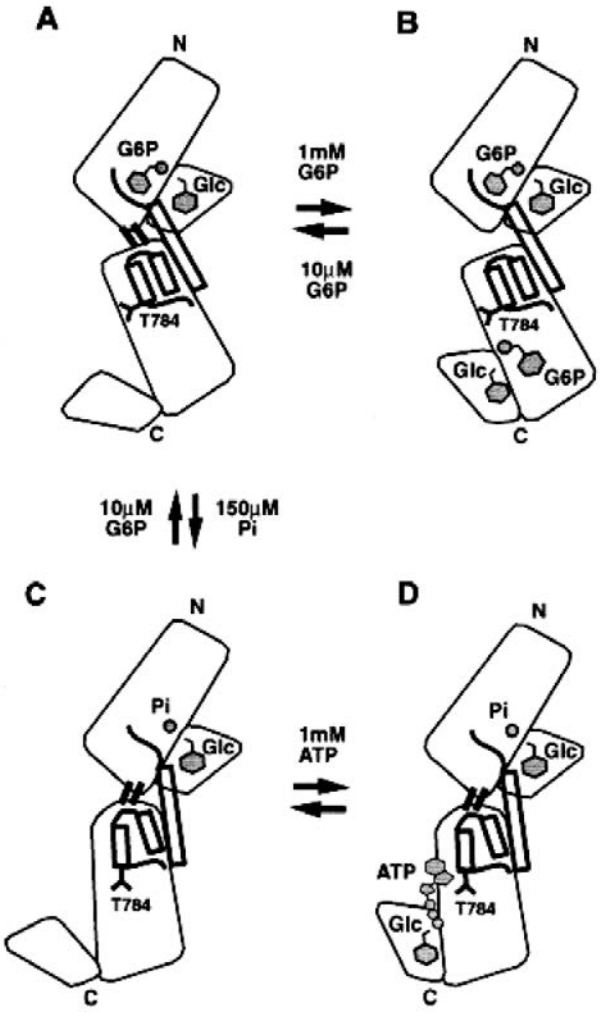

Figure 1. Allosteric states of the hexokinase I monomer. The conformation of monomeric hexokinase varies in response to ligation of its active site (C-terminal half) and its vestigial active site (N-terminal half). (a) In the presence of low concentrations of Glc-6-P, the allosteric interface between the N and the C-terminal halves maintains the flexible subdomain in an ATP-antagonistic state, in which Thr784 blocks the base-binding pocket for the nucleotide. (b) In the presence of elevated concentrations of Glc-6-P, the N and C-terminal halves are decoupled, with Glc-6-P bound directly to the active site, overlapping the ATP pocket. (c) Sufficient levels of P_i displace Glc-6-P from the N-terminal half and allow a rigid-body rotation of that half relative to the C-terminal half. The allosteric interface now stabilizes the ATP-compatible conformation of the flexible subdomain, removing Thr784 as a steric obstacle to ATP association. (d) ATP binds to the P_i-stabilized conformer of hexokinase. (Reprinted from Ref.17 with permission)

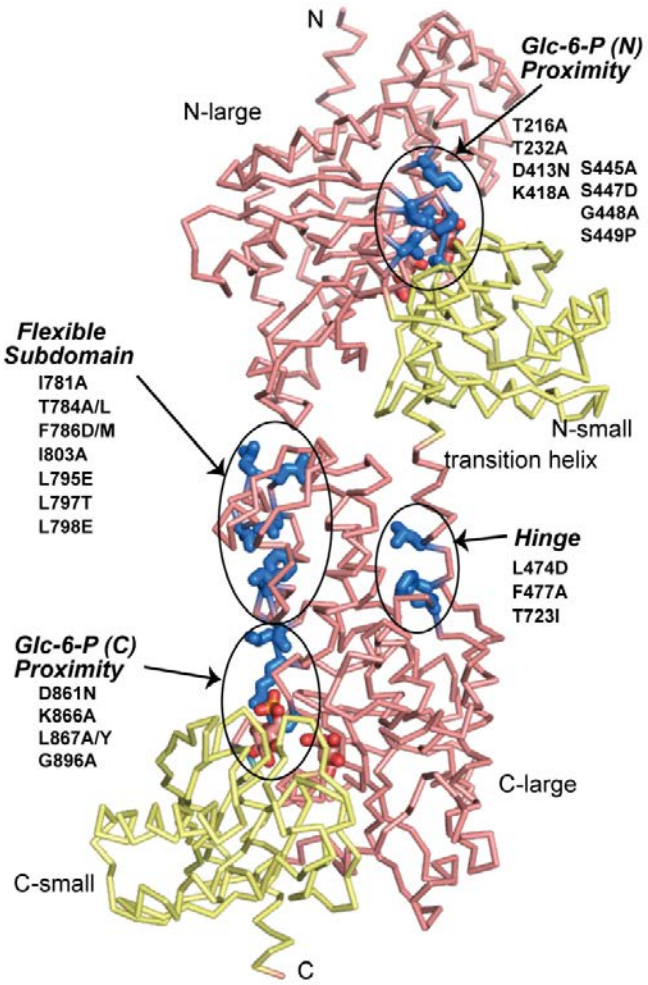

Figure 2. Overview crystal structure of wild type HKI•Glc-6-P•Glc complex (Chapter 2, this thesis). Large domains (16-74, 210-447 for N-terminal half; 467-522, 658-895 for C-terminal half) are pink; small domains (75-209, 448-465 for N-terminal half; 523-657, 896-913 for C-terminal half) are yellow. Glc-6-P and Glc are stick models. The residues mutated in this report are colored blue. (The illustration was generated with PyMOL).

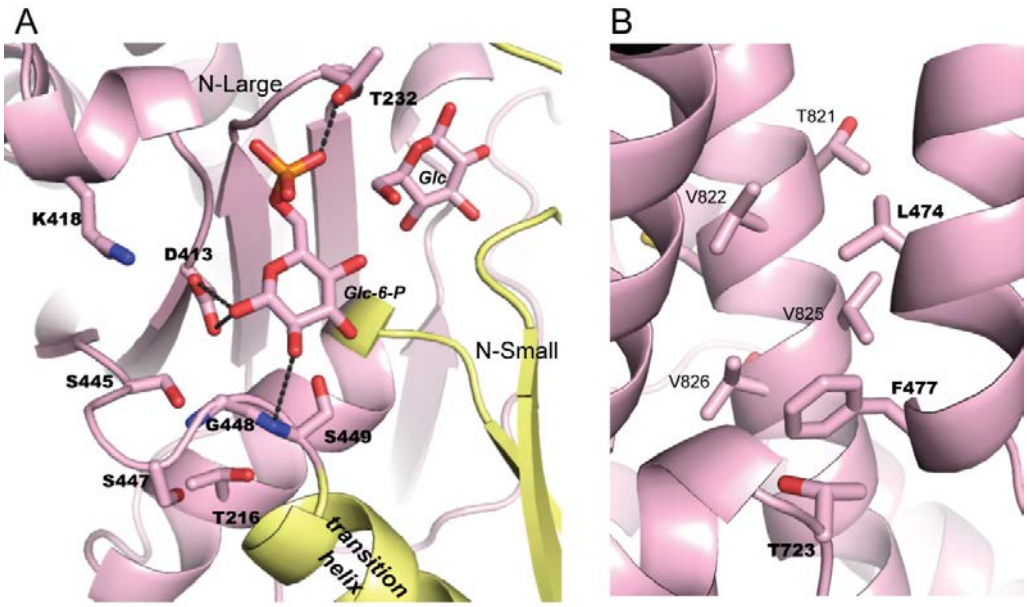

Figure 3. N- and C-terminal ends of the transition helix. Structural details in the Glc-6-P pocket, N-terminal half (A) and the C-terminal end of the transition helix (B). The structure is from Chapter 2, this thesis, wild-type HKI•Glc-6-P•Glc complex. (The illustration was generated with PyMOL).

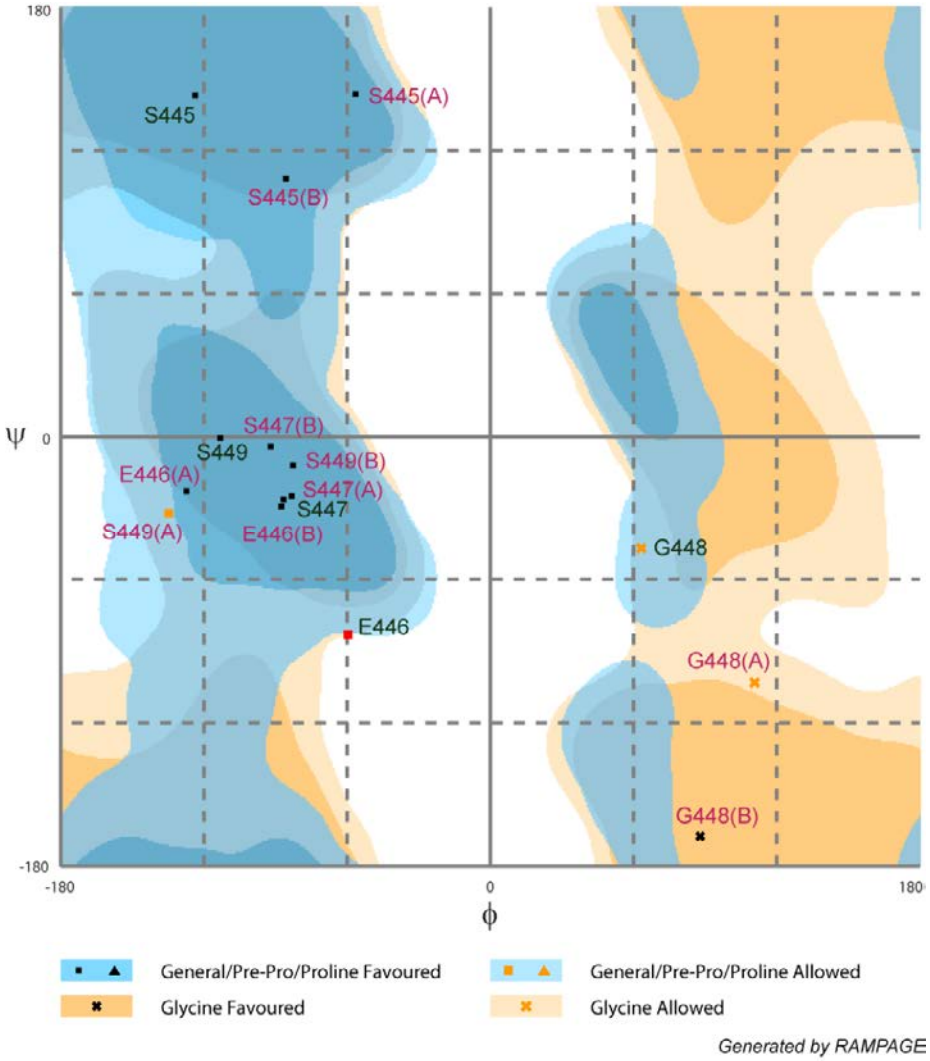

Figure 4. Ramachandran Plot of Loop 445–449. Main chain angles from the Glc-6-P•Glc complex (labeled magenta with chain A and B shown, from the HKI•Glc-6-P•Glc structure, Chapter 2, this thesis) and the HKI•P_i•Glc complex (labeled dark green, PDB: 1HKC).

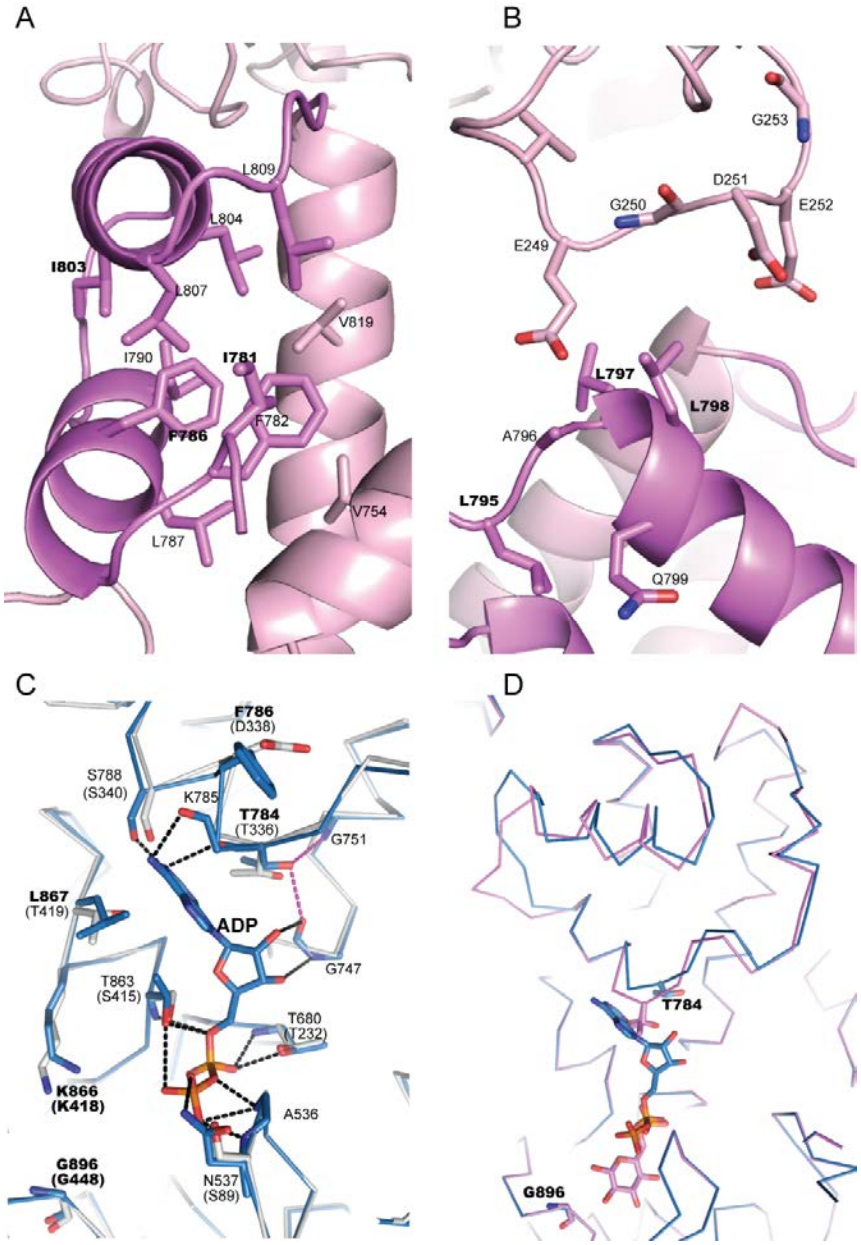

Figure 5. Structural details of the flexible subdomain. A. hydrophobic pocket of F786 with the side chain buried in the core of the flexible subdomain. From the HKI•Glc-6-P•Glc structure, Chapter 2, this thesis. B. the interface between the N- and C-terminal halves. Residues of the flexible subdomain are dark purple and others are light purple. C. ADP binding pocket from structure 1DGK with C-terminal half (blue) superimposed to N-terminal half (light gray). The side chains residues that involved in direct ADP binding or putatively contribute to ADP binding are labeled and the corresponding partners in N-half are marked in parenthesis. The main chain residues involved in ADP binding are labeled only for C-half HKI. D. Flexible subdomain from HKI•ADP•Glc (1DGK, blue) and HKI•Glc-6-P•Glc (pink) complexes superimposed based on C-terminal half large domain. T784 from Glc-6-P are in two states. The backbone of Gly is shown. Names of mutated residues are bold fonts. (The illustration was generated with PyMOL).

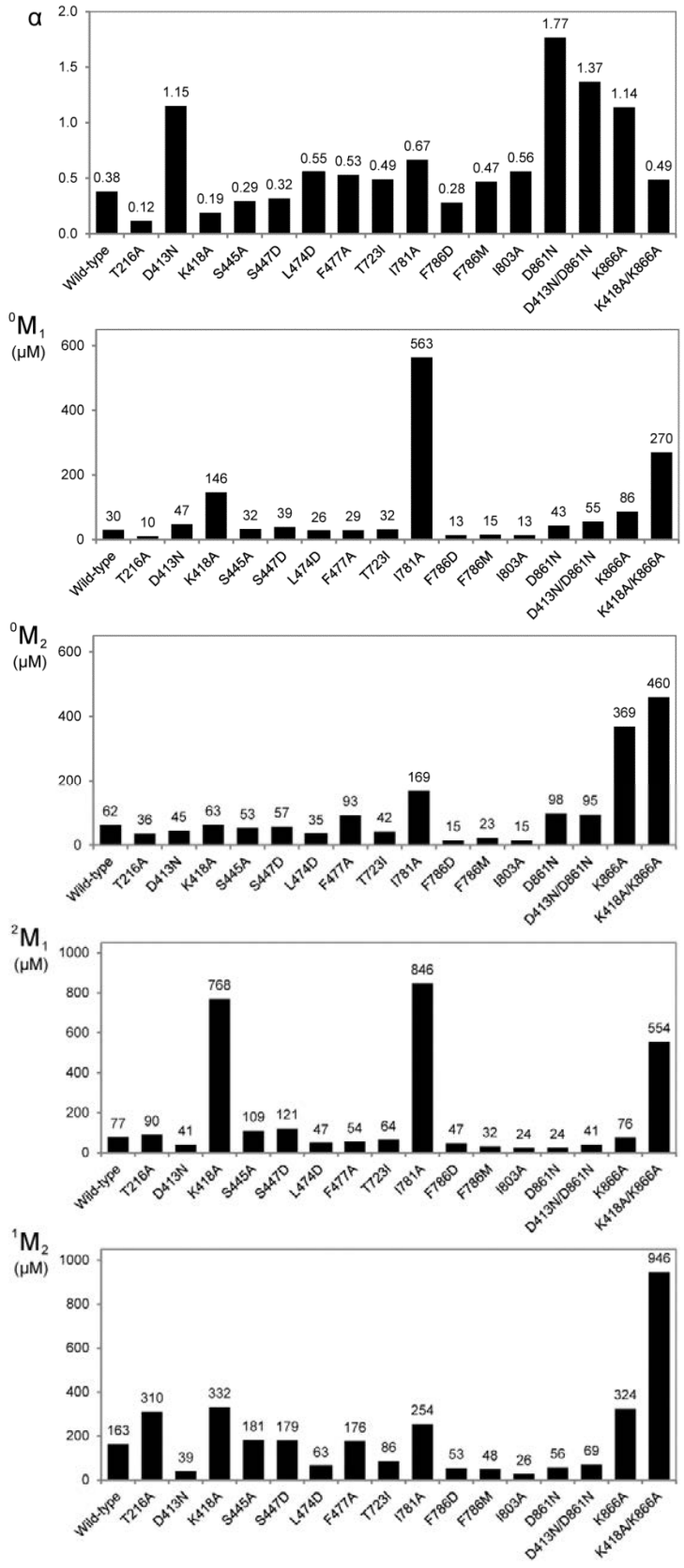

Figure 6. Histogram of cooperativity parameter α and site affinity constants for wild-type HKI and mutants.

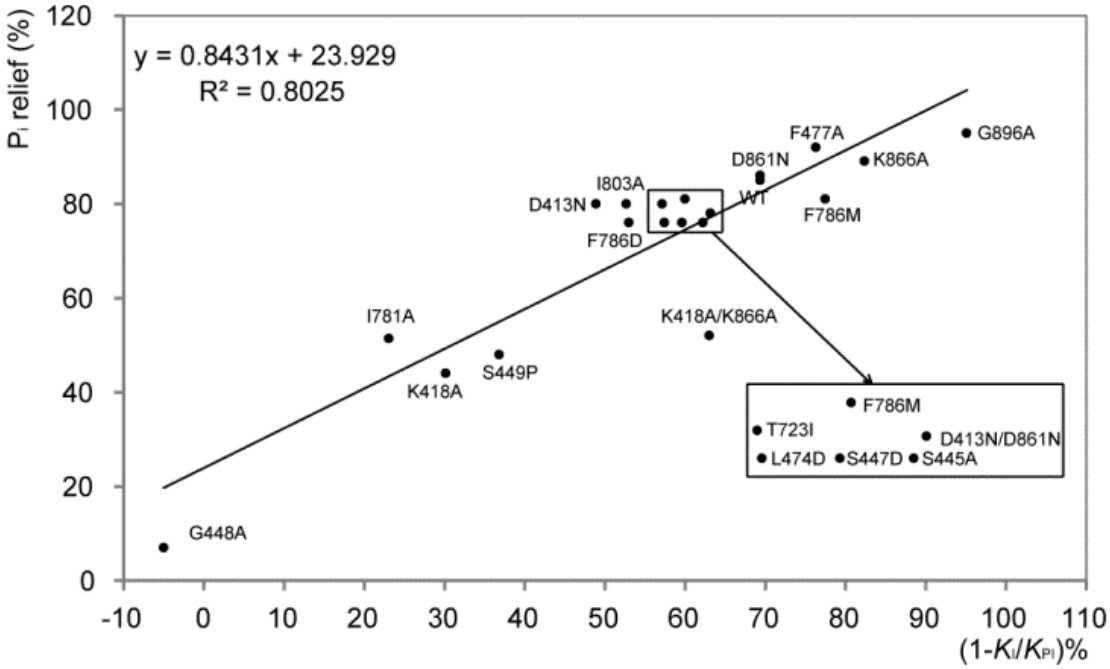

Figure 7. Correlation between P_i-relief and (1-K_I/K_{PI}).

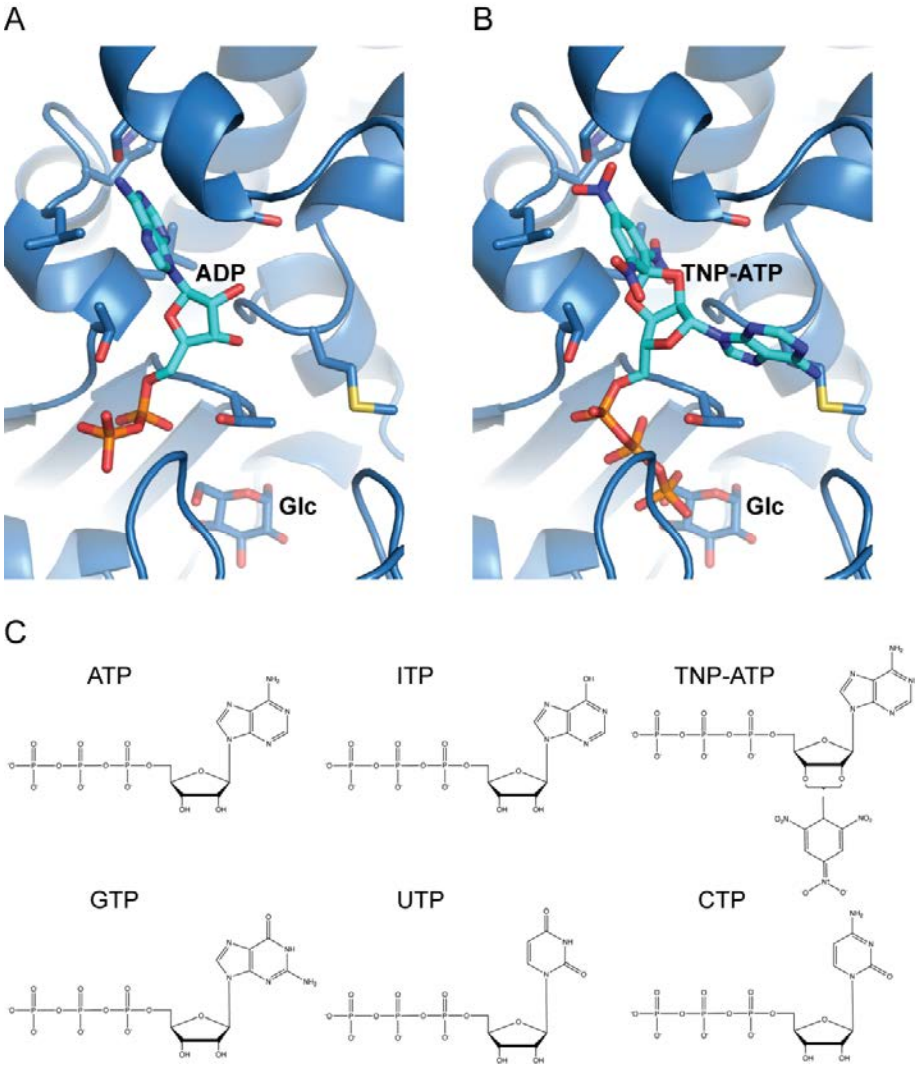

Figure 8. Alternative binding for nucleotides. A. ADP pocket of HKI structure from 1DGK. B. possible TNP-ATP bound HKI structure from modeling. TNP-ATP is shown as two derivatives, 2'-(or-3')-O-(trinitrophenyl) adenosine 5'-triphosphate. (The illustration was generated with PyMOL) C. Nucleoside triphosphates and derivatives. (The illustration was generated with Bio-Draw).

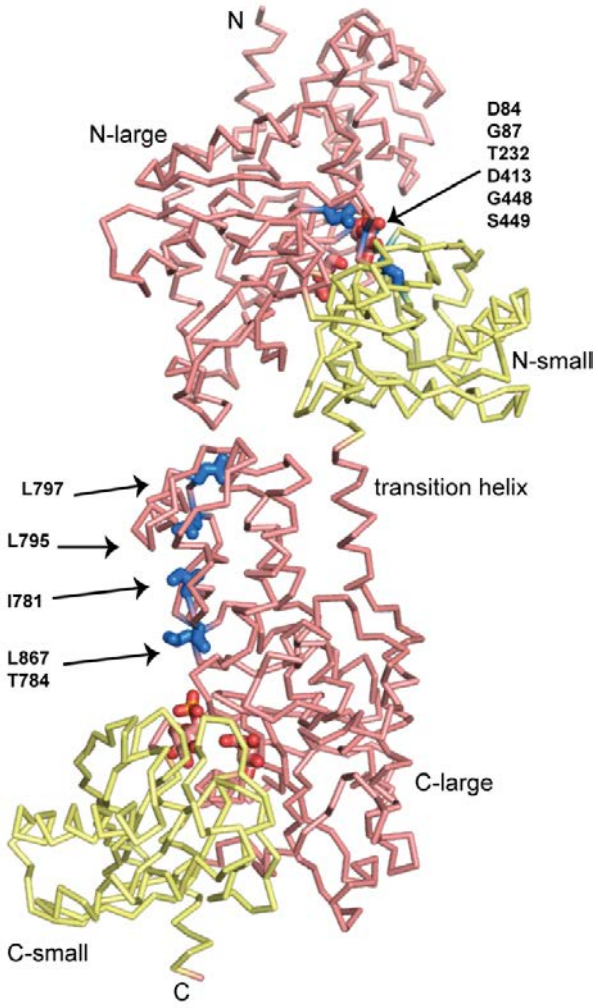

Figure 9. Residues involved in Glc-6-P allosteric inhibition. Large domains (16-74, 210-447 for N-terminal half; 467-522, 658-895 for C-terminal half) are s pink and small domains (75-209, 448-465 for N-terminal half; 523-657, 896-913 for C-terminal half) are yellow. Residues causing significant change in inhibition properties are blue. Glc and Glc-6-P are stick models. (The illustration was generated with PyMOL).

References

1. Gonzalez, C., Ureta, T., Sánchez, R., and Niemeyer, H. (1964) Multiple molecular forms of ATP: hexose 6-phosphotransferase from rat liver. *Biochem. Biophys. Res. Commun.* **16**, 347-352
2. Grossbard, L., and Schimke, R.T. (1966) Multiple hexokinases of rat tissues. Purification and comparison of soluble forms. *J. Biol. Chem*. **241**, 3546-3560
3. Katzen, H.M. (1967) The multiple forms of mammalian hexokinase and their significance to the action of insulin. *Adv. Enzyme Regul*. **5**, 335-356
4. Katzen, H.M., and Schimke, R.T. (1965) Multiple forms of hexokinase in the rat: tissue distribution, age dependency, and properties. *Proc. Natl. Acad. Sci. U.S.A.* **54**, 1218-1225
5. Wilson, J.E. (1995) Hexokinase. *Rev. Physiol. Biochem. Pharmacol*. **126**, 65-198
6. Tsai, H.J. and Wilson, J.E. (1996) Functional organization of mammalian hexokinases: both N- and C-terminal halves of the rat type II isozyme possess catalytic sites. *Arch. Biochem. Biophys.* **329**, 17-23
7. White, T.K., and Wilson, J.E. (1989) Isolation and characterization of the discrete N- and C-terminal halves of rat brain hexokinase: retention of full catalytic activity in the isolated C-terminal half. *Arch. Biochem. Biophys*. **274**, 375-393
8. Arora, K.K., Filburn, C.R., and Pedersen, P.L. (1993) Structure/function relationships in hexokinase. Site-directed mutational analyses and characterization of overexpressed fragments implicate different functions for the N- and C-terminal halves of the enzyme. *J. Biol. Chem*. **266**, 5359-5362
9. Kawai, S, Mukai, T, Mori, S, Mikami, B, and Murata, K. (2005) Hypothesis: structures, evolution, and ancestor of glucose kinases in the hexokinase family. *J. Biosci. Bioeng*. **99**, 320-330
10. Easterby, J.S, and O'Brien, M.J. (1973) Purification and properties of pig-heart hexokinase. *Eur. J. Biochem*. **38**, 201-211
11. Holroyde, M.J., and Trayer, I.P. (1976) Purification and properties of skeletal muscle hexokinase. *FEBS Lett*. **62**, 215-219

12. Ureta, T. (1982) The comparative isozymology of vertebrate hexokinases. *Comp. Biochem. Physiol*. **71B**, 549-555
13. Manning, T.A., and Wilson, J.E. (1984) Inhibition of brain hexokinase by a multisubstrate analog results from binding to a discrete regulatory site. *Biochem. Biophys. Res. Commun.* **118**, 90-96
14. Aleshin, A.E., Zeng, C., Bourenkov, G.P., Bartunik, H.D., Fromm, H.J., and Honzatko, R.B. (1998) The mechanism of regulation of hexokinase: new insights from the crystal structure of recombinant human brain hexokinase complexed with glucose and glucose-6-phosphate. *Structure.* **6**, 39-50
15. Mulichak, A.M., Wilson, J.E., Padmanabhan, K., and Garavito, R.M. (1998) The structure of mammalian hexokinase-1. *Nat. Struct. Biol*. **5**, 555-560
16. Aleshin, A.E., Fromm, H.J., and Honzatko, R.B. (1998) Multiple crystal forms of hexokinase I: new insights regarding conformational dynamics, subunit interactions, and membrane association. *FEBS Lett*. **434**, 42-46
17. Aleshin, A.E., Kirby, C., Liu, X., Bourenkov, G.P., Bartunik H.D., Fromm, H.J., and Honzatko, R.B. (2000) Crystal structures of mutant monomeric hexokinase I reveal multiple ADP binding sites and conformational changes relevant to allosteric regulation. *J. Mol. Biol*. **296**, 1001-1015
18. Aleshin, A.E., Zeng, C., Bartunik, H.D., Fromm, H.J., and Honzatko, R.B. (1998) Regulation of Hexokinase I: Crystal Structure of Recombinant Human Brain Hexokinase Complexed with Glucose and Phosphate. *J. Mol. Biol*. **282**, 345-357
19. Zeng, C., and Fromm, H.J. (1995) Active site residues of human brain hexokinase as studied by site-specific mutagenesis. *J. Biol. Chem*. **270**, 10509-10513
20. Fang, T.Y., Alechina, O., Aleshin, A.E., Fromm, H.J., and Honzatko, R.B. (1998) Identification of a Phosphate Regulatory Site and a Low Affinity Binding Site for Glucose 6-Phosphate in the N-terminal Half of Human Brain Hexokinase. *J. Biol. Chem*. **273**, 19548-19553
21. Liu, X., Kim, C.S., Kurbanov, F.T., Honzatko, R.B., and Fromm, H.J. (1999) Dual Mechanisms for Glucose 6-Phosphate Inhibition of Human Brain Hexokinase. *J. Biol. Chem.* **274**, 31155-31159

22. Ellison, W.R., Lueck, J.D., and Fromm, H.J. (1974) Studies on the kinetics and mechanism of orthophosphate activation of bovine brain hexokinase. *Biochem. Biophys. Res. Commun*. **57**, 1214-1220
23. Ellison, W.R., Lueck, J.D., and Fromm, H.J. (1975) Studies on the mechanism of orthophosphate regulation of bovine brain hexokinase. *J. Biol. Chem*. **250**, 1864-1871
24. Chou, A.C., and Wilson, J.E. (1974) Rat brain hexokinase: glucose and glucose-6-phosphate binding sites and C-terminal amino acid of the purified enzyme. *Arch. Biochem. Biophys.* **165**, 628-633
25. Skaff, D.A., Kim, C.S., Tsai, H.J., Honzatko, R.B., and Fromm, H.J. (2005) Glucose 6-phosphate release of wild-type and mutant human brain hexokinases from mitochondria. *J. Biol. Chem*. **280**, 38403-38409
26. Purich, D.L., and Fromm, H.J. (1971) The kinetics and regulation of rat brain hexokinase. *J. Biol. Chem.* **246**, 3456-3463
27. Smith, A.D., and Wilson, J.E. (1991) Effect of ligand binding on the tryptic digestion pattern of rat brain hexokinase: relationship of ligand-induced conformational changes to catalytic and regulatory functions. *Arch. Biochem. Biophys*. **291**, 59-68
28. Zeng, C., Aleshin, A.E., Hardie, J.B., Harrison, R.W., and Fromm, H.J. (1996) ATP-binding site of human brain hexokinase as studied by molecular modeling and site-directed mutagenesis. *Biochemistry*. **35**, 13157-13164
29. Liu, F., Dong, Q., Myers, A.M., and Fromm, H.J. (1991) Expression of human brain hexokinase in Escherichia coli: purification and characterization of the expressed enzyme. *Biochem. Biophys. Res. Commun.* **177**, 305-311
30. Laemmli, U.K. (1970) Cleavage of structural proteins during the assembly of the head of bacteriophage T4. *Nature*. **227**, 680-685
31. Bradford, M.M. (1976) A rapid sensitive method for the quantitation of microgram quantities of protein utilizing the principle of protein-dye binding. *Anal. Biochem.* **72**, 248-252
32. Ferrari, R., and Crane, R. (1959) 1,5-Anhydro-D glucitol 6-phosphate and its use for the specific inhibition of the hexokinase reaction in tissue homogenates. *Arch. Biochem. Biophys.* **80**, 372-377

33. Drueckes, P., Schinzel, R., and Palm, D. (1995) Photometric microtiter assay of inorganic phosphate in the presence of acid-labile organic phosphates. *Anal. Biochem*. **230**, 173-177
34. Leatherbarrow, R.J. (2010) GraFit Version 7, Erithacus Software Ltd., Horley, U.K.
35. Hashimoto, M., and Wilson, J.E. (2002) Kinetic and regulatory properties of HK I(+), a modified form of the type I isozyme of mammalian hexokinase in which interactions between the N- and C-terminal halves have been disrupted. *Arch. Biochem. Biophys.* **399**, 109-115
36. Aleshin, A.E., Malfois, M., Liu, X., Kim, C.S., Fromm, H.J., Honzatko, R.B., Koch, M.H., and Svergun, D.I. (1999) Nonaggregating mutant of recombinant human hexokinase I exhibits wild-type kinetics and rod-like conformations in solution. *Biochemistry*. **38**, 8359-8366
37. Zeng, C., Aleshin, A.E., Chen, G., Honzatko, R.B., and Fromm, H.J. (1998) The roles of glycine residues in the ATP binding site of human brain hexokinase. *J. Biol. Chem.* **273**, 700-704
38. Shen, L., Gao, Y., and Honzatko, R.B. (2012) High-affinity recognition of ligands by the glucose 6-phosphate binding sites of mammalian hexokinases. (to be submitted)
39. Toyoshima, C., Yonekura, S., Tsueda, J., and Iwasawa, S. (2011) Trinitrophenyl derivatives bind differently from parent adenine nucleotides to Ca^{2+}-ATPase in the absence of Ca^{2+}. *Proc. Natl. Acad. Sci. U.S.A.* **108**, 1833-1838

Chapter VI. General Conclusion

The work described in this thesis represents a significant advancement in our knowledge of the mechanism of allosteric regulation of human hexokinase Type I. Chapter II presents a series of crystalline complexes and molecular dynamics simulations of recombinant human HKI with glucose 6-phosphate (Glc-6-P), 1,5-anhydro-D-glucose 6-phosphate (1,5-anhydroGlc-6-P), 2-deoxyglucose 6-phosphate (2-deoxyGlc-6-P) and mannose 6-phosphate (Man-6-P). For 2-deoxyGlc-6-P and Man-6-P, the C-terminal half tends toward an open conformation as MD simulations progress, consistent with early stages of ligand dissociation, whereas 1,5-anhydroGlc-6-P, adopts a stable, alternative binding mode in a slightly open conformation of the C-terminal half which differs from that of Glc-6-P. This alternative binding mode might reflect synergistic binding of two molecules of 1,5-anhydroGlc-6-P to sites with unequal constants of dissociation, as indicated by the kinetics data of D413N and/or D861N enzymes (D413 and D861 interact with 1-OH groups of Glc-6-P). Simulations of the Glc-6-P complex of D413N HKI demonstrate a N-terminal half conformation similar to that of the 1,5-anhydroGlc-6-P complex of wild-type HKI. The N-terminal half is open slightly relative to the N-terminal of wild-type HKI with bound Glc-6-P. The data indicate differences in the response of HKI to Glc-6-P and 1,5-anhydroGlc-6-P, suggesting an important role for the 1-OH group of the physiological inhibitor that has been overlooked. Finally, the foundation is laid for a site-affinity model that is further developed in subsequent chapters.

Chapter III presents crystalline complexes and molecular dynamics simulations of recombinant human HKI with glucose 1,6-bisphosphate (Glc-1,6-P_2), as well as the kinetics studies of specific mutant forms of HKI with respect to Glc-1,6-P_2. 1,5-AnhydroGlc-6-P is a nonlinear competitive inhibitor with respect to ATP, whereas Glc-1,6-P_2 is a linear competitive inhibitor up to a concentration of 400 μM. The crystal structure of HKI with Glc-1,6-P_2 and molecular dynamics implicate Lys418 (N-terminal half) and Lys866 (C-terminal half) in stabilizing hydrogen bond networks in inhibitor binding pockets. The kinetics of inhibition of K418A and/or K866A mutants support the significant of these lysyl side chains in inhibition. P_i-relief of inhibition is re-examined in the context of a new

kinetic model, which identifies a complex that allows both P_i and inhibitor to bind to the enzyme simultaneously. Under experimental conditions of saturating P_i, the equilibrium constant for the dissociation of inhibitor from the enzyme•phosphate•inhibitor complex is taken as the dissociation of inhibitor from the C-terminal half, thus determining one of four site affinity constants. One determined constant, along with other information, allows the complete numerical assignment of all site-affinity constants and a cooperativity parameter governing interactions between inhibitory sites. The following conclusions arise from site-affinity values: Inhibitor binds to the N-terminal half with high affinity relative to the C-terminal half of HKI. P_i affords relief of inhibition caused by inhibitor binding to the N-terminal half. Binding sites for inhibitors at the N- and C-terminal halves are coupled antagonistically.

Chapter IV is a study of glucose as (Glc) as a synergist and antagonist of HKI inhibition by 1,5-anhydroGlc-6-P. At submillimolar concentrations of Glc, the binding of Glc-6-P is synergistic with Glc; however when Glc concentration is high, the binding of 1,5-anhydroGlc-6-P is undermined. Effective inhibition of wild-type HKI requires two bound molecules of Glc, and that the binding of Glc to the active site is critical to potent inhibition by 1,5-anhydroGlc-6-P. Glc binding to the active site controls the binding affinity of allosteric inhibitors at sites within the same half and in the opposite half of HKI.

Chapter V presents the effects of directed mutations in regions putatively responsible for the allosteric inhibition of HKI, the N-terminal half pocket for Glc-6-P and the C-terminal half flexible subdomain. Using the site affinity model developed in Chapters II and III, site affinity constants are determined for a significant sampling of mutant enzymes. The effects of mutations are consistent with the proposed model of allosteric regulation due to Aleshin *et al*. Allosteric inhibition involves a Glc-6-P induced rotation of the N-terminal half about the end of the transition helix connecting the N- and C-terminal halves of HKI. Nonbonded contacts between the N-terminal half and the flexible subdomain of the C-terminal half undergo adjustments due to the rotation of the N-terminal half, the consequence of which is a state that blocks the base-binding pocket for ATP.

Acknowledgment

I would express my deepest gratitude to Dr. Richard B Honzatko, my major professor, for his guidance and support through my graduate study. Dr. Honzatko has been a great mentor and an excellent example of an academic scientist. I also like to thank Dr. Herbert J. Fromm for his advice and support. I would like to thank my colleagues: Muneaki Watanabe, Nimer Mehyar and Yang Zhou, for their help, encouragement and friendship. In addition, I would like to express my sincere gratitude to Yang Gao, my colleague and one of my best friends, who put large effort into hexokinase I structure simulation studies and gave me tons of useful advices on nearly every part of my research. Special thanks for my committee member for their time and effort for my thesis.

I would like to thank my parents for their understanding and support over all these years. My best friend, Yun Lu is always there whenever I have any trouble. I would like to thank all my friends, Ruo Xu, Qiaohui Lin, Lei Yang and Lifeng You for their friendship and help. Finally, special thanks go to my dearest cat KiKi, who accompanied me through all those hard work nights and warm my heart with his soft tummy and unconditional love.